

AMERICAN UNIVERSITY OF BEIRUT

TWO- AND THREE-DIMENSIONAL CHEMICAL WAVES IN
THE REACTION-DIFFUSION SYSTEM OF MERCURIC
IODIDE IN HYDROGEL MEDIA

by
MAHMOUD MALIK AL AYASS

A thesis
submitted in partial fulfillment of the requirements
for the degree of Master of Science
to the Department of Chemistry
of the Faculty of Arts and Sciences
at the American University of Beirut

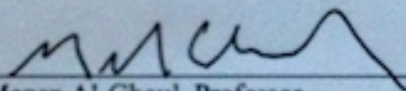
Beirut, Lebanon
May 2014

AMERICAN UNIVERSITY OF BEIRUT

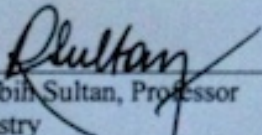
TWO- AND THREE-DIMENSIONAL CHEMICAL WAVES IN
THE REACTION-DIFFUSION SYSTEM OF MERCURIC
IODIDE IN HYDROGEL MEDIA

by
MAHMOUD MALIK AL AYASS

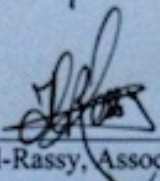
Approved by:



Dr. Mazen Al-Ghoul, Professor
Chemistry
Advisor



Dr. Rabih Sultan, Professor
Chemistry
Member of Committee



Dr. Houssam El-Rassy, Associate Professor
Chemistry
Member of Committee

Date of thesis defense: May 2, 2014

AMERICAN UNIVERSITY OF BEIRUT

THESIS, DISSERTATION, PROJECT RELEASE FORM

Student Name: Al Ayass Mahmoud Malik
Last First Middle

Master's Thesis Master's Project Doctoral Dissertation

I authorize the American University of Beirut to: (a) reproduce hard or electronic copies of my thesis, dissertation, or project; (b) include such copies in the archives and digital repositories of the University; and (c) make freely available such copies to third parties for research or educational purposes.

I authorize the American University of Beirut, **three years after the date of submitting my thesis, dissertation, or project**, to: (a) reproduce hard or electronic copies of it; (b) include such copies in the archives and digital repositories of the University; and (c) make freely available such copies to third parties for research or educational purposes.

Salim
Signature

12/5/2014
Date

ACKNOWLEDGMENTS

Foremost I would frankly like to devote my tremendous gratitude to my advisor Dr. Mazen Al-Ghoul for his exceptional guidance, constructive criticism and patience over the many years of both undergraduate and graduate research. I would like to thank him for his valuable advice and for granting me a hospitable atmosphere to carry out my research. I accredit my knowledge and the level of my degree to his assistance, and without him this thesis would not have been accomplished.

I would also like to give my appreciation to the committee members Dr. Rabih Sultan and Dr. Houssam El-Rassy for their helpful comments on this thesis and for their support.

Sincerely, I would like to express my acknowledgment of any effort or assistance granted to me by all the faculty members throughout my residency at the Chemistry Department. I am especially grateful to Mr. Issam Sleiman for his assistance with the administrative tasks necessary for completing my Master's program.

Many friends shared this experience with me and I would like to thank them all from the bottom of my heart. I have been blessed to know all of them. I thank Naim Saad, Mazen Al Mawla, Manal Ammar, Daniel Saliba, Malak El Dayeh and Malek Jaafar for the stimulating work we have performed together and for all the fun we have had in the past years.

Last but not least, I dedicate this achievement to my loving family, who have devoted their entire life for my success and comfort. Their unequivocal confidence in my character and abilities is the reason behind my accomplishments today.

AN ABSTRACT OF THE THESIS OF

Mahmoud Malik Al Ayass for Master of Science
Major: Chemistry

Title: Two- and Three-Dimensional Chemical Waves in the Reaction-Diffusion System of Mercuric Iodide in Hydrogel Media

In our study, we will investigate a simple reaction-diffusion process that embraces a pattern formation of traveling chemical waves in an “excitable” system based on the simple precipitation reaction between mercuric chloride and potassium iodide in a solid hydrogel media. The reaction involves a redissolution of the precipitate upon excess outer concentration. In the gel media, we observe three different polymorphs: orange (tetragonal), β -yellow (orthorhombic) and α -red (tetragonal). Amongst these polymorphs, the orange and yellow are the kinetically favored and appear early in the reactions, yet they are both metastable and transform readily to the most stable and thermodynamically favored red polymorph.

We first report a 2D system that incorporates superdiffusive radially propagating waves exhibiting unusual cusp-like borders. These waves result from a leading precipitation reaction (wavefront) and a trailing redissolution (waveback) between the initially separated reactants to produce the HgI_2 precipitate in a thin sheet of the solid hydrogel (agar) medium. The propagation dynamics is accompanied by the continuous polymorphic transformations between the metastable orange/yellow crystals and the stable red crystals of HgI_2 . We study the dynamics of wavefront and waveback propagation, which reveals interesting anomalous superdiffusive behavior without the involvement of external enhancement of motion. We predict that the dynamics are dependent on the outer iodide concentration in which a transition from superdiffusive to subdiffusive transport occurs. Inner mercuric concentrations apply an impact on the structure of the precipitation band where it converts from the unusual cusp-like form to the cusp-free regular form. While gel concentration affects the speed of propagation of the wave, it has no effect on its shape or on its superdiffusive dynamics. Microscopically, we show that the macroscopic wave propagation and polymorphic transformations are accompanied by an Ostwald ripening mechanism in which larger red HgI_2 crystals are formed at the expense of smaller yellow HgI_2 crystals.

Second, we explore the behavior of our system in a 3D setup, which comprises the nucleation of superdiffusive traveling chemical waves without external forcing. These waves include: single-wave circular targets, rotating spirals, and ripple-like cardioid structures, in addition to phase waves. We provide a phase diagram as function of the initial concentrations of the reactants that expresses the probability of formation of each pattern. We analyze the spatio-temporal evolution of these chemical waves. We

also find that the initial concentrations of the reactants have an important role in the pattern selection and wavelengths of propagating waves. We also investigate the breakup of the waves and show that the breakdown of ripples and spirals is a consequence of a Doppler-like instability, while the targets undergo a boundary defect-mediated breakup.

Third, we analyze the gradual growth of the HgI_2 crystals in a thin 1D tube. We confirm that the sequence of crystal transformation agrees with the Ostwald Rule of Stages. However, we find a region, of initial inner iodide concentration, where a stationary pattern of alternating metastable/stable crystals forms.

CONTENTS

ACKNOWLEDGMENTS.....	v
ABSTRACT	vi
LIST OF ILLUSTRATIONS	xi
chapter	
I. INTRODUCTION	1
A. Historical Overview	1
B. Reaction-Diffusion Systems in Nature	4
1. Living Systems.....	5
2. Nonliving Systems	8
C. Pattern Formation in Oscillatory Reactions and Excitable Systems.....	9
1. Homogeneous Oscillatory Reaction: the Belousov- Zhabotinsky (BZ) Reaction	11
2. Heterogeneous Oscillatory Reaction: Catalytic CO Oxidation on Platinum.....	14
3. Self-Organized Patterns in Solid Hydrogel Media	22
a. Pattern Formation in the Copper Hydroxide System	25
b. Pattern Formation in the Aluminum Hydroxide System..	27
D. Anomalous Transport: Superdiffusion.	28
E. Crystal Structure and the Properties of Mercuric Iodide	30
F. Preface of this Work.....	33
G. Experimental Methods.....	34

II. SUPERDIFFUSIVE CUSP-LIKE WAVES AND THEIR TRANSITION TO REGULAR REACTION BANDS.....	36
A. Experimental Setup.....	37
B. Results and Discussion	38
1. Wave Dynamics	38
2. Horizontal Speed of Cusp Formation.....	42
3. Effect of Initial Outer Iodide Concentration	44
4. Effect of Initial Inner Mercuric Concentration	48
5. Effect of Agar Gel Percentage	50
6. Macro- and Microscopic structures.....	52
 III. THREE-DIMENSIONAL SUPERDIFFUSIVE CHEMICAL WAVES	 60
A. Experimental Setup.....	61
B. Results and Discussion	62
1. Detailed Chemistry	62
2. Spatiotemporal Patterns	64
a. Effect of Concentrations.....	64
b. Superdiffusive Targets	67
c. Three-Dimensional Targets	70
d. Spirals and Ripples.....	72
e. Phase Wave	76
f. Pattern Breakup.....	77
3. Relationship between chemical waves and cusped precipitation band	80
 IV. ALTERNATING METASTABLE/STABLE PATTERN OF THE CRYSTALLINE POLYMORPHS OUTSIDE THE OSTWALD RULE OF STAGES	 84
A. Experimental Setup.....	85
B. Results and Discussion	86

V. CONCLUSION	92
A. Summary	92
B. Future Work	94
REFERENCES	96

ILLUSTRATIONS

Figure	Page
1. 1 Classical Liesegang rings.....	2
1. 2 Examples of living and nonliving reaction–diffusion systems.....	5
1. 3 Turing patterns and traveling waves in the Belousov-Zhabotinsky reaction.....	6
1. 4 Spiral wave propagation in the cardiac muscle	8
1. 5 Reconstructed and non-reconstructed surfaces of the three Pt planes.....	17
1. 6 PEEM images of rotating spirals forming in the CO oxidation reaction.....	18
1. 7 Spontaneous breakup of a spiral wave in the reduced KEE model	22
1. 8 Cu(OH) ₂ precipitate patterns	26
1. 9 Al(OH) ₃ precipitate patterns	28
1. 10 The crystal structures of the three polymorphs of HgI ₂	32
2. 1 Schematic representation of the 2D reactor.....	38
2. 2 Spatio-temporal evolution of the irregular precipitation band.....	41
2. 3 Spatio-temporal progress of the bursting wavefront.....	42
2. 4 Plot of cusp formation speed versus outer iodide concentration	43
2. 5 Log-log plots of the wavefront and waveback displacement versus time	45
2. 6 Width variation as a function of outer iodide concentration	46
2. 7 Plot of change of the slope values with change of outer	47
2. 8 Plot of waveback displacement (d_b) vs. wavefront displacement (d_f)	48
2. 9 Transition from an irregular cusped to a regular smooth structure.....	50
2. 10 Log-log plots of displacements of wavefronts versus time	52
2. 11 Features of the red and yellow polymorphs at transformation intersection.....	54

2. 12	Panel of SEM images of various regions of the precipitation band.....	56
2. 13	Plot of width vs. time of red, yellow and entire precipitation band.....	59
3. 1	Schematic representation of the 3D experimental setup.....	62
3. 2	Three different self-organized patterns forming in HgI ₂ precipitate	63
3. 3	Phase diagram as a function of the outer [I ⁻] ₀ and inner [Hg ²⁺] ₀	66
3. 4	Plots of radius (R) vs. time (t) plots of targets. Inset Log (R) vs. Log (t)	69
3. 5	Spatio-temporal evolution of the target patterns.....	69
3. 6	SEM images of 3D target.....	71
3. 7	Spatio-temporal evolution of rotating spirals	72
3. 8	Plots of wavelengths of spiral and ripple patterns versus inner [Hg ²⁺] ₀	74
3. 9	Plots of wavelengths of spiral and ripple patterns versus outer [I ⁻] ₀	74
3. 10	Plots of the radius traveled by the wavetrain of ripples.....	76
3. 11	Evolution of the phase wave in HgI ₂	77
3. 12	Time evolution of the propagating wave patterns until their breakup.....	78
3. 13	Spatio-temporal evolution in a rectangular gel slab	82
4. 1	Snapshot of four tubes with different initial inner iodide concentrations.....	88
4. 2	Evolution panel of the alternating yellow (metastable)/red (stable) pattern.....	90

CHAPTER I

INTRODUCTION

A. Historical Overview

Simply by observing life and nature around us we realize that our world is manufactured by means of two principal factors: Change and motion. These two factors define and continuously evolve the existence of everything around us, on scales as small as atomic to as large as global. New molecules are created upon the movement and collision of other simpler molecules; life developments are conserved due to migration of cells to fulfill their functions; organisms assemble to accomplish cooperative tasks, such as producing offspring or even competing against each other. “The subtle relationship between change and motion gives rise to an astounding richness of natural phenomena, and often manifests itself in the emergence of intricate spatial or temporal patterns¹.”

Chemists were the pioneers in conducting formal study of such pattern-forming systems. Chemistry as a discipline is defined as the study of matter, or in a different way, it's the study of change. Specifically molecular changes and their motion acquired highest concern. The end of the nineteenth century witnessed the building foundation of the basic laws describing the kinetics of chemical reactions therefore explaining the means in which molecules travel through different media to react with each other. At that time of history, it was foreseeable that some curious chemist will mix up these two

ingredients to produce a system, in which chemical reactions were coupled in some nontrivial way to the motions of the participating components.

In 1896, this was truly accomplished by the German chemist, Raphael Liesegang². In his seminal experiment, Liesegang observed periodic precipitation in a gel matrix, as a result of movement and reaction of particular pairs of inorganic salts (Fig. 1.1). The puzzling aspect of his discovery lied in the mechanism itself. No chemical reaction claims or even simply suggests the development of such spatially periodic patterns. The vagueness of the origin of this observation ignited immense curiosity in the minds of many scientists at the time. Yet Liesegang was definite that the occurrence of these patterns was due to the movement of the ions and molecules with respect to each other.

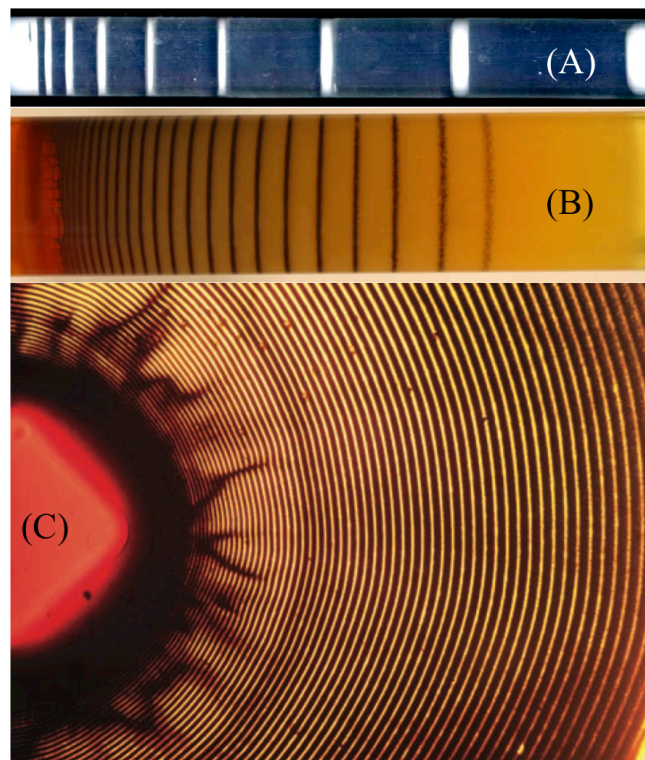


Fig. 1. 1 Classical Liesegang rings appearing in several different systems of inorganic precipitates. (A) $\text{NH}_4\text{OH} + \text{MgCl}_2$ system in PVA gel column producing $\text{Mg}(\text{OH})_2$ precipitate³. (B-C) $\text{AgNO}_3 + \text{K}_2\text{Cr}_2\text{O}_7$ system in gelatin producing $\text{Ag}_2\text{Cr}_2\text{O}_7$ precipitate^{1,4}.

However, by the early 1900s, similar reactions involving traveling chemicals in diverse arrangements producing interesting spatial patterns became very abundant. In 1910, all these reactions were collected by the French chemist, Stéphane Le Duc, in his book entitled “Théorie Physico-Chimique de la Vie et Générations Spontanées” (Physical–Chemical Theory of Life and Spontaneous Creations)⁵, in which he also speculated the importance of such patterns in biological systems. His conclusions about the similarities between the salt precipitate patterns and biological processes, such as mitosis, were certainly inaccurate nevertheless his work was somewhat farsighted. Several decades later, his analogy towards living systems became understood. This was deduced when his static patterns were accompanied by structures exhibiting spatio-temporal variation, alteration in color and propagating chemical waves.

Having the capability of recreating life-like behavior in a test tube elevated the attention towards migrating reactions and led to the unification of chemists, physicists, biologists, mathematicians and engineers to investigate new realms of reactions in motion. This gave rise to many theoretical studies in the field, which produced new branches of science, particularly, nonlinear chemical kinetics and dynamic system theory. This brought upon the development of powerful mathematical tools and computational resources which were used to model and explain a vast amount of previously puzzling phenomena, including the formation of skin patterns in certain animals, ecological behaviors and various body activities, such as impulses in the nervous system⁶. All these advances have made migration/reaction systems a scientific norm and a major element in the evolution of the world.

Yet, despite the unquestionable successes achieved by the nonlinear studies, pattern forming chemical systems have not been sufficiently integrated in our modern

technology. Migration/reaction systems have the capability of imitating nature and constructing new designs to control small-scale processes, making them perfectly suitable for applications in micro- and nanotechnology. Applying reactions in motion to their full potential will create countless possibilities not only in discovery of new phenomena, but also in the construction of micro- and nano-structures of practical significance, without the interference of humans. The motivation arises from the idea of learning from the ability of nature to design chemical systems encoded in space and time to execute desired tasks, without attempting to create ‘artificial life’. This will bring us to limit our discussion to the most common and simplest approach to reactions in motion, thus focusing on the so-called reaction–diffusion (RD) systems.

B. Reaction-Diffusion Systems in Nature

The universality of RD systems and the creativity in their usage by nature is expressed in a large number of examples, existing in both living and nonliving (Fig 1.2) creations at a wide range of length scales. Our purpose is to acquire inspiration from these examples to set a building block towards developing our own RD microsystems.

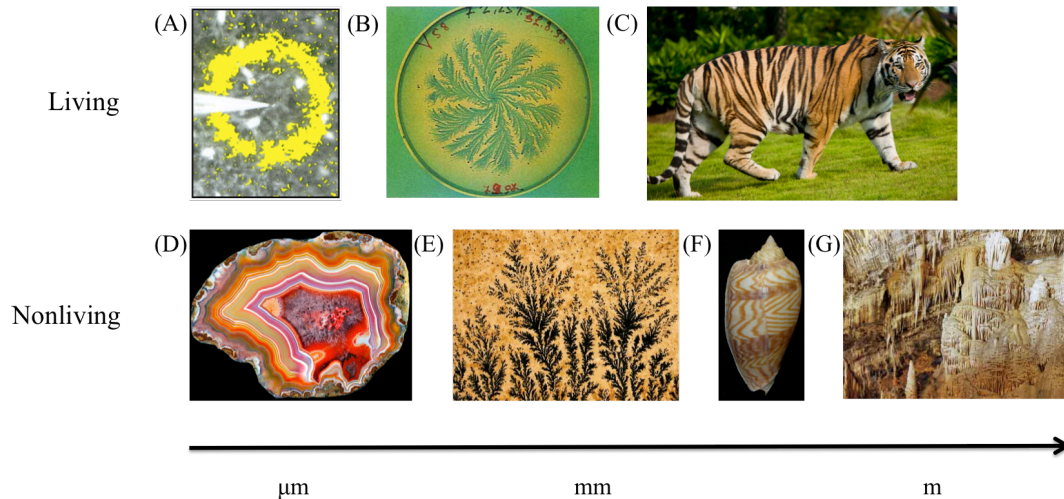


Fig. 1.2 Examples of living (A–C) and nonliving (D–G) reaction–diffusion systems on a range of length scales. (A) Calcium waves propagating in a retinal cell after mechanical stimulation⁷. (B) Vortex growth of a bacterial colony⁸. (C) Turning patterns on a tiger⁶. (D) A polished cross-section of an Argentinian agate. (Courtesy of agatelady.com). (E) Fractal structures forming on limestone⁹. (F) *Amoria undulate* seashell exhibiting triangular-like patterns formed by a reaction-diffusion process¹⁰. (G) Jeita grotto stalactites. (Courtesy of jeitagrotto.com).

1. *Living Systems*

Starting the discussion with examples existing in living organisms in nature we convey the vital role played by RD systems in their functionality. It is interesting to vision how any organism can carry out a biological or chemical reaction without the involvement of migrating components. Such evidence linking RD systems to living bodies were not recognized so long ago. The work of Alan Turing¹¹ in the 1940s and Boris Belousov¹² in the 1950s initiated the studies in this field and revolutionized the notion of nonlinear chemical dynamics that is much better understood nowadays. Turing predicted that certain diffusing reactive activator/inhibitor species are able to spontaneously break the symmetry of an initially uniform mixture of both and result with stationary concentration patterns¹¹. The experimental evidence of Turing’s predication took a long time to appear, when in 1990, De Kepper¹³ presented the

Chlorite-iodide-malonic acid (CIMA) reaction in an open system with considerably different diffusion coefficients of the activator and inhibitor species (Fig. 1.3A). On the other hand, Belousov unveiled a new class of systems giving rise to spatiotemporal oscillatory reactions resulting from nonlinear coupling between reaction and diffusion. Such reactions exhibited propagating chemical waves (Fig 1.3B).

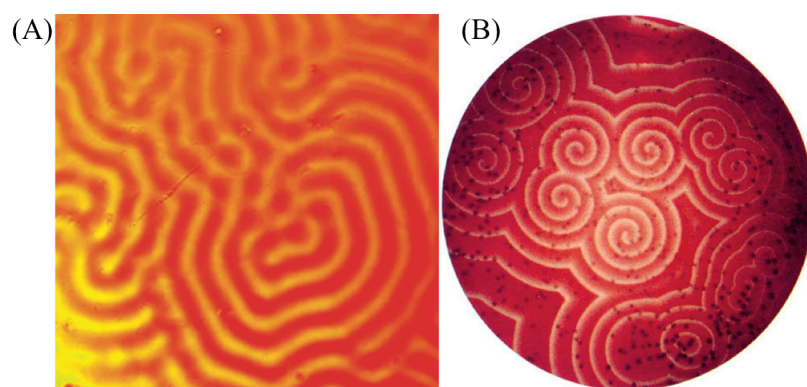


Fig. 1. 3 (A) Turing patterns appearing in a CIMA reaction¹⁴. (B) Traveling waves of spiral patterns forming in the Belousov-Zhabotinsky reaction¹⁵.

It is important to understand how crucial the findings of Turing and Belousov are concerning direct impact on living organisms. They comprise the necessary ingredients, such as nonlinear coupling and feedback loops, that when combined together in the proper sequence can deliver various regulatory processes in cells, tissues and organisms. For example Turing-like instabilities can motivate organism development by distinguishing initially stable chemical mixtures into areas of specific structure or function. In addition, oscillatory chemical reactions can acquire the role of biological clocks that synchronize particular events in the body, and chemical signals could be delivered by the means of chemical waves, such as nerve impulses. These

elements are combined in many biological examples operating at a range of length scales; some of these examples are illustrated in the upcoming sections.

Calcium signals traveling within cells by means of oscillatory reactions or chemical waves, play a crucial part in regulating a numerous variety of intercellular and intracellular activities. These oscillations occurring as a function of time are the outcome of a complex RD mechanism^{7,16-18}. Several aspects of energetics and metabolism depend on RD mechanisms. The most important example lies in the process of glycolysis, which is coordinated by glucose-induced oscillations that induce NADH and proton waves to break down sugars and produce high-energy ATP molecules¹⁹. Also, communication between sites that produce ATP (mitochondria) and sites consuming ATP (cell nuclei) is enhanced via RD, which is important for regular cell functioning. Complex RD mechanisms have been naturally developed to deliver needed ATP to ATP-deficient regions using spatially distributed enzymes, collectively known as a 'phosphoryl wires'. The ATP propagates from one enzyme to the next in a flux-wave manner, which makes it reach the desired site in more rapid time than a purely diffusive transport^{20,21}. RD processes are not limited to operating on single cells; cases prevail confirming their effect on groups of cells that make up entire organs. The most important example to this case, having severe consequences on health, is the electrical excitation in the cardiac tissues, which propagates a spiral (Fig. 1.4)²², and may lead to life-threatening cardiac arrhythmias such as ventricular tachycardia and fibrillation^{23,24}. RD processes have also expressed significance in several other operations in organisms: they mediate direct involvement in the growth and development of limbs²⁵; they manage defense mechanisms constructed by organism populations^{26,27}, a strategy employed by bacteria colonies, grown in inadequate nutrients, by forming stationary

nonequilibrium patterns²⁷; and they give rise to spectacular skin patterns, forming through a Turing-like mechanism, in animals like zebras, giraffes and tigers^{6,28}.

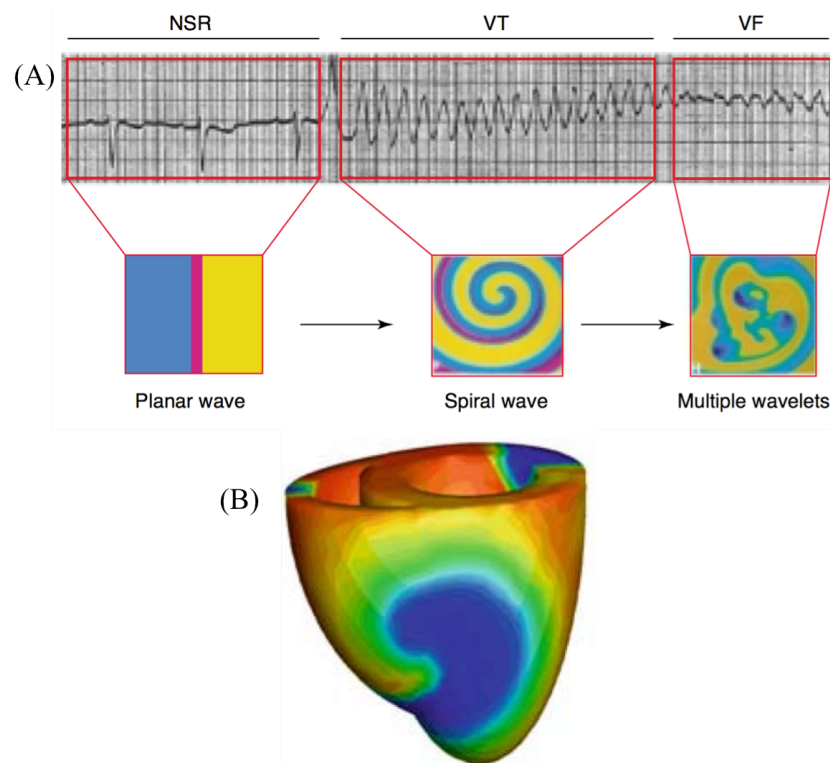


Fig. 1.4 (A) Proposed evolution of the spiral wave propagation in the cardiac muscle displaying the transition from a normal cardiac rhythm to ventricular fibrillation. Transition from normal sinus rhythm (NSR) to ventricular tachycardia (VT) and ventricular fibrillation (VF), as recorded on the surface electrocardiogram. Initial state shows a planar wave that transitions to a single spiral wave which later breaks up into multiple spiral waves²⁹. (B) Simulation of a spiral wave pattern appearing on a cardiac muscle³⁰.

2. *Non-living Systems*

Nonliving creations, unlike living systems, do not employ complex RD processes for regulating and signaling mechanisms. They simply apply RD by the means of inorganic chemicals to build spatially extended structures. Such inorganic salts react in nature to produce many different kinds of precipitates that compose the vital components of alternating layers that characterize the oscillatory zoning textures of

many natural minerals, which include plagioclase, garnet, augite or zebra spa rock³¹⁻³³. A captivating example involving a two-mineral deposition is the alternating pattern formed by defect-poor quartz and defect-rich chalcedony observed in iris agates³⁴. The patterns and bandings formed in these minerals reveal a remarkable similarity to the formation of Liesegang rings, which suggests that their creation is also governed by similar mechanisms. Another famous example of nonliving shapes owing their formation to RD processes, are cave stalactites. They involve: hydrodynamic flow of a thin layer of water carrying Ca^{2+} and H^+ , along the length of the stalactite; CaCO_3 reactions; and CO_2 diffusion³⁵. The alternating thickness of the fluid layer along the shape of the stalactites controls the processes of CO_2 diffusion and CaCO_3 precipitation. Limestone surfaces have also expressed interesting fractal structures driven by RD⁹. They are characterized in terms of simple redox RD equations, because they are comprised of residues of hydrous iron or manganese oxides that crystallize upon exposure to air when supersaturated iron or manganese diffuse through the limestone³⁶. Lastly, RD processes have also served to understand the pigmentation and front formation appearing on complex seashell structures¹⁰.

C. Pattern Formation in Oscillatory Reactions and Excitable Systems

Oscillatory and excitable media are the two main ‘ingredients’ found in many of the examples we stated earlier. This area of RD processes has received its fame and tremendous amount of attention from scientists owing to the aspect of formation of self-organized patterns. Researchers in chemistry^{1,37-40}, physics^{41,42} and biology^{7,25,43,44} have

indulged in many investigations in this field and discovered various significant results of high relevance to their domains.

A further definition of the two ‘ingredients’: oscillatory chemical reactions undergo the fluctuations in concentration of intermediate and catalyst species with time. This behavior is a result of the decrease in the Gibbs free energy of the overall reaction happening far from thermodynamic equilibrium. As the species interact, they are coupled with diffusion thus leading to spatial inhomogeneities in the form of traveling waves of chemical activity in which their concentrations are far above or below those in the bulk mixture⁴⁵. On the other hand, excitable media are extended systems functioning far from equilibrium exhibiting uniform rest states that are regularly stable yet vulnerable to the slightest perturbations. When perturbed with an inadequate stimulus the system will return back to its initial state and maintain its uniformity, but when the perturbation is large enough the system fires a signal triggering wave propagation. Depending on the type of perturbation implemented, a variety of wave patterns can be generated, such as solitary waves, target-like patterns, and spiral waves⁴⁶.

The concept of macroscopic chemical waves and patterns was only familiar to scientists a little more than a 100 years ago. The first time the development of waves and patterns from chemical reactions coupled with diffusion was presented at the main meeting of the Deutsche Bunsengesellschaft für Angewandte Physikalische Chemie, held in Dresden, Germany in May 1906. Robert Luther, Director of the Physical Chemistry Laboratory in Leipzig presented his work on RD fronts in autocatalytic chemical reactions⁴⁷. He proposed an equation describing the velocity of these novel waves, $V = a(KDC)^{1/2}$, where a is a numerical factor, K is the reaction rate constant, D is the diffusion coefficient and C is the concentration. He also claimed that they might

have common characteristics with propagating action potentials in nerve cell axons. The great physical chemist Walther Nernst, present at the meeting, questioned his work and speculations. He required a derivation to Luther's wave velocity equation and believed that nerve impulses are way too fast compared to chemical waves. Luther did respond to the criticism by explaining the origin of his equation and by demonstrating examples of autocatalytic chemical reactions that exhibit propagating waves. From then onwards this branch of nonlinear dynamics grew exponentially and now we do know that RD waves and nerve impulses actually have a fundamental similarity, which underlies in their mathematical description. The theoretical work of Fisher⁴⁸ and Kolmogorov *et al.*⁴⁹ around 30 years later, was further influenced by Luther's ideas and simplified many phenomena of propagating fronts.

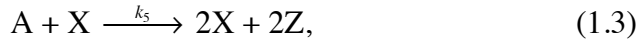
The paper entitled "The Chemical Basis of Morphogenesis" published in 1952 by Alan Turing¹¹ the famous British mathematician is considered the beginning of modern research on pattern formation. This paper today stands as one of the most important contributions of its century and has improved a great number of studies on self-organizing patterns in systems far from equilibrium. It ignited strong research in the fields of physical and chemical systems to discover new spatiotemporal activity; in addition, it constructed the basis of modern theories of biological patterns.

1. Homogeneous Oscillatory Reaction: the Belousov-Zhabotinsky (BZ) Reaction

The first homogeneous oscillatory chemical reaction was reported by Bray in 1921 when he performed the iodate-catalyzed decomposition of hydrogen peroxide⁵⁰. Back in the time, oscillatory reactions received lots of skepticism because they were

believed to disobey the second law of thermodynamics. 30 years later, one year before Turing's paper, a Soviet Union chemist named Boris P. Belousov discovered another oscillating chemical reaction in a liquid phase. The oscillations occurred in the [Ce(IV)/Ce(III)] ratio during the cerium-ion-catalyzed oxidation of citric acid by bromate ion. Belousov could not publish his discovery, since he received a lot of criticism from fellow scientists, until 1958. Another chemist from the Soviet Union, Anatoly M. Zhabotinsky developed the reaction further by substituting the citric acid substrate with malonic acid and substituting the oxidation–reduction indicator ferroin for the cerium catalyst⁵¹. The product was a strong oscillatory reaction with remarkable color alterations that is now known as the Belousov- Zhabotinsky (BZ) reaction. Nowadays, it is considered the ancestor of many pattern-forming systems in nonlinear dynamics. The unstirred BZ reaction mixture was found to display spectacular spatiotemporal wave behavior. In the early works of Zhabotinsky^{12,52} and Winfree^{53,54}, they characterized the properties of the propagating waves in the quasi-two-dimensional (2D) layers of the solution. Later on, in 1971, self-sustaining wave sources rotating about a phase singularity were observed in the BZ reaction and were labeled as spiral waves, owing to the patterns they formed⁵⁵. In the 1980s, as digital imaging technology advanced, accurate measurements and characterization were performed on these spiral waves, thus bring forward insightful information about the unknown patterns of that time^{56,57}.

In 1972, Field, Körös, and Noyes developed a mechanism on which the modeling of the BZ reaction depended on, this model was called the FKN mechanism⁵⁸. The crucial factors of this mechanism were captured in a three-variable model called the Oregonator⁵⁹, which is comprised of 5 chemical steps:



where the variable $X = [\text{HBrO}_2]$, $Y = [\text{Br}^-]$ and $Z = [\text{Ce}^{4+}]$ (the oxidized catalyst). The constants $A = [\text{BrO}_3^-]$, $B = [\text{malonic acid}]$ and $P = [\text{HOBr}]$ represent the reactant and product species. X regenerates rapidly by an autocatalytic reaction in step (1.3) after a critical consumption of Y in steps (1.1) and (1.2). However, Y inhibits X , representing delayed negative feedback. The oxidized catalyst Z is produced by the oxidation of the metal ion catalyst in the autocatalytic process (1.3). In step (1.5) Z regenerates Y and resets the oscillatory process. The Oregonator gives a rough model, due to the deficiency of details about the reaction. Therefore, the interpretation of the parameter f depends on the authors, since in some models it has a constant value⁶⁰ and in other recent studies it has been claimed that it is proportional to the concentration of the organic species, mainly bromomalonic acid $(\text{BrCH}(\text{COOH})_2)$ ⁶¹. The effect of the bromomalonic acid is not included in the Oregonator model.

The rate equations of the Oregonator model are the following:

$$\frac{dX}{dt} = k_3AY - k_2XY + k_5AX - 2k_4X^2 \quad (1.6)$$

$$\frac{dY}{dt} = -k_3AY - k_2XY + \frac{1}{2}k_0fBZ \quad (1.7)$$

$$\frac{dZ}{dt} = 2k_5AX - k_0BZ \quad (1.8)$$

The system does not include the diffusion terms. This is because a well-mixed system case is considered, which leads to the minimization of concentration gradients, therefore no diffusive transport exists. Concentrations of the species (B) and of the bromate (A) are set to be constant.

2. Heterogeneous Oscillatory Reaction: Catalytic CO Oxidation on Platinum

Some chemical reactions in the gas phase also have great potential yet cannot happen. Nevertheless, these reactions become possible when aided by adsorption on a catalytic metal surface. Such chemical reactions are widely under investigation and used in chemical industry and in environmental technology. Industrially, the catalysts usually include porous materials and micro-particles. Experimentally, perfect surfaces of single crystals of metals are commonly favored. These experiments, using surface chemical adsorption, are typically conducted under very low pressures of gaseous reactants, which prevents strong thermal effects and the development of hydro-dynamical flows³⁹.

These conditions secure an atmosphere very suitable for development of nonequilibrium reaction-induced wave patterns in a surface chemical reaction. A reaction chamber containing the catalytic metal surface is continuously supplied with gaseous reactants. Therefore, under ultra-low pressures the mixing of reactants in the chamber is practically instantaneous. Only a monolayer of molecules adsorb onto the metallic catalyst surface, which is where the reaction itself takes place. As the molecules diffuse towards each other on the surface, they collide and react thus forming the products that go back into the gas phase. The delivery of the gases into the chamber sustains a well-controlled supply of reactants, and the products along with excess reactants are steadily pumped away.

The formation of nonequilibrium patterns in a 2D RD system, formed by adsorbed reactants on the catalytic surface, is a characteristic behavior of bistable, excitable or oscillatory media. Such patterns have characteristic length scales of micrometers and time scales of seconds. Special methods of optical and electron microscopy is used to observe and analyze them⁶². A common technique is the photoemission electron microscopy (PEEM), which is based on the effect of photoelectron emission from the metal surface under ultraviolet (UV) light irradiation. Real-time imaging can be processed, using this method, of the lateral distribution of the adsorbed species with spatial resolution of about 1 μm .

Several different surface reactions forming nonequilibrium pattern formation have been reported⁶³. The CO oxidation on single platinum (Pt) crystals is the most extensively investigated surface chemical reaction. In this reaction, CO₂ is produced, and goes back to the gas phase, by the reaction between CO and O₂ that are both adsorbed on the catalytic metal surface. This process has high practical significance owing to its application in catalytic convertors installed in car exhaust pipes to reduce environmental pollution by CO. The net reaction $2\text{CO} + \text{O}_2 \rightarrow 2\text{CO}_2$ follows the Langmuir–Hinshelwood scheme:



where, * denotes a free adsorption site on the catalytic surface. In reaction (1.10), oxygen undergoes dissociative adsorption. The O atoms adsorbed, are bound much more strongly to the surface than the CO molecules. Therefore, the CO can desorb and

diffuse on the surface more freely. At usual experimental temperatures (below 600 K), such processes are negligible for adsorbed O atoms. Since the reaction is performed at temperatures above 300 K, the CO₂ produced desorbs immediately into the gas phase, leaving behind it a free space for new adsorbates.

The properties of the CO oxidation occurring on surfaces of single Pt crystals, significantly depends on which crystallographic plane is used to carry out the reaction. Reactions on the Pt(111) surface, exhibit only bistable behavior. This happens between the reactive state mainly dominated by O₂ and the nonreactive state, which is dominated by CO. This bistability is a consequence of asymmetric inhibition of adsorption. Which means that, O₂ covered platinum surfaces is able to adsorb CO molecules, while, CO covered surfaces inhibit O adsorption, thus ‘poisoning’ the reaction. Bär *et al.* developed a two-variable kinetic model, describing bistability and front propagation in the CO oxidation on Pt(111)⁶⁴.

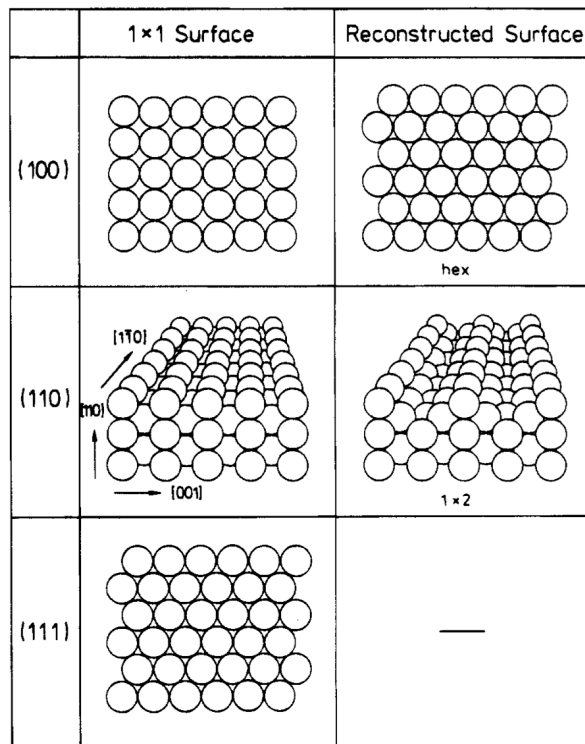


Fig. 1. 5 Reconstructed and non-reconstructed surfaces of the three Pt planes⁶³.

Much richer dynamics were observed when the CO oxidation was carried out on the Pt(110) crystallographic plane. It displayed significant oscillatory and excitable kinetics upon specific initial reactant temperatures and partial pressures. The oscillatory behavior of the system brings upon structural changes of the metal surface, which results in complex dynamics⁶³. The Pt atoms available in the open Pt(110) are constantly undergoing a spontaneous geometrical rearrangement through a process known as surface reconstruction. This rearrangement occurs between the 1×1 arrangement, which corresponds to Pt atoms in the top layer of the metal as in the bulk, and the 1×2 “missing row” geometry (Fig. 1.5). As the CO molecules continue adsorbing on the reconstructed Pt(110) surface, a critical coverage is reached when the surface reconstruction is removed and the surface returns to its 1×1 geometry that

corresponds to the bulk of the metal. Such reactions displaying surface structural alterations have much slower reaction rates thus resulting in additional inertial feedback leading to the possibility of oscillations and excitability. Figure 1.6 displays the temporal evolution of some spiral patterns forming on the Pt(110) plane.

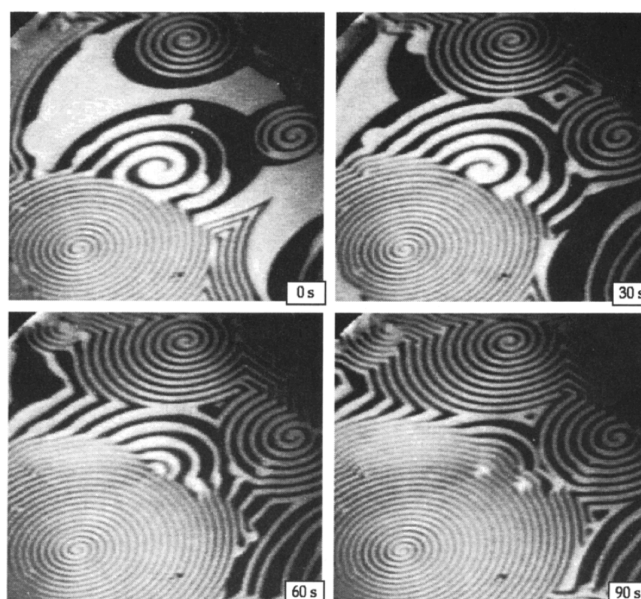


Fig. 1. 6 PEEM images of rotating spirals forming in the CO oxidation reaction on the Pt(110) plane⁶⁵.

The Pt(100) plane also undergoes a similar adsorbate-induced structural phase transition. The reconstructed state of this surface is referred to as the “hex” geometry (Fig. 1.5). Kinetic oscillations are also an important characteristic of the CO oxidation happening on this surface⁶³.

PEEM was used to observe the first experimental pattern formation occurring in the CO oxidation reaction on Pt(110). It has unveiled a big variety of self-organized patterns, such as rotating spiral waves, target patterns, standing waves and irregular wave regimes^{66,67}. Spiral waves appearing in the excitable regime were confirmed to nucleate and pin to surface defects and were characterized by a distribution of rotation

periods⁶⁵. However, drifting free spirals were also observed over the surface resulting from intrinsic meandering or variations of reaction parameters.

The mathematical model formulated by Ziff *et al.*⁶⁸ brought forward the proposal of the general Langmuir–Hinshelwood mechanism. However, this model does not take into consideration the aspects of dissociative adsorption of oxygen on platinum and the asymmetry of inhibition, which are fundamental properties of the bistable reaction. The initial theoretical model that considered surface reconstruction of the Pt(100) was proposed by Imbihl *et al.*⁶⁹. It described the alteration of the adsorbate coverages on the “hex” and 1×1 phases of Pt(100) and the phase transition between the two substrate phases by the means of four coupled ordinary differential equations (ODEs).

The leading model describing the CO oxidation reaction on the Pt(110) surface was the Krischer–Eiswirth–Ertl (KEE) model, which well explained the oscillations and excitable behavior of the system⁷⁰. This model is formulated in terms of three variables, u , v and w . First, u , is the local CO coverage, i.e., the fraction of CO adsorption sites on the metal surface that are occupied by adsorbed CO molecules. Second variable, v , is the local oxygen coverage. Third variable, w specifies the local fraction of the surface area occupied by the non-reconstructed 1×1 structural phase. The rate equations of the KEE model are:

$$\frac{\partial u}{\partial t} = k_1 s_{CO} p_{CO} (1 - u^3) - k_2 u - k_3 uv + D \nabla^2 u \quad (1.12)$$

$$\frac{\partial v}{\partial t} = k_4 p_{O_2} [s_{o,1 \times 1} w + s_{o,1 \times 2} (1 - w)] (1 - u - v)^2 - k_3 uv \quad (1.13)$$

$$\frac{\partial w}{\partial t} = k_5 \left(\frac{1}{1 + \exp((u_0 - u) / \delta u)} - w \right) \quad (1.14)$$

The first term in Eq. (1.12) defines the CO adsorption process. The rate constant of adsorption is k_1 , s_{co} represents the sticking coefficient for CO molecules, and p_{co} represents the partial pressure of the CO gas. The fraction of free CO sites is not only proportional to $1 - u$, instead, it includes a $1 - u^3$ factor, which is done to take into consideration that a weakly attached CO precursor was available at the Pt surface before the actual formation of the physical adsorbed state of a CO molecule. The second term simply defines the CO desorption process while the third term defines the reaction between adsorbed CO and O_2 molecules. The last term defines the diffusion of the adsorbed CO on the Pt surface.

The kinetics of the adsorbed O_2 molecules is expanded in Eq. (1.13). The first term defines the rate of adsorption, which is dependent on the partial pressure of oxygen molecules, p_{O_2} . The rate is defined to be proportional to the square of the fraction of oxygen adsorption sites available, which is represented by $(1 - u - v)^2$. Because O_2 undergoes dissociative adsorption, each O_2 molecule requires two free adsorption sites on the surface for each of its atoms. In addition, the fact that excess CO on the surface inhibits adsorption of O_2 is also taken into consideration in this case. This implies that new O_2 molecules can only adsorb to sites that are both CO- and O-free. The last term defines the chemical reaction on the surface. The usual experimental conditions include temperatures low enough that makes oxygen firmly bound to the surface, which leads to neglecting its desorption and surface diffusion from the equation. The sticking coefficient of oxygen is dependent on the state of the Pt surface. It has different values in each of the non-reconstructed 1×1 , $s_{\text{O}, 1 \times 1}$ and the reconstructed 1×2 , $s_{\text{O}, 1 \times 2}$.

Eq. (1.14) is phenomenological explanation of the kinetics of the phase transition. The completely CO covered surface corresponds to the non-reconstructed 1×1 phase, while the reconstructed 1×2 phase corresponds to the CO-free surface. At intermediate coverages of CO, the surface acquires microscopic properties of both structural phases. In this equation it is assumed that at constant CO coverage, the local fraction (w) of the surface area in the non-reconstructed phase approaches, $w(u) = [1 + \exp((u_0 - u)/\delta u)]^{-1}$. The rate constant k_5 corresponds to the process at which the variable w approaches the equilibrium value $w(u)$.

The surface reconstruction process is slow. CO adsorption initiates on the reconstructed surface, where w is approximately zero, next the reconstruction is gradually lifted leading to the increase in the value of w . Since on the non-reconstructed surface the sticking coefficient of CO is smaller and in addition to its consumption in the reaction, its coverage decreases. This results in reversing the structural phase transition. The cycle repeats itself, with a period judged by the rate constant k_5 , giving rise to interesting oscillatory kinetics.

Spontaneous development of turbulence has been observed in these reactions, when taking into consideration diffusion of CO molecules, which is a result of the destabilization of the state with uniform oscillations with respect to phase modulations (the Benjamin–Feir instability). Numerical analysis of the coefficients of the complex Ginzburg–Landau equation for the KEE model, gives direct solutions for the instabilities⁷¹.

Figure 1.7 contains a sequence of images displaying the evolution of transformation of a uniformly oxygen covered surface state to the spontaneous development of chemical turbulence, in the reduced KEE model. The formation of irregular wave fronts and several fragments of rotating spiral waves characterize such turbulence. The recurrent breakup of the spiral waves, results in formation of new spiral wave fragments at different positions. At suitable choice of partial pressure of gases in the chamber, such spatiotemporal chaos is present in a broad range of temperatures⁷².

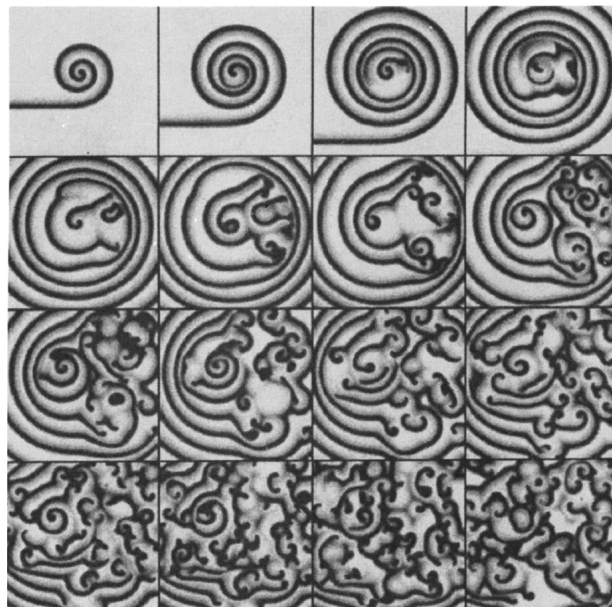


Fig. 1. 7 Images representing spontaneous breakup of a spiral wave in the reduced KEE model of the CO oxidation reaction⁷³.

3. Self-Organized Patterns in Solid Hydrogel Media

The two previous examples described coupling between reaction and diffusion to produce self-organized patterns in fluid media (solution or gas). Even if the patterns form spontaneously in such media, they are easily destroyed and completely disappear

upon mixing of the system. Therefore, scientists needed a stronger more robust, yet permeable material to support a permanent formation of the RD patterns. The solution to this issue was found in the rigid matrices of solid gels.

Gel forms as a material of a porous network of particles, such as monomers, oligomers or polymers, which occupy the whole volume of a liquid medium. This network forms in response to a variety of effects, which include temperature decrease (cooling), chemical reaction initiation, or sometimes sound waves⁷⁴, depending on each system⁷⁵. The classification of the gel comes according to the type of solvent it contains and type of intermolecular interactions supporting its structure. Gels absorbing aqueous solutions are termed hydrogels, while gels absorbing organic solutions are termed organogels. Noncovalent, intermolecular interactions between the gel-forming molecules form physical gels such as agarose, gelatin or syndiotactic poly(methyl methacrylate). On the other hand, covalent crosslinking of the component monomers/polymers construct chemical gels such as poly[acrylamide-co-(ethylene glycol dimethacrylate)]. The initiation of gelation of both physical and chemical gels results in a significant increase in viscosity of the solution followed by solidification.

One of the most important reasons gels are very widely employed in separation experiments is because of their porous networks that suppress convective and/or turbulent flows while allowing transport by diffusion. This ease of mass transport gives gels their ideal reputation for use in RD processes and ensures that structures and patterns that form do not easily wash away by accidental mixing of the underlying fluid. In addition, gels can supply significant supports for several types of chemical reactions such as crystal formation. Crystallization in gel is a diffusion-dominated process, and the absence of hydrodynamic flows and diminished diffusion coefficients, due to

obstacles in the gel network, decreases the flux of the molecules at the growing crystal faces⁷⁶. Accordingly, the crystal growth process is slower and more balanced, and no sedimentation of large crystals is experienced in the growing medium. Growth of inorganic substances in gel-supported media can result with high quality crystals of dimensions in the centimeter scale⁷⁷.

The gel we are concentrating on in this work is agar hydrogel. It has strong mechanical and chemical properties and relatively high degree of elasticity. Chemically, agar is an unbranched, uncharged polysaccharide (i.e., sugar) consisting of (1 → 3)-β-D-galactose and (1 → 4)-3,6-anhydro-α-L-galactose alternating repeat units and acquired from cell membranes of some species of red algae or seaweed. Depending on the specific origin of the agar, its degree of methoxylation and its bulk concentration, it is required to heat to 70 – 95 °C to disperse the gel particles and gels between 25 and 42 °C. The gelation process is reversible, and it encompasses conversion from an alternating, disordered coil conformation in solution to a solid, ordered structure with connection regions joined by hydrogen bonds.

Once it has gelled, agar can relatively withstand many types of organic and inorganic substances. It can splendidly contain inorganic pH buffers and solutions of proteins and/or DNA. They function really well in gel electrophoresis or gel filtration chromatography. Their structures are stable for days or weeks even when saturated with aqueous solutions of inorganic salts (AgNO₃, CuSO₄, K₂CO₃...). The gel structure is bound to degrade faster upon acidic substances, and that is due to proton-mediated disruption of hydrogen bonds between polysaccharide chains. Nevertheless, it can withstand high concentrations of acids or bases (2 M) for several hours or even for weeks if the concentration is diluted.

a. Pattern Formation in the Copper Hydroxide System

Péter Hantz^{78,79} performed a simple precipitation reaction between two inorganic substances, copper chloride (CuCl_2) and sodium hydroxide (NaOH). His experiments were carried out in two types of gel media, the first was poly(vinyl)alcohol (PVA) and the second was agar hydrogel. These gels were chosen since they are neutral and easy to handle, while having a network that does not disturb the precipitation reactions. The gels were dissolved in a CuCl_2 solution to prepare the inner electrolyte of the system, and NaOH solution was used as the outer electrolyte and co-precipitate. Hantz observed many different interesting patterns forming in various experimental setups.

He first reports the pattern formation in thin gel sheets. As the outer electrolyte, NaOH , diffuses into the gel containing the inner electrolyte, CuCl_2 , a one-dimensional diffusion front is produced. Before this front, there exists a region where both reactants are present. This region is called the excitable region, since it is the location where precipitation and pattern formation can occur. In this excitable region there appears a reaction front, which encompasses the primary $\text{Cu}(\text{OH})_2$ precipitate. As diffusion proceeds, a broader precipitation band is formed. The formation of this precipitation band is disturbed by defect points encountered in the gel media. As the distorted front progresses, these points develop into wedge-like, precipitate-free areas. Therefore the precipitation front gets divided into different regions. The progression of diffusion gives rise to diagonal borders at which the reaction halts thus separating the previously formed precipitate from the wedge-like void areas. These static surfaces are called passive borders. The surfaces that are still in motion and forming new precipitate are referred to as regressing edges. The lengths of these edges decrease as diffusion

progress, thus the trapezoidal shape they are forming with the diagonal passive edges disappears to form a triangular-like shape with a cusp at its tip. Hantz referred to these shapes as Meinhardt peaks, owing to their similarity to pattern formations on some seashells described in Meinhardt's book: *The algorithmic beauty of seashells*¹⁰. Figure 1.8 represents the patterns observed by Hantz in thin gel sheets.

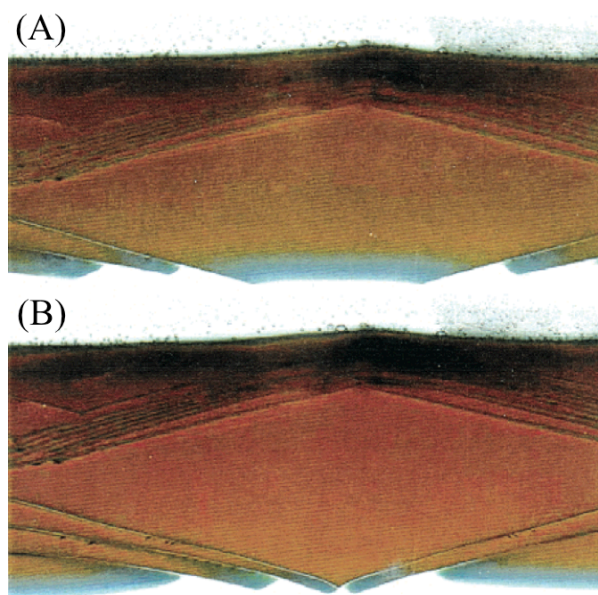


Fig. 1. 8 Consecutive images of the $\text{Cu}(\text{OH})_2$ precipitate pattern forming in thin gel sheets when reacting CuCl_2 and NaOH ⁸.

A second type of experiments performed by Hantz was in Petri dishes. He allowed the gel to settle and gelate in a wide-diameter Petri dish. Minutes after he poured the outer electrolyte into the surface of the gel, he observed fascinating pattern formation of cardioid-like, spiral and target structures. These patterns were directly related to the produced 2D patterns and showed significant correspondence with each other.

b. Pattern Formation in the Aluminum Hydroxide System

Volford et al.⁸⁰ investigated another system exhibiting self-organized spatiotemporal patterns forming in gel media. This system involves a simple RD process based on the precipitation and complex formation reaction of aluminum hydroxide ($\text{Al}(\text{OH})_3$) from its co-precipitates, aluminum chloride (AlCl_3) serving as the inner electrolyte and sodium hydroxide (NaOH) serving as the outer electrolyte. The excess of outer ions, results in the redissolution of the precipitate thus forming the complex $[\text{Al}(\text{OH})_4]^-$. The outer electrolyte diffuses perpendicularly with respect to the gel surface where the precipitation patterns emerge coexisting with traveling waves. Upon initialization of the reaction, a unique kind of self-organization initiates in formation of traveling waves and double-spiral formation resulting in cardioid patterns inside the precipitation layer, without any external perturbation. The “excitability” of the system can be altered by the means of initial inner concentration ($[\text{AlCl}_3]_0$). As excitability decreased (i.e. lower inner concentration) the double-spirals turned into single circular traveling waves. Such self-organization existed in a small range of $[\text{Al}^{3+}]_0 = (0.28\text{--}0.34 \text{ M})$ at a fixed concentration of the outer electrolyte, $[\text{NaOH}]_0 = 2.50 \text{ M}$.

They also performed experiments in the thin (1 mm) gel sheets to study the dynamics of wave propagation. This showed the behavior of the wave perpendicular to the surface of the gel where the pattern formation occurs. The precipitation layer propagating down the gel showed interesting features. Its leading front exhibited waves that annihilated each other as similarly described by the study on seashell patterns¹⁰. Figure 1.9 shows the $\text{Al}(\text{OH})_3$ precipitation patterns appearing in gel media.

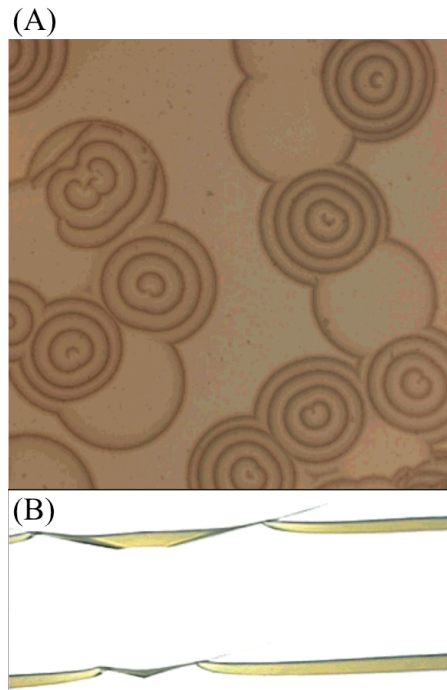


Fig. 1. 9 Al(OH)₃ precipitate pattern forming in thin gel sheets when reacting AlCl₃ and NaOH⁸⁰.

D. Anomalous Transport: Superdiffusion.

It is very significant how much front and wave propagation phenomena are encountered in physical⁴¹, chemical^{1,38} and biological systems^{42,81,82}. The difference in each system brings upon a different nature of the fronts and waves (e.g., electromagnetic, elastic, excitable waves or diffusion fronts). However, a common feature is that they travel with finite velocity i.e. the wave front displacement is linearly proportional to time ($r \sim t$), or in other cases, like diffusion, fronts progress with a decreasing velocity with time, therefore the front displacement is always linearly proportional to the square root of time ($r \sim t^{0.5}$). This brings upon two main ways to characterize mass transport in front and wave propagation in space; the first case

includes advective motion (finite velocity) and the second case includes Brownian or eddy motion (diffusive).

In a typical diffusion process the mean square displacement of particles (*MSD*) is a linear function of time ($MSD \sim t^{2\alpha}$), where exponent α is equal to 0.5, i.e. $2\alpha = 1$. However, anomalous transport has been encountered in some other types of systems. Anomalous diffusion⁸³ is defined as a transport process with a nonlinear relationship with time. The transport is labeled superdiffusive when the exponent α is greater than 0.5. Superdiffusion can be observed when tracer trajectories become discontinuous as a result of extremely long jumps (Lévy flights), which leads to mixing between distant regions of the medium⁸⁴⁻⁸⁶. On the other hand, the transport is labeled subdiffusive when the exponent α is lower than 0.5. Subdiffusion is found in heterogeneous media that exhibit disordered or porous surfaces that are able to trap traveling particles. Gels⁸⁴ and metal-organic frameworks (MOFs)⁸⁷ serve as the best examples of such material.

In chemical systems, the dynamics of fronts and waves are governed by two main factors: the interplay between mixing in the system (transport phenomena) and the interaction between the different species (e.g., chemical reactions). Normally, the mixing is purely a result of molecular diffusion due to the underlying Brownian motion. Classical reaction-diffusion equations (RDE) are effectively employed in both homogeneous and heterogeneous media to describe the evolution of waves and fronts⁶. Specifically, RDE are capable of explaining chemical wave propagation in the Belousov-Zhabotinsky (BZ) reaction and similar reactions. Interestingly in the BZ reaction, the typical diffusion of species and nonlinear chemical interactions between them result with finite velocities of their propagating waves^{86,88,89}. In addition, precipitation fronts in Liesegang systems⁹⁰ exhibit normal diffusive dynamics. Yet,

even though underlying Brownian motion is constantly available as a microscopic mechanism for transport, numerous exceptions have been encountered in complex systems to exhibit anomalous transport. In these systems, anomalous sub- and superdiffusion mechanisms are the driving force governing the physics of transport. Several examples are encountered in turbulent fluids⁹¹, chaotic dynamics⁹² and disordered media⁹³.

In chemistry, new experiments have reported the existence of superdiffusive chemical waves only when they are exposed to external interference that enhanced diffusion. Such enhancements include chaotic flow created by Faraday waves^{85,86}, azimuthal motion of counter-rotating vortices⁹² and simple stirring-induced hydrodynamic turbulence⁹⁴.

E. Crystal Structure and the Properties of Mercuric Iodide

In this work the material we are focusing on is mercury (II) iodide (HgI_2). Among the mercury (II) halides, HgI_2 forms the greatest number of captivating solid phases that adopt a remarkable variety of crystal structures. Owing to this fact, extensive studies have been conducted on this compound using numerous techniques in vision of its opto-electronic properties and technological importance⁹⁵. Hundreds of articles have been published on this material and have been compiled and reviewed in the work of M. Piechotka⁹⁶. HgI_2 is known to crystallize into three different polymorphs that are red, orange and yellow color⁹⁷. These three polymorphs have also shown interesting transformations in gel media⁹⁸⁻¹⁰⁰.

The red polymorph comprises layers of corner-shared HgI_4 tetrahedra, with the I-atoms forming a cubic close packing (ccp) of spheres having the Hg-atoms occupying the tetrahedral voids, where all I–Hg–I and Hg–I–Hg angles are tetrahedral¹⁰¹. The orange polymorph is slightly different from the red in that its Hg-atoms distribution in the ccp arrangement of I-atoms is different. It exhibits corner-shared Hg_4I_{10} supertetrahedra as building blocks that construct its three distinctive tetragonal crystal structures^{102,103}. On the other hand, the yellow polymorph has a very different molecular structure of almost linear (178.3°) I–Hg–I molecules and an orthorhombic crystalline symmetry, at room temperature^{101,104}. Expectedly, this results in a deformed packing of the iodine atoms. It has six-coordinated spheres in its closest-packed layers which are stacked roughly midway between cubic close packing (ccp) and hexagonal close packing (hcp). Therefore, the sub-structure of iodine can be described to be distantly associated with a body-centered cubic (bcc) structure¹⁰⁴. Each Hg-atom is surrounded by six I-atoms, 2+4, with two close and four relatively more distant, thus forming a distorted octahedral structure. Figure 1.10 displays the structures of HgI_2 polymorphs at ambient conditions.

At ambient conditions, the orange and yellow phases are both metastable, therefore when mechanically touched they readily transform into the thermodynamically stable red phase, each in its own manner. However, the orange form is significantly more stable than the yellow form. The orange crystals first form irregularly shaped red nuclei that spread and transform within hours, whilst preserving its external shape. Whereas, the yellow crystals form a red front, at the point of contact that propagates rapidly, within seconds, to transform the whole crystal within seconds and significantly distorts its structure. The transformation from orange to red seemingly

involves only the movement of Hg-atoms in an invariable *ccp* matrix of I-atoms. In contrast, the transformation from yellow to red indicates a complete rearrangement of the atoms^{97,105}.

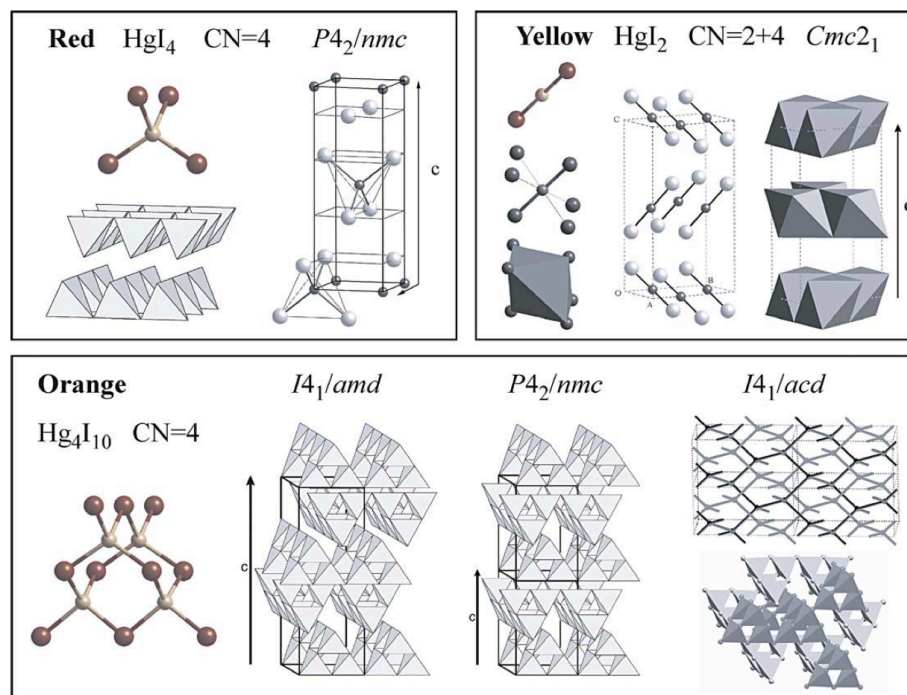


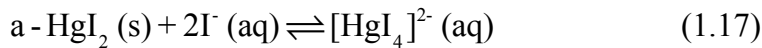
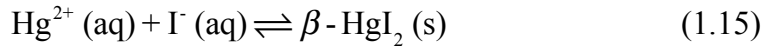
Fig. 1.10 The crystal structures of the three polymorphs of HgI_2 . The red polymorph has a tetragonal crystalline symmetry. The orange polymorph exhibits three different structures constructed of corner-shared Hg_4I_{10} super-tetrahedra¹⁰⁵.

When crystallizing HgI_2 from solvent, at ambient conditions, the solvent is required to rapidly evaporate for the formation of the yellow^M polymorph, indicating that the crystallization of this form is governed by kinetics. A Raman spectra study of HgI_2 solution in 2-chloroethanol reveals its existence in the form of molecules¹⁰⁴. Therefore we acquire an interpretation of the kinetic effect that brings upon this sequence of crystallization: while the formation of HgI_4 tetrahedra requires the breaking of bonds, the pre-existing molecules promptly pack to form the yellow polymorph. On the contrast, the orange polymorph is also kinetically favored over the stable red form

yet the reason is vague. In both structures, there exists four shortest Hg–Hg distances, yet it is reasoned that the Hg distribution in the orange form is more globular, thus less ordered, than the planar distribution in the red form, hence somewhat more homogenous making it the favored form¹⁰⁵.

F. Preface of this Work

In this work, we study wave propagation in a heterogeneous system based on the precipitation reaction between mercuric chloride (HgCl₂) and potassium iodide (KI) to form mercuric iodide (HgI₂) precipitate, which upon excess iodide undergoes redissolution to form the complex [HgI₄]²⁻:



where $\beta\text{-HgI}_2$ is the yellow polymorph of mercuric iodide with an orthorhombic crystalline symmetry and $\alpha\text{-HgI}_2$ is the red polymorph with a tetragonal symmetry¹⁰¹. In Chapter two, we will discuss the propagation of fronts in a two-dimensional setup exhibiting precipitation bands forming irregular cusp-like contours of the leading and trailing edge propagating radially from the center of the reactor. This band creates captivating precipitation patterns concomitant with the sequential polymorphic transformation between the yellow/orange and red polymorphs of the crystalline HgI₂. In Chapter three, we will discuss observations in a three-dimensional setup combining the

coexistence of moving precipitation patterns and traveling waves typical to excitable and oscillatory media^{12,80}. A multitude of wave patterns, including targets, spirals, ripples as well as phase waves, are observed. Their propagation dynamics is shown to be superdiffusive and their breakup leads to defect-mediated chemical turbulence. In Chapter four, we will discuss experiments carried out in a one-dimensional setup expressing a phenomenal behavior of crystal formation, in which an alternating pattern forms combining the metastable yellow polymorph and the stable red polymorph of mercuric iodide. We investigate the disagreement of this crystal growth with the notorious Ostwald rule of stages¹⁰⁶.

G. Experimental Methods

The materials used in all our experiments are constituted of mercuric chloride (Fischer Chemical), potassium iodide (Merck) and agar gel (Bacto). We carry out the reactions in gel media. We prepare stock solutions, using double distilled water, of both mercuric chloride (HgCl_2) and potassium iodide (KI) according to the required concentrations. We dissolve agar powder in a volume of solution required by using a magnetic stirring rod on a stirring/hot plate. Depending on which solution is used, we result with the inner electrolyte. When heating, we maintain the temperature of the mixture at a range within 80–90 °C. To ensure that no errors in the concentration occur we cover the beakers while stirring and make sure that the solutions never reach to the boiling point. The solutions continue to mix until they become clear and no gel particles remain floating. When the solution mixtures are complete, we deliver them to the intended experimental setup. We then place the prepared gel mixture in a chamber

equipped with a thermostat that maintains the temperature at 20 ± 0.2 °C. The gels are left for 2 hours for their gelation and aging processes to complete. The simple aqueous solution of the corresponding co-precipitate, serves as an outer electrolyte for the experiments.

Next, we proceed with the performance of the reaction by pouring the outer electrolyte on to the solidified gel (initialization step). The temperature of the medium is maintained at ambient room conditions during the reaction. We monitor the diffusion under a high-resolution digital camera (Cannon EOS 450D) connected to an iMac with a built-in remote shooting software, where the camera options can be altered according to needed specifications. The mode that we use for our analysis takes a clear focused shot of the setups and the software can be set to automatically take a snapshot according to a pre-specified time intervals (minimum 5 seconds). We leave the reactions to proceed under continuous snapshots, thus producing a sequence of images. Combining these images produces a clear time evolution of the diffusion of precipitate in our system. This experimental procedure is the same for all experiments carried out, but only the reactor and setup in which the reaction is performed differs from study (i.e. chapter) to another. Each experimental setup will be explained in its corresponding chapter.

CHAPTER II

SUPERDIFFUSIVE CUSP-LIKE WAVES AND THEIR TRANSITION TO REGULAR REACTION BANDS

The significant role of RD processes has been revealed in several disciplines exhibiting interesting self-organized pattern formation^{1,6,38,41,42,107}. In particular, RD processes with initially separated reactants have been widely investigated theoretically¹⁰⁸⁻¹¹¹, computationally¹¹²⁻¹¹⁴, and experimentally¹¹⁵⁻¹¹⁸. They are categorized by the presence of a propagating reaction band or front commonly observed in various systems^{10,78,80,119}.

In the current study, we carry out our precipitation reaction in a two-dimensional setup (described in the Experimental Setup section) in which a precipitation band with irregular cusp-like contours, of the leading and trailing edge, propagates radially from the center of the reactor. This band creates attractive precipitation patterns coexistent with the sequential polymorphic transformation between the yellow/orange and red polymorphs of the HgI₂ crystals. The alteration of initial outer and inner concentrations has shown great impact on the speed and the shape of the propagating band. One key result reveals a superdiffusive nature of the transport in this system, without any external modulation that might enhance diffusion. We will also describe the microscopic dynamics accompanying the wave propagation.

A. Experimental Setup

In the study conducted in this chapter, the gel mixture we produce contains Hg^{2+} as the inner electrolyte. We transfer this mixture while hot to a circular, two-dimensional Liesegang reactor (Fig. 2.1A & 2.1B) in which the reaction-diffusion is to take place. The reactor is comprised of a base plate that holds the gel mixture, which in its turn is covered by a second plate of smaller diameter having a reservoir in its center, via which the hot inner mixture is to be delivered. The covering plate is equipped with spacers, of 0.7 mm thickness, that separate it from the base plate thus producing a thin sheet of gel layer in which the outer would radially diffuse. Next, we cover the plates and place them in a chamber equipped with a thermostat that maintains the temperature at 24.0 ± 0.2 °C. We leave the gels for 2 hours for their gelation and aging processes to complete. After the mixtures have gelled, the outer electrolyte, in this case Γ^- is also delivered via the central reservoir, which commences the reaction-diffusion process (initialization step).

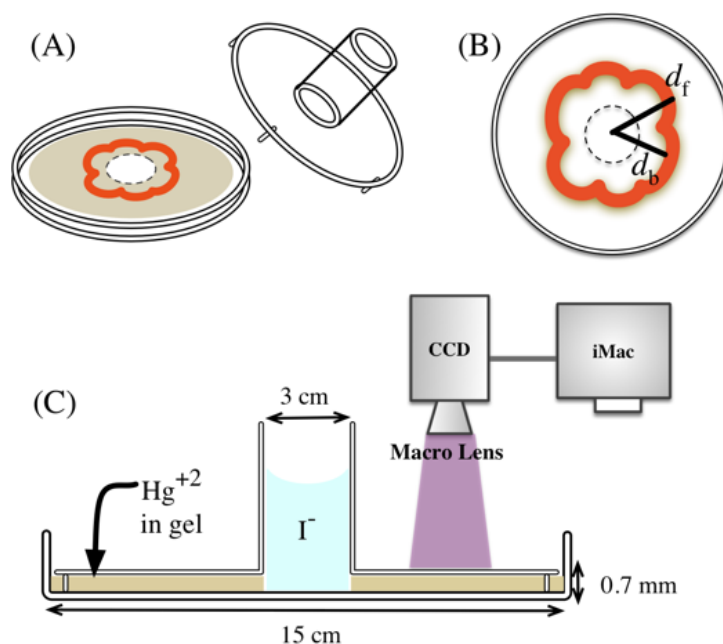


Fig. 2. 1 Schematic representation of the 2D reactor we use to carry out the precipitation-diffusion reactions. (A) Two circular plexiglass plates; first is the base plate holding the gel mixture and the second is the top plate that has a smaller diameter, equipped with a delivery reservoir at its center in addition to 0.7 mm spacers. (B) Top view representation of the radially propagating irregular precipitation band. The two black bold lines from the center of the reactor represent the displacement of the wavefront (d_f) and the waveback (d_b) that we monitor temporally to study the dynamics of the bands. (C) Side-view of the full experimental setup displaying the two plexiglass plates with their dimensions. The positions of both the gel mixture containing the inner electrolyte and the outer electrolyte are specified. The sketch on the right side represents the macro-lens camera connected to an iMac; in addition, the position at which the snapshots of the propagating bands are captured.

B. Results and Discussion

1. Wave Dynamics

When we initiate the reaction, the outer electrolyte diffuses into the gel containing the inner electrolyte to form a two-dimensional diffusion front. In the area following this front, a gel region forms in which both the reactants exist. This gel section is referred to as the excitable region, and it is where precipitation and pattern formation occurs. In this region, there also exists a zone, termed the reaction front, at

which the primary HgI_2 precipitate forms. This primary precipitate mainly involves the two kinetically favored forms of HgI_2 , the orange and the yellow polymorphs. They are both metastable at ambient conditions, which in their turn later transform to the red polymorph, the final and most stable structure of the crystals. As time elapses, the precipitation band of HgI_2 progresses radially away from the center of the reactor, giving rise to a traveling wavefront. In the meantime, because of the excess outer iodide concentration present, redissolution of the formerly formed HgI_2 band produces the colorless complex K_2HgI_4 thus giving rise to a propagating waveback. This relationship between precipitation and redissolution reactions results in the complex dynamics of the ring-like band studied in this system.

This band is analyzed over a broad range of initial reaction concentrations of inner and outer reactants (elaborated in upcoming sections). We detect the propagation of an irregularly shaped precipitation band with cusp-like borders from both sides (front and back). During its spatio-temporal evolution, the band experiences a remarkable polymorphic transformation between the yellow/orange and red polymorphs of HgI_2 . This transformation occurs in a way as if the β -yellow- HgI_2 crystals are dissolving to yield needle-like structured α -red- HgI_2 crystals. Figure 2.2 displays the spatio-temporal evolution process of a single irregular band forming the cusp-like pattern. The interruption of precipitate formation at certain points in the wavefront seems to be the reason behind these unusual structures. During the wavefront propagation through the gel, these points develop to become empty regions (precipitate-free). Thus, the wavefront splits up into portions called reaction zones, each being limited by regressing edges. These edges are accompanied by two diagonal passive edges on their sides that limit the no precipitate regions from the diffusing band. This results in the appearance

of a trapezoidal shape formed by the regressing edge and the two passive edges. This shape has proven to be a very important qualitative property of the pattern. As diffusion advances, the length of the regressing edges decreases, forcing the approaching passive edges to meet and annihilate each other. At these annihilation points the precipitation halts, thus producing a small triangular cusp, possibly because of the depletion of the reactants in their surroundings. After a short period from when this occurs, the reactants are replenished, thus new wavefronts are able to develop anywhere along the passive edges, mostly at the wedge-like empty regions (precipitate-free). These wavefronts appear in a different manner of the previously conceived cusp formation. They are produced in a bursting way resulting in curve shaped precipitation front as opposed to the linear features of the aforementioned cusps. Figure 2.3 displays the evolution of such bursting wavefronts.

Pair production and annihilation of traveling waves have been observed on several seashell patterns. Mathematical models based on nonlinear reaction-diffusion equations have reproduced this behavior¹⁰. Similar cusp-like patterns, forming in gel media, were also encountered in the $\text{Cu}(\text{OH})_2$ ⁷⁸ and $\text{Al}(\text{OH})_3$ ⁸⁰ systems.

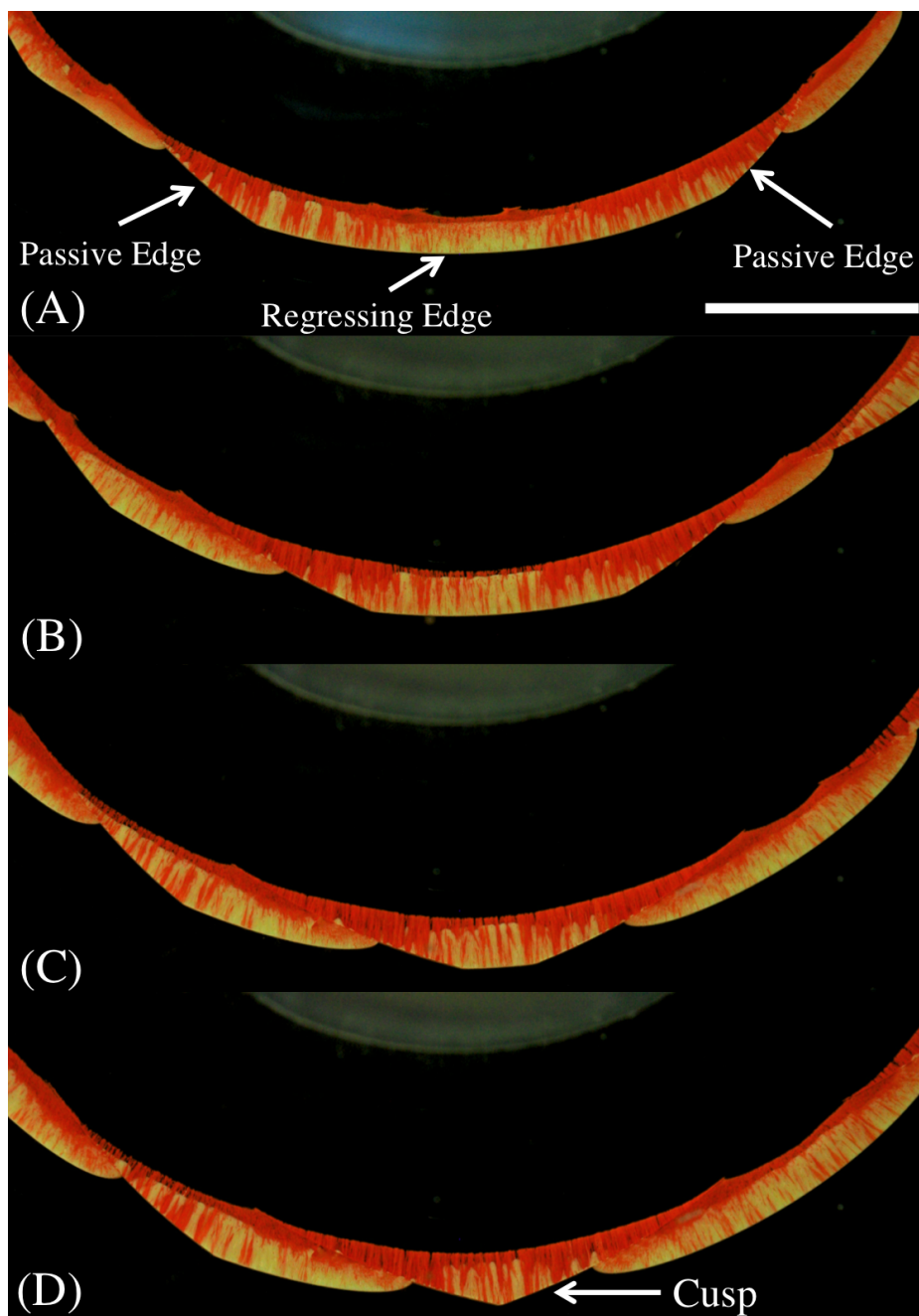


Fig. 2. 2 Sectional, top view snapshots of the radially diffusing irregular precipitation band describing the spatio-temporal progress of cusp pattern development and formation. Initial conditions: inner, $[\text{Hg}^{2+}]_0 = 0.21 \text{ M}$ in 1% per volume agar gel, outer, $[\text{I}^-]_0 = 3.0 \text{ M}$. Time after initialization: (A) 135 minutes, (B) 165 minutes, (C) 190 minutes, (D) 200 minutes. Scale bar represents 0.5 cm.

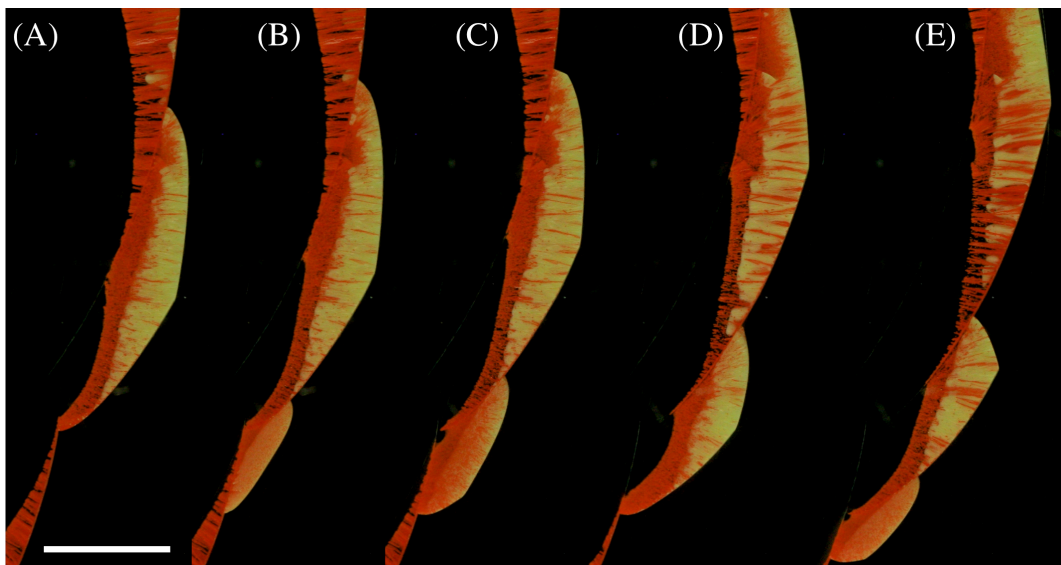


Fig. 2.3 Sectional, top view snapshots of the radially diffusing irregular precipitation band displaying the spatio-temporal progress of the bursting wavefront, appearing at the bottom part of the band. Initial conditions: inner, $[\text{Hg}^{2+}]_0 = 0.21 \text{ M}$ in 1% per volume agar gel, outer, $[\Gamma]_0 = 3.0 \text{ M}$. Time after initialization: (A) 350 minutes, (B) 360 minutes, (C) 370 minutes, (D) 400 minutes, (E) 425 minutes. Scale bar represents 0.3 cm.

2. Horizontal Speed of Cusp Formation

The speed of formation of the cusps is an important aspect to analyze. As it appears to us, the length of the regressing edge decreases, as the passive edges, of the trapezoidal shaped structure, approach each other horizontally. From these terms, to calculate the speed at which the cusps are forming, we need to measure the rate at which the length of the regressing edge is disappearing. A range of different outer concentrations at constant inner concentration is chosen to perform these measurements. For comparison of the range of concentrations, we pick out cusps forming in same time interval in each setup. A noticeable effect is detected in the alteration of the outer concentration. The horizontal speeds of passive edges, leading to cusp formation, are calculated to be constant with time. Yet, when we compare different outer

concentrations, the speed of the wavefront increases linearly as a function of concentration increase. Figure 2.4 shows the linear trend of speed values at each outer concentration. It is clear that the highest outer concentration has the highest speed of cusp formation, while speed becomes lower as concentration decreases. We also measure speeds of cusp formation at different stages of the diffusion, of each specific setup, and conclude that at later stages of the reaction the cusps forming are slower. This is reasoned to be a consequence of the larger size of the cusp forming as a result of precipitation band broadening that takes place at later stage of the diffusion.

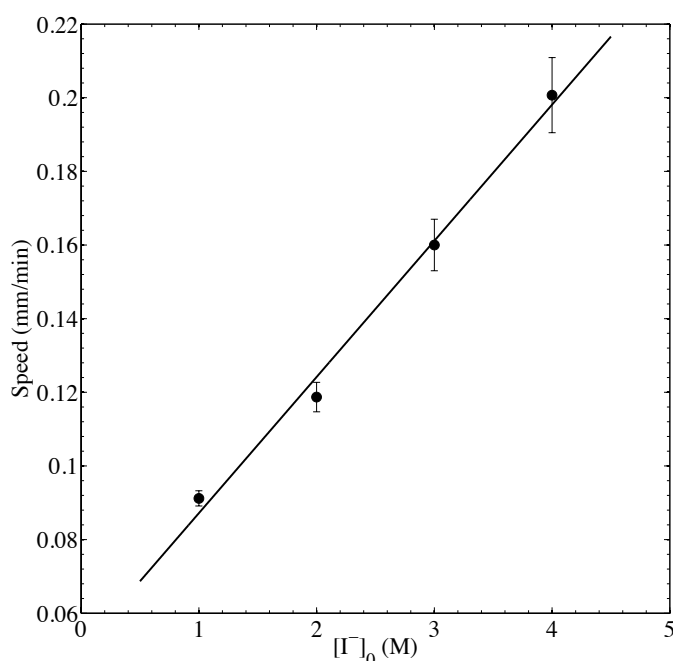


Fig. 2. 4 Plot displaying the alteration of cusp formation speed as a function of outer iodide concentration. Initial conditions: inner, $[Hg^{2+}]_0 = 0.21$ M in 1% per volume agar gel. Outer, $[I^-]_0 = 1.0, 2.0, 3.0$ and 4.0 M. The linear fit in the plot has an $R^2 = 0.9922$, with a slope = 0.03698 and y-intercept = 0.05019 .

Another important characteristic of the wavefronts is provided by the angle forming between the passive edge and the regressing edge. It is characterized by two speeds: the perpendicular speed of the regressing edge in the reaction zone and the

lateral speed of the passive edges. The angles in all patterns forming are found to be changing, and have values decreasing from 162° to 158° as diffusion progresses further. This outcome implies that the perpendicular speed of wavefront diffusion is not constant, and actually is diminishing.

3. Effect of Initial Outer Iodide Concentration

We investigate, in this section, the effect of the initial outer electrolyte concentration, $[\text{I}^-]_0$, on the dynamics of the wavefront and the waveback. At constant inner concentration, we alter the outer concentration, which gives us a variety of concentration gradients to investigate, leading to an important sum of information about the interactions. We use a reference setup with initial conditions (inner, $[\text{Hg}^{2+}]_0 = 0.21$ M in 1% agar gel at 24.0 ± 0.2 °C). The range of outer concentrations includes $[\text{I}^-]_0 = (1.0, 2.0, 3.0, 4.0, 4.5, 5.0, 6.0)$ M. With time evolution, we measure the wavefront displacement (d_f) and as well as the waveback displacement (d_b) from the center of the reactor. We then analyze the velocities of the two aforementioned fronts by producing log-log plots (Fig. 2.5) relating displacement with diffusion time. Consequently, we can obtain information about the dynamics of the width of the propagating precipitation band. The plots, of both waves, show a noteworthy relation between the outer concentration and the velocities, in which the lowest concentration has, the slowest velocity of propagation and as the concentration increases the velocities gradually increase as well. This is reasoned to be because of the larger concentration gradients resulting in more rapid propagation of both waves. Typically, all the waves express decreasing velocities with a sharp transition emerging at outer concentrations higher

than 4.0 M as shown in Fig. 2.5. This transition is not only constricted to their velocity, but also they possess dissimilar features as compared to other concentrations. Their propagating precipitate bands themselves get significantly thinner and lose their cusp-like shape when the outer concentration increases. This behavior is illustrated in Fig. 2.6 showing a width comparison of the bands from three different outer concentrations. It is very evident that the width of the band produced by the outer 1.0 M is about three times wider than that produced by the outer 5.0 M. This can be described using the correlation between wavefront and waveback displacement (Fig. 2.8), which shows significant increase in velocity of waveback propagation at higher outer electrolyte concentrations relative to lower values of concentrations, thus giving rise to a waveback of relatively higher redissolution rate the wavefront producing new precipitate which brings upon this decrease in precipitation band width at high outer concentrations.

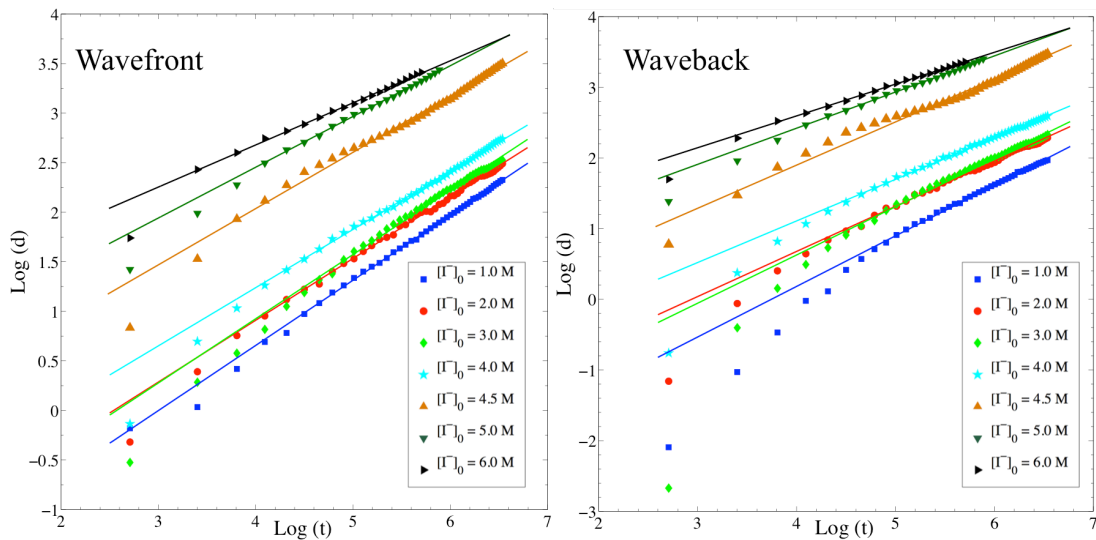


Fig. 2. 5 Log-log plots of the wavefront displacement (d_f) and waveback displacement (d_b) of the diffusing precipitation bands as a function of time (t). Left plot represents the wavefront and the right plot represents the waveback. Initial conditions: inner, $[\text{Hg}^{2+}]_0 = 0.21$ M in 1% per volume agar gel. A range of different initial outer concentrations are tested: $[\text{I}^-]_0 = 1.0, 2.0, 3.0, 4.0, 4.5, 5.0$ and 6.0 M.

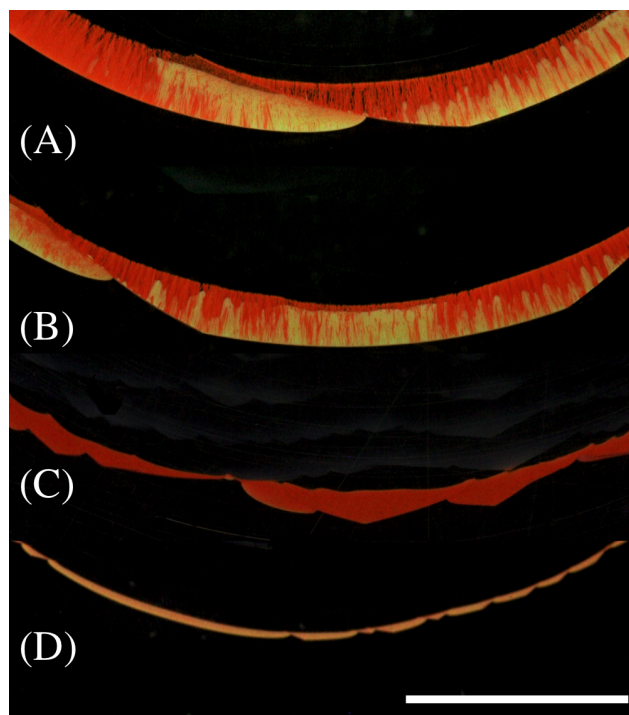


Fig. 2. 6 Sectional, top view snapshots of the radially diffusing irregular precipitation bands. Time after initialization ~ 150 minutes. They express the difference in width as a function of outer iodide concentration. Initial conditions: inner, $[\text{Hg}^{2+}]_0 = 0.21$ M in 1% per volume agar gel. Outer, $[\text{I}^-]_0 =$ (A) 1.0 M, (B) 3.0 M, (C) 4.0 M and (D) 5.0 M. Scale bar represents 0.5 cm.

We linearly fit the log-log plots in Fig. 2.5 to evaluate their slopes (α for the wavefront and β for the waveback). In a typical diffusion-limited process the mean squared displacement of particles (d^2) is linearly proportional to time ($d^2 \sim t^{2\alpha}$), resulting in an exponent α equal to 0.5, owing to the fact that usually mixing is solely due to diffusion of molecules as a result of the underlying Brownian motion. However, our results presented in Fig. 2.7 uncover that the slopes α and β varied between 0.55 and 0.73, in the range of outer concentrations between 1.0 M and 4.5 M, indicating an anomalous superdiffusive behavior for the precipitation wavefront and redissolution waveback. This superdiffusive behavior arises without any external involvement or enhancement of motion. Furthermore, a sharp transition in the values of α and β , to

around 0.5 (normal diffusive behavior), happens as the outer concentration reaches to 5.0 M and continues to drop to values below 0.5 that correspond to a subdiffusive regime, that is usually expected in a gel matrix diffusion due to entrapment of traveling particles¹. It is important to note as well that the values of β are greater than the values of α over the majority of the values in the range of outer concentrations and this aspect has principal implications on the alteration of the width of the band as it evolves with time. In Fig. 2.5, both d_f and d_b are shown to exhibit the following time laws: $d_f = at^\alpha$ and $d_b = bt^\beta$ then the width can be defined as $w = d_f - d_b$. When $\beta > \alpha$, the width increases in time to reach a maximum at $t_{max} = (a\alpha/b\beta)^{1/(\beta-\alpha)}$ then it starts decreasing until the bands is completely dissolved ($w = 0$).

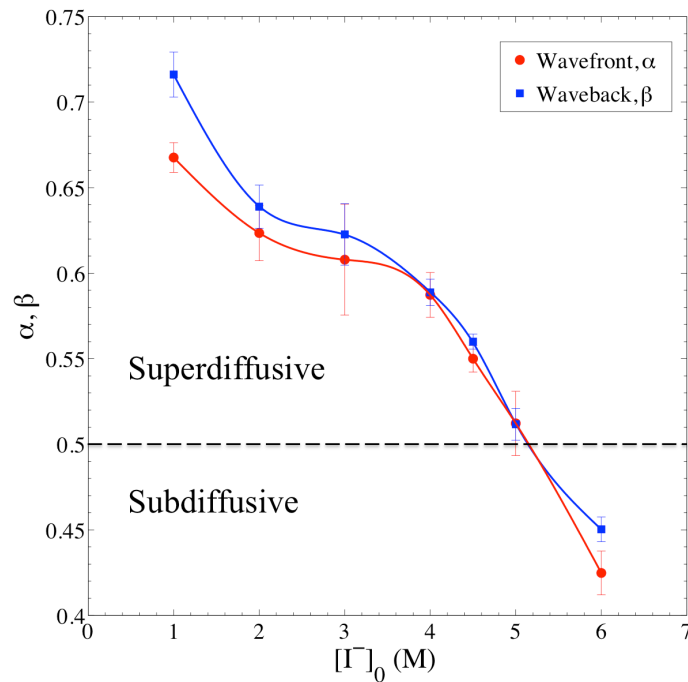


Fig. 2. 7 Plot displaying the change of the slope values (α for wavefront and β for waveback), in the relation $\log(d) \sim (\text{slope})\log(t)$, (d is displacement in mm and t is time in minutes) with change of outer, $[I^-]_0$ at constant inner, $[Hg^{2+}]_0 = 0.21$ M and 1% agar. Dashed line indicates the value 0.5 at which the dynamics is consistent with the normal diffusive profile. Error bars included representing the confidence range.

In Fig. 2.8 we report the correlation between the wavefront displacement and waveback displacement corresponding to values of Fig. 2.5. In this plot, we find that for all outer electrolyte concentrations the displacements have a relationship that is linear to a high extent.

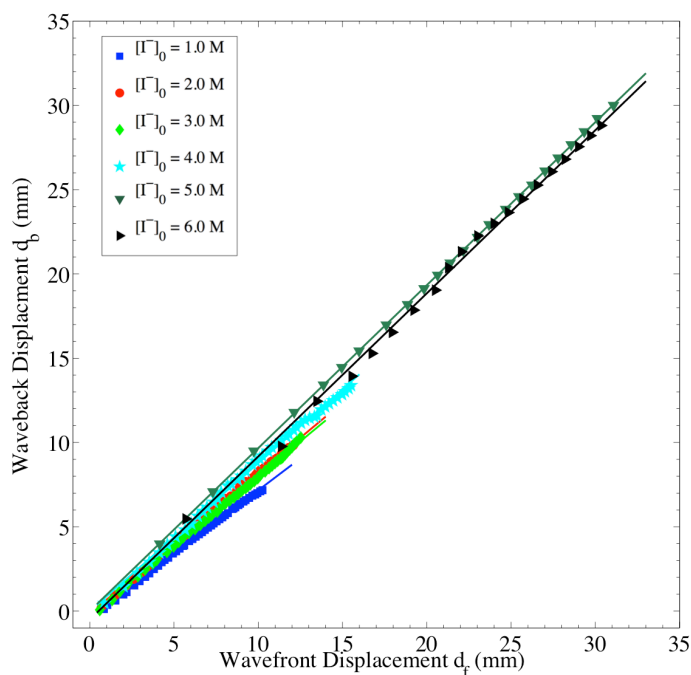


Fig. 2. 8 Plot of the waveback displacement (d_b) vs. the wavefront displacement (d_f) of the diffusing precipitation bands. Initial conditions: inner, $[\text{Hg}^{2+}]_0 = 0.21$ M in 1% per volume agar gel. A range of different initial outer concentrations are tested: $[\text{I}^-]_0 = 1.0, 2.0, 3.0, 4.0, 5.0$ and 6.0 M.

4. Effect of Initial Inner Mercuric Concentration

Altering the inner mercuric concentration unveils a remarkable impact on the actual structure of the propagating precipitation band. The irregularly shaped band with cusp-like pattern (Fig. 2.9A) normally appears at relatively higher concentrations, and as the inner concentration decreases, the precipitation band continuously converts to a ring-like band with undistorted boundaries (Fig. 2.9C). We developed particular interest in the transition between these two structures. As our analysis confirm, an inflection

region exists in the initial inner mercuric concentration below which one can only produce a regular smooth precipitation band and above which only irregular cusp patterned bands form. We test inner concentrations ranging from 0.10 to 0.24 M at a constant outer concentration of 4.0 M and constant gel percentage (1%). The inflection region is established to exist in the range 0.16 to 0.19 M where the precipitation band expresses both structures we encounter, at different stages of the reaction. The band propagation starts with a cusp pattern formation, however at later stages of the reaction/diffusion the irregular form of the structure eventually fades away to bring upon a regular ring precipitation band (Fig. 2.9B). Furthermore, we never encounter an event in which the transition is from regular band to irregular band, the reaction always happens in a manner whereby irregularity stabilizes to form a final regular structure. All the concentrations above the inflection region display the cusp-like pattern formation of the precipitation band, and all the concentrations below it show completely regular structures. It is noteworthy to mention that the bands displayed anomalous superdiffusive dynamics before and after the aforementioned transition, because the values of slopes α and β we calculate range between 0.55 and 0.65. This confirms that the inner concentration has an impact only on the structure of the precipitation band and at the same time the structure itself has no influence on the spatio-temporal dynamics of the reaction.

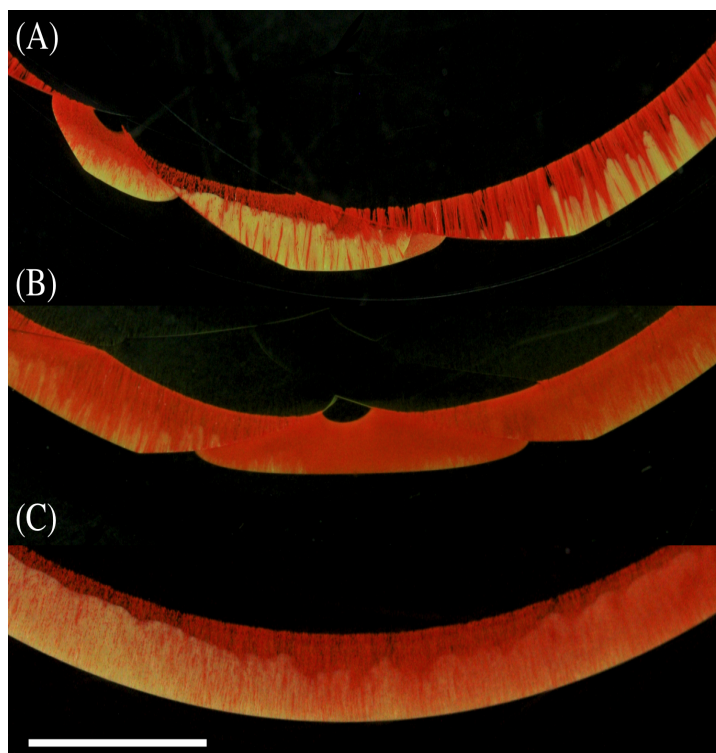


Fig. 2. 9 Sectional, top view snapshots of the radially diffusing precipitation bands describing the transition from an irregular cusped structure to a regular smooth structure, as a function of inner mercuric concentration. (A) Irregular cusp-like shaped precipitation band produced by initial conditions: inner, $[\text{Hg}^{2+}]_0 = 0.21 \text{ M}$ in 1% agar gel, outer, $[\text{I}^-]_0 = 4.0 \text{ M}$. (B) Precipitation band at midway point of transition exhibiting features of both regular and irregular structures. Initial conditions: inner, $[\text{Hg}^{2+}]_0 = 0.19 \text{ M}$ in 1% per volume agar gel, outer, $[\text{I}^-]_0 = 4.0 \text{ M}$. (C) Regular ring-like shaped precipitation band produced by initial conditions: inner, $[\text{Hg}^{2+}]_0 = 0.15 \text{ M}$ in 1% per volume agar gel, outer, $[\text{I}^-]_0 = 4.0 \text{ M}$. The snapshots are taken at ~ 400 minutes after initialization. All the precipitation bands express the polymorphic transformation of the HgI_2 yellow and red crystals. Scale bars represents 0.5 cm.

5. Effect of Agar Gel Percentage

We also investigate the effect of the gel concentration. For this purpose, we prepare a reference setup that serves as a control in all experiments with initial conditions as follows: inner concentration, $[\text{Hg}^{2+}]_0 = 0.21 \text{ M}$ in 1% of volume agar gel and outer concentration, $[\text{I}^-]_0 = 4.0 \text{ M}$, at $24.0 \pm 0.2 \text{ }^\circ\text{C}$. This combination of conditions yields the cusp-like patterns and exhibits anomalous superdiffusive dynamics.

Therefore, the experiments we carry out are in order to detect any deviations from these characteristics.

In the current experiment, gel percentage in the volume of mercuric solution is the variable and all the other concentrations are kept constant. The gel percentages under study are 1%, 2% and 3%. In Fig. 2.10 we report the linear fits of the log-log plots we produce from the measurements of wavefronts displacement with time. The plots express a definite effect on the velocity of the wavefront caused by the gel percentage, in that the lowest gel percentage (1%) has relatively the highest velocity and the highest gel percentage (3%) has the slowest velocity. While predicting that the speed of the wavefront is dependent on the gel percentage, we also confirm that the slopes α and β are invariant yielding values close to 0.6. Reproducibility of the results is verified by several repetitions of these tests.

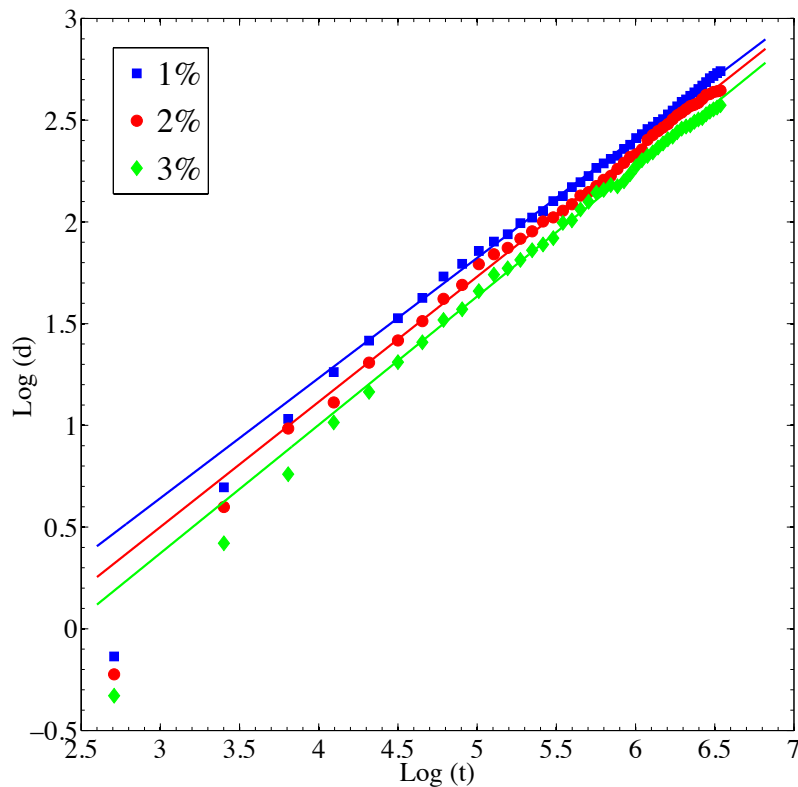


Fig. 2. 10 Log-log plots of displacements (d_f) of wavefronts of the diffusing precipitation bands with respect to time (t). Initial conditions: inner, $[\text{Hg}^{2+}]_0 = 0.21 \text{ M}$; outer, $[\text{I}^-]_0 = 4.0 \text{ M}$. Three different agar gel percentage per volume are tested: 1%, 2% and 3%.

6. Macro- and Microscopic structures

During the propagation of the precipitation band, it undergoes an attractive transformation between the orange, yellow and red crystalline polymorphs of HgI_2 . We observe this transformation at a gradual rate in the gel media, which makes it easier to analyze every step that is proceeding. In the early stages of diffusion, the orange and yellow polymorphs are the primary constituents of the precipitate. On the macroscopic scale, the orange form does not adopt a definite structure, moreover it does not survive for a relevant period of the propagation time and entirely transforms to the next more stable polymorph, which is normally the red polymorph. Cases have been encountered,

in gel media, in which the orange polymorph transforms to the relatively less stable yellow polymorph. Next, the metastable yellow (yellow^M) polymorph (β -HgI₂), appears as a webbing of tightly packed crystal strands and dominates the full width of the precipitation band. As the propagation continues, the yellow form also gradually transforms to give rise to the most stable form, the red polymorph (α -HgI₂). The transformation occurs in a fashion as if the needle-like structured α -red-HgI₂ crystals appear from under the dissolving yellow crystals. This transformation is not the only process happening, it is also complemented by a morphological conversion of the crystalline forms. The β -yellow-HgI₂ adopts an orthorhombic crystalline symmetry, with the Hg-atoms having a coordination number of 2+4, with two close I-atoms and four relatively far, thus forming a distorted octahedral structure. On the other hand, the α -red-HgI₂ has a tetragonal crystalline symmetry, with Hg-atoms each surrounded by 4 I-atoms thus forming HgI₄ tetrahedra, that are corner-linked and form a sheet on a larger scale¹⁰⁵. Since both the red and orange polymorphs adopt cubic closest packing of atoms (*ccp*), the transformation from orange to red apparently only involves the movement of Hg atoms in the unchanging *ccp* matrix of I-atoms. In contrast, a complete rearrangement of the atoms occurs in the transformation from yellow to red^{97,105}.

Extensive work on crystallization of the yellow and red crystals by evaporation from several organic solvents has been published¹²⁰. Yet we implement a different technique of crystal growth, which embraces the formation of the HgI₂ crystal structures in gel media. Figure 2.11 displays a time evolution of a single precipitation band focused on the intersection where polymorphic transformation occurs and illuminating the structures of the red and yellow crystals.

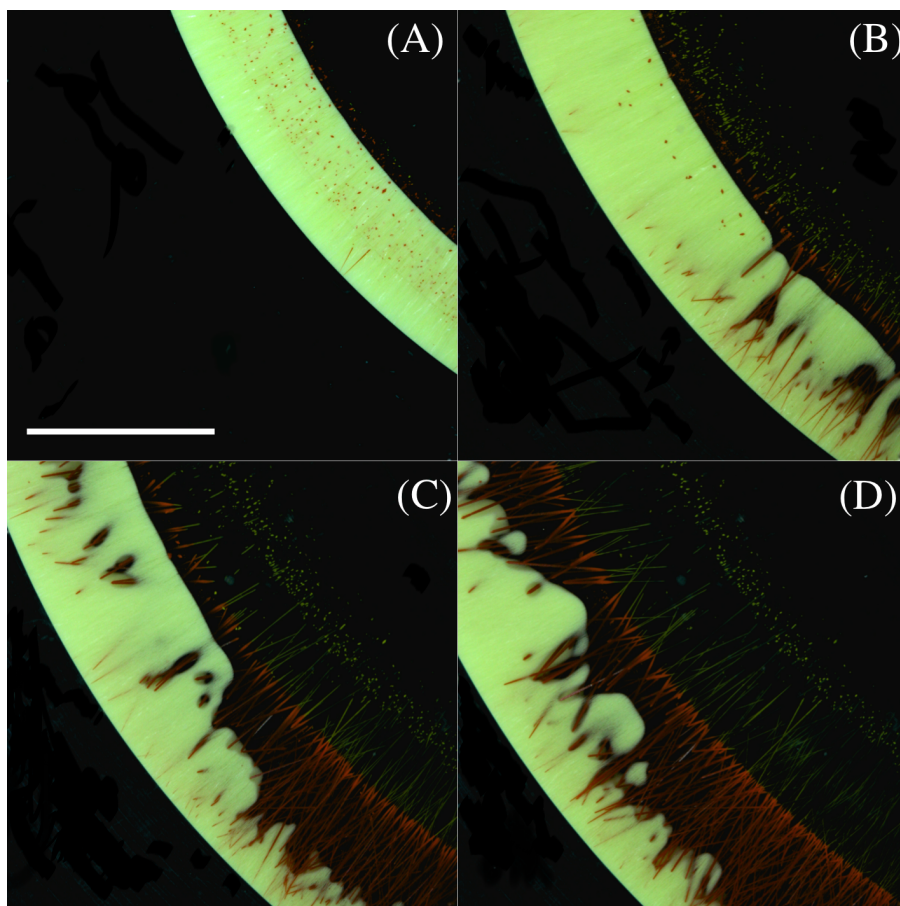


Fig. 2. 11 Top view snapshots of the precipitation band evolution illustrating the structural features of the red and yellow HgI_2 polymorphs, in gel media, at the intersection at which the polymorphic transformation occurs. The yellow polymorph grows as a webbing of strands of crystals with tiny branching structures and the red polymorphs grows as needle-like structures. Initial conditions: inner, $[\text{Hg}^{2+}]_0 = 0.10 \text{ M}$ in 1% per volume agar gel ; outer, $[\text{I}^-]_0 = 1.0 \text{ M}$. Time after initialization: (A) 100 minutes (B) 400 minutes (C) 700 minutes (D) 900 minutes. Scale bar represents 0.5 cm.

The following procedure is applied to describe the structures of the crystals microscopically. After several hours of diffusion, the precipitation band would have covered approximately half the radius of the reactor, thus the polymorphic transformation would also be in its mid-stages (shown in Fig. 2.11). Therefore to analyze the crystal structures at the intersection of the red and yellow polymorphs, we remove the gel layer containing the precipitation band cautiously from inside the reactor whilst preserving the structure and features of the crystals inside it. We then place it in a

freeze-drying machine to form a dried up mold of the gel containing the crystals, which makes the sample more convenient to inspect without imposing any damage to its contents. Next, we observe the sample under a scanning electron microscope (SEM), using an in beam detector, to illustrate the microscopic qualities of the crystals we produce. The images we capture display various attractive morphological structures of both HgI₂ polymorphs. Figure 2.12 shows a panel of different images of several samples representing various parts of the precipitation band with false coloring to indicate the yellow and red regions.

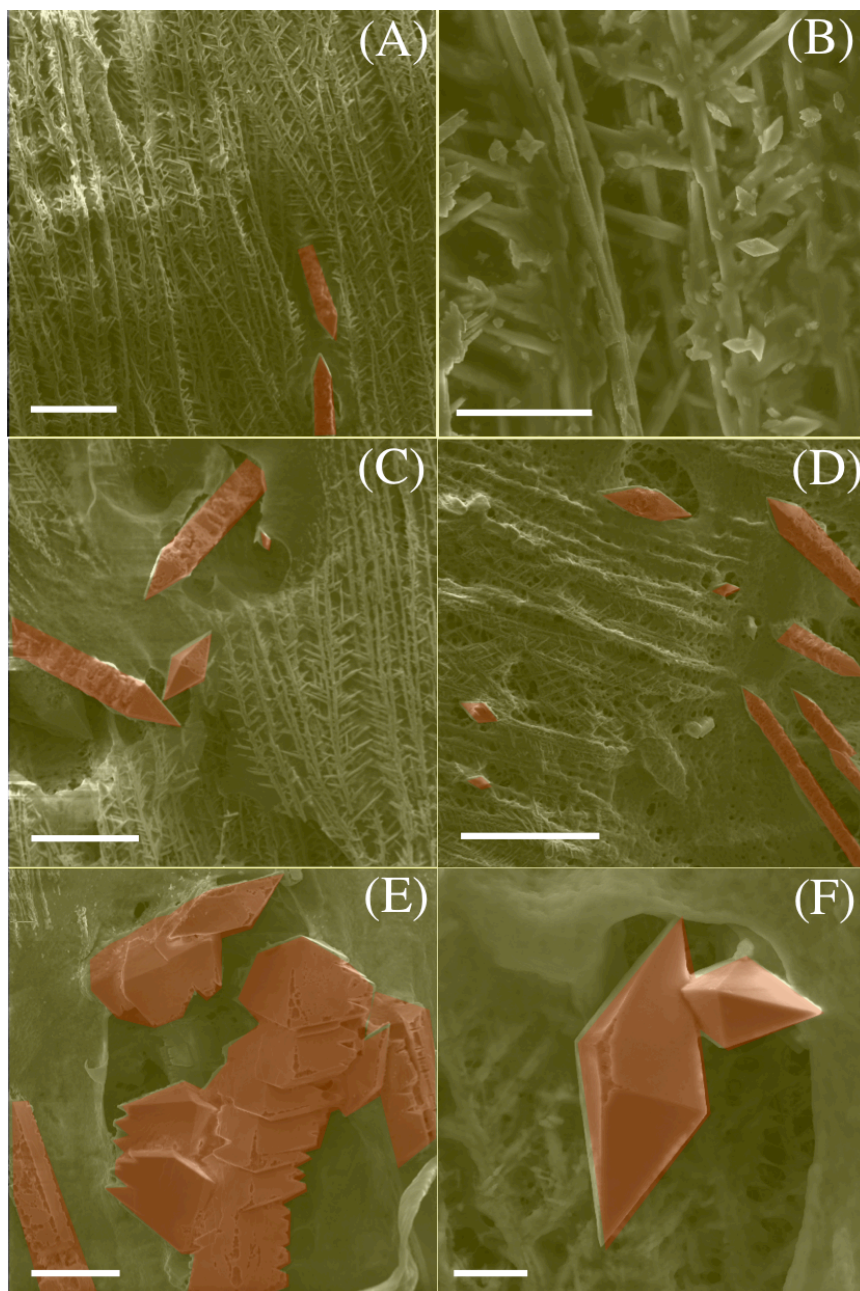


Fig. 2. 12 Panel showing several SEM images captured of various regions of the precipitation band. False coloring added on the images to indicate the real colors of the crystals. Initial conditions: inner, $[\text{Hg}^{2+}]_0 = 0.10 \text{ M}$ in 1% per volume agar gel, outer, $[\text{I}^-]_0 = 1.0 \text{ M}$. (A) A webbing of tightly packed crystal strands with branching structures, in the yellow region. Scale bar represents 100 μm . (B) A magnified image of a yellow region showing the small, undeveloped octahedral shaped crystals carried by the branching crystal strands. Scale bar represents 20 μm . (C-D) These images display the intersection edge between the yellow and red regions of the precipitation band. The yellow region appears as the tightly packed crystal strands, while the large crystals protruding out of the yellow region are the red needles with their various forms. Scale bars in (C) and (D) represent 100 and 200 μm , respectively. (E) A red needle crystal structure formed by a side-to-side overlap of large octahedrally shaped crystals. Scale bar represents 50 μm . (F) A large octahedrally shaped crystal in the red region. Scale bar represents 20 μm .

The yellow region appears as a packed network of crystal strands, with each strand having branching structures that spread throughout its entire length. When we apply a closer view, small octahedrally (square bipyramidal) structured crystals with sizes ranging between 3 and 5 μm appear on the strands. On the other hand, the red region shows numerous yet very similar structures. The fully-grown crystals macroscopically appear as needles, yet under the SEM, the microscopic structure reveals that each needle is made of several octahedra stacked on top of each other. Some appeared to have pointy extremities, like pyramids, owing to the fact that they are constructed perfectly on top of each other in a head-to-head manner. Other needles formed saw-tooth structures that are built in a similar way as the aforementioned needles, yet the octahedra are stacked in a sideways fashion. We also observe several single octahedral crystals that are not stacked to form a needle structure. These octahedra are very similar to the ones appearing in the yellow form yet have sizes ranging between 50 and 90 μm which makes them nearly 20 times larger. Such a behavior brings upon a confirmation to the fact that Ostwald ripening^{90,121} is taking place in the gel during the transformation between yellow and red crystals whereby larger crystalline $\alpha\text{-HgI}_2$ forms at the expense of the smaller $\beta\text{-HgI}_2$. The Ostwald ripening mechanism involves the reconstruction of octahedral Hg(II) in the layers from the orthorhombic $\beta\text{-HgI}_2$, which in fact, involves the breaking and forming of bonds, preceded by a dissolution-reformation process. All this also involves a morphological change of the crystals in the two phases, where smaller octahedral structures are preferred in the β -polymorph, whereas larger octahedra are preferred in the α -polymorph.

We also conduct a spatio-temporal evolution analysis on a setup corresponding to the regular precipitation band by combining the images captured of the RD process. The evolution expresses a well-defined polymorphic transformation. From the early stages of diffusion, the yellow polymorph emerges and dominates the whole width of the precipitation band. As the diffusion progresses, the needles of the red polymorph start appearing from under the yellow mesh extending from the waveback to near the center of the band. As we described earlier, the precipitation band experiences an increase in width as it diffuses further in the reactor. At some point of the diffusion the band is three-quarters comprised of red needles and the rest is yellow (yet we observe cases where the entire precipitation band is dominated by the red polymorph). Afterwards, a rather appealing transition occurs in which the polymorphic transformation adopts an oscillatory behavior. As the red polymorph covers three-quarters of the band, we notice that the yellow to red transformation halts, yet diffusion at the leading wavefront continues to produce new yellow crystals, while the red needles start disappearing due to the dissolution at the waveback. As this behavior regenerates, a time is reached where the precipitation band is dominated by the yellow polymorph again, and the cycle repeats itself. This behavior is quantitatively described in Fig. 2.13, which shows the alteration of the entire precipitation band width as a function of time, in addition to the oscillations of width values of both yellow and red polymorphs regions occurring with wavefront and waveback propagation.

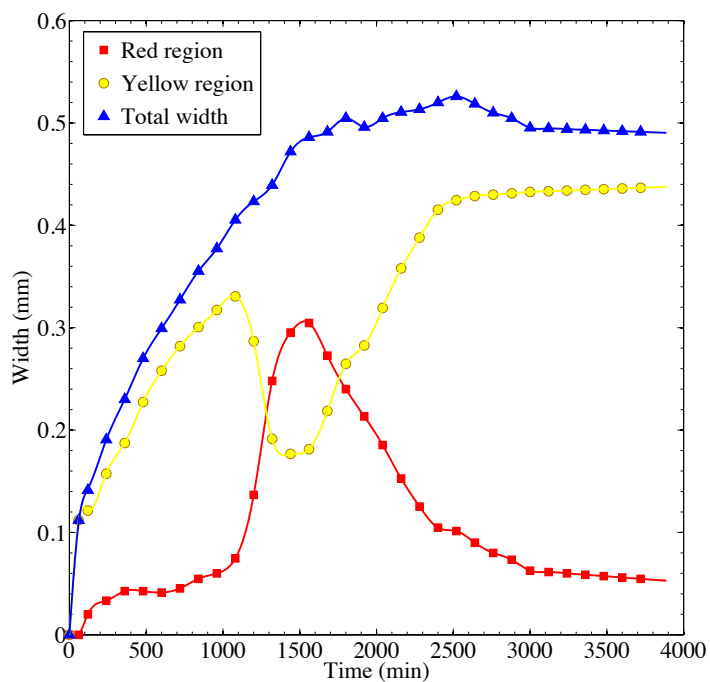


Fig. 2. 13 Plot of alteration of precipitation band width with respect to time. Red and yellow curves represent the oscillations in the red and yellow regions, respectively and the blue curve represents the change in width of the entire precipitation band. Initial conditions: inner, $[\text{Hg}^{2+}]_0 = 0.10 \text{ M}$ in 1% per volume agar gel ; outer, $[\text{I}^-]_0 = 1.0 \text{ M}$.

CHAPTER III

THREE-DIMENSIONAL SUPERDIFFUSIVE CHEMICAL WAVES

In both homogeneous systems, such as the Belousov-Zhabotinsky (BZ) reaction¹², and heterogeneous systems, such as the catalytic oxidation of CO on Pt crystal planes⁶⁶, travelling waves give rise to many interesting pattern formations, which can take the form of spirals or circular targets⁸⁰. The rotation and propagation of such patterns instigate deformations in the medium of reaction. These deformations cause the spirals to breakup and lead to chaotic behavior that produce complex spatiotemporal patterns⁴². Such spatiotemporal chaotic states have been discovered to have critical impact on the cardiac tissue, consequently leading to ventricular fibrillations and sudden deaths²⁹. This issue gave rise to extensive investigations to understand the origin and mechanism that produce such spiral waves and chaotic states. Both experimental and theoretical studies have been carried out aiming towards reducing ventricular fibrillation and maintaining regular functioning of the heart^{24,29,44,82,122}.

In this chapter, we study the precipitation reaction occurring on the surface of the gel medium. This is applied by performing the reactions in small Petri dishes that provide a large enough surface area to monitor the gel interface from above. Our observations involve the coexistence of traveling precipitation patterns and propagating waves typical to excitable and oscillatory media^{12,80}. A variety of wave patterns are encountered which include targets, spirals, ripples in addition to phase waves. The

dynamics of their propagation is shown to be superdiffusive. On the other hand, we also confirm that the breakup of the patterns leads to defect-mediated chemical turbulence.

A. Experimental Setup

In the current study, after the completion of the gel/solution mixtures containing the inner electrolyte (Hg^{2+}), we deliver them to small Petri dishes (47.0 mm diameter). We transfer approximately 10 mL of the solution to each Petri dish, which produces a gel thickness of about 7 mm. We then cover the dishes and place them in the thermostatic chamber that maintains the temperature at 24.0 ± 0.2 °C. The gels are left for 2 hours for their gelation and aging processes to complete. After the mixtures have gelled, the outer electrolyte (I^-) is simply poured on top of the gel surface, thus producing a large circular precipitation layer that diffuses perpendicularly into the gel.

The mode that we use on our camera for the reaction analysis takes a snapshot of the setup every 5 seconds. The reactions proceed for around 15–30 minutes each; therefore with our settings we produce well about 180–360 snapshots of the reactions. Combining these frames produces a clear time evolution of the traveling chemical waves in our system. The experimental setup is represented in Fig. 3.1.

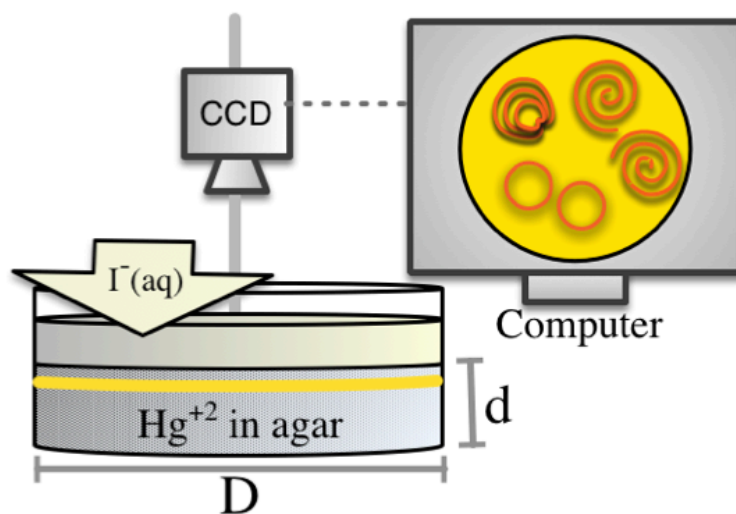


Fig. 3. 1 Schematic representation of the experimental setup under which the snapshots of the reactions are captured using a computer-controlled CCD and transferred to the computer for display and further analysis. The outer iodide concentration is added to agar gel containing the mercuric ions. The yellow precipitation front propagates downward due to redissolution in excess iodide. The screen on the right display the captured from above wave patterns as appearing in the yellow front parallel to the gel interface. The diameter of the reactor is $D = 47.0$ mm and the width of the gel $d = 7.0$ mm.

B. Results and Discussion

1. Detailed Chemistry

Our experimental observations incorporate the best of the two worlds; in the sense that it combines moving precipitation patterns, like in the Liesegang phenomenon and traveling waves, like in excitable media, occurring perpendicular to the diffusion flux vector of the outer electrolyte invading the gel. In our system, the Hg^{2+} ions (inner electrolyte) are uniformly distributed in the agar gel. This is followed by the delivery of Γ ions (outer electrolyte) on top of the gel surface, which in turn diffuses into the gel to produce HgI_2 precipitate.

Immediately after contact between the two electrolytes, a thin layer of the precipitate ($\sim 70\text{--}150\ \mu\text{m}$) forms at the gel surface which is the primary interface between the inner and outer solutions. As the diffusion proceeds, the excess outer electrolyte reacts with the precipitation layer to form the complex $[\text{HgI}_4]^{2-}$ (redissolution), thus making it appear like a downward propagating front. Meanwhile, as we monitor the surface from above, parallel to the interface, we observe distinct self-organized patterns forming inside the whole width of the thin precipitation disk. Figure 3.2 presents the three different self-organized patterns we encounter in our system.

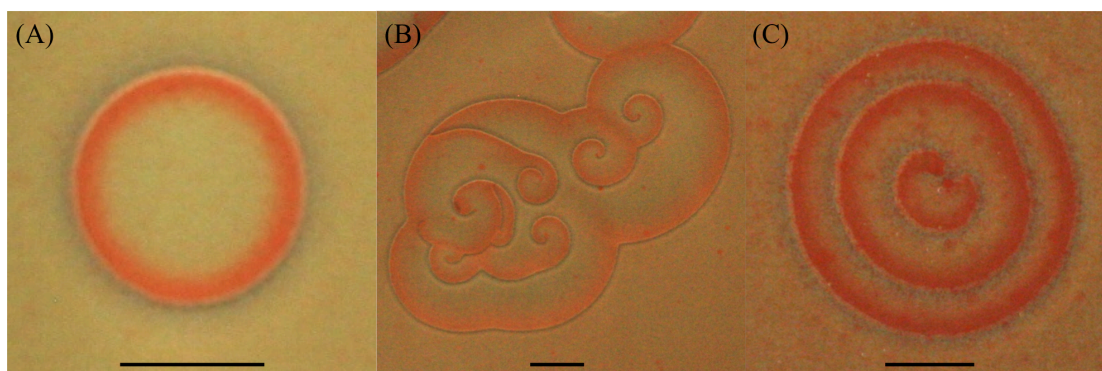


Fig. 3. 2 Three different self-organized patterns forming in HgI_2 precipitate (top view). Initial conditions, (A) Target, $[\text{Hg}^{2+}]_0 = 0.22\ \text{M}$, $[\text{I}^-]_0 = 1.0\ \text{M}$, 350 s after initialization; (B) Spirals, $[\text{Hg}^{2+}]_0 = 0.24\ \text{M}$, $[\text{I}^-]_0 = 5.0\ \text{M}$, 460 s after initialization; (C) Ripples, $[\text{Hg}^{2+}]_0 = 0.22\ \text{M}$, $[\text{I}^-]_0 = 4.0\ \text{M}$, 420 s after initialization. The scale bar represents 0.25 cm.

Accurate examination of the snapshots captured of the pattern evolution unveil that tiny bubbles are entrapped on the gel surface, while solidifying, which are serving as nucleation sites for all the propagating patterns. In addition, the glass boundary of our Petri dishes is also an important nucleation site, which produces somewhat irregularly shaped patterns. The reported measurements and descriptions entirely correspond to patterns nucleating at the center of the Petri dishes without any boundary obstruction.

When precipitation is initiated, the first HgI_2 polymorph to appear is the orange form, which directly transforms to the yellow form ($\beta\text{-HgI}_2$). The nucleation of chemical waves is found to be possible in both polymorphs. The spatial evolution of the waves over a particular region originates on a steady background of a kinetically favored HgI_2 precipitate. The chemical wave itself acts as a transformation wave, enforcing an increase in red- $\alpha\text{-HgI}_2$ and a consequential decrease in yellow- $\beta\text{-HgI}_2$. Directly after the wave a quasi-steady region equivalent to the post-wave composition of $\beta\text{-HgI}_2$ exists resulting from the slow drop of $\alpha\text{-HgI}_2$. As the wave travels, the colorless complex of redissolution appears as an intermediate of the polymorphic transformation reaction, which occurs when $\beta\text{-HgI}_2$ readily transforms to $\alpha\text{-HgI}_2$. Furthermore, it is significant in all of our experiments that the traveling wave is highlighted by a colorless contour. This contour is reasoned to be the complex $[\text{HgI}_4]^{2-}$ forming due to the excess iodide solution. The spatial description given is somewhat close to what is described in the alteration of red and blue colors observed in the BZ reaction¹²³, yet it is very distinctive and complex in its type owing to the fact that it involves an interplay between diffusion of a chemical wave coupled with a polymorphic transformation of crystalline precipitate, along with a redissolution process, all occurring in a heterogeneous mixture, in a porous medium (the gel).

2. Spatiotemporal Patterns

a. Effect of Concentrations

As illustrated in Figure 3.2, we observe several types of traveling wave patterns in our system, which include: single-wave circular targets, spirals and ripples

similar to a cardioid originating from a double spiral. The initial reaction concentrations confirm to be the primary judge on: the selection of the patterns, their coexistence and their characteristic wavelengths. During propagation the structure of the patterns are relatively preserved. Upon collision, the waves combine and deplete each other, thus causing their eventual loss in stability and their breakup into chaotic patterns. In Fig. 3.3 we display a phase diagram that qualitatively describes the probability of pattern formation. The figure relates a range of inner and outer concentrations signifying specifically which pattern has the greatest probability to nucleate at each pair of inner/outer concentration combinations. We reproduce the experiments several times and combine the results to give the precise probabilities that are present in Fig 3.3. As the figure reveals, spiral waves have the highest probability of appearance at high outer concentrations and as concentration decreases, the target patterns become more probable to nucleate. The amazing phase wave (explained later in this chapter) that we observe clearly appears at the outer concentration of 1.0 M specifically.

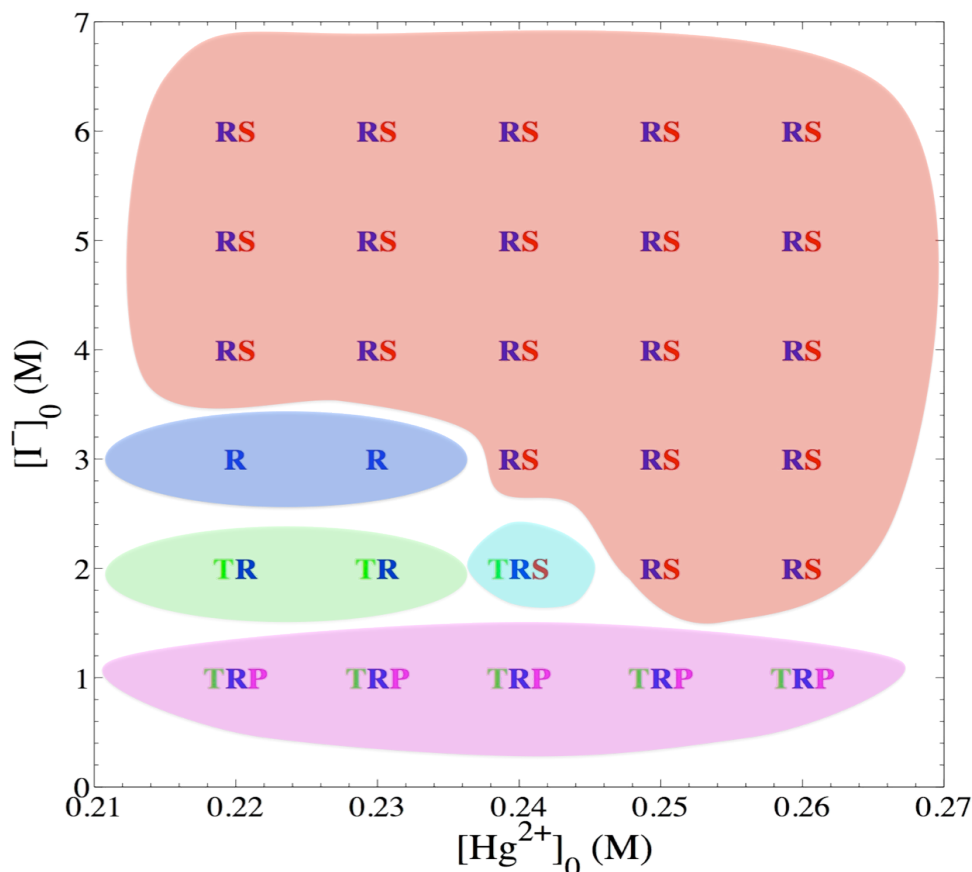


Fig. 3.3 Phase diagram as a function of the outer $[I^-]_0$ and inner $[Hg^{2+}]_0$, showing the most probable type of self-organized patterns appearing at every pair of inner/outer concentrations. Notations: (P) Phase wave, (T) Target, (R) Ripple, (S) Spiral.

It is noteworthy to state that the nucleating self-organized patterns are highly dependent on the initial mercuric concentration, $[Hg^{2+}]_0$, in the gel medium. They only appear in a limited range labeled the “excitable region” which exists between 0.16 M and 0.26 M of $[Hg^{2+}]_0$. The outer electrolyte plays the role of determining the probability of which pattern is going to majorly nucleate. As Fig. 3.3 shows, at high outer values the major patterns are spirals and ripples, yet as we go lower in concentration, targets become the more major pattern to be observed. Another role of the outer electrolyte noticed, is the actual quantity of nucleation sites that actually produce a pattern. At initial iodide concentration, $[I^-]_0 = 1.0\text{--}2.0$ M, experiments show

nucleation of about 40–50 patterns, but when the concentration increased to 3.0 M and above, the count dropped to less than 10 patterns. Therefore simply to increase the probability of nucleation we decrease outer concentration, yet we expect a crowded reactor with small patterns. If we require a larger and clearly pattern we increase the outer concentration.

b. Superdiffusive Targets

In this section we turn our focus towards target patterns specifically. These patterns are circular waves that develop from small modified areas that can act as pacemakers as a result of slight perturbations such as dust particles, gas bubbles or surface defects³⁹. In homogenous media, these regions typically have a local oscillation frequency higher than that of uniform oscillations^{124,125}. On the other hand, in our system the targets nucleating at the entrapped air bubbles in the gel, lack continuous stimulation. Because of the moderate availability of such perturbative bubbles in our media, several circular patterns are distinctly observed. Yet no initiation of targets can be present when the gel preparation is cautiously performed with the elimination of these bubbles.

Our next concern is the displacement profiles illustrating the diffusion of our targets in time; therefore we produce the Log-Log plots (inset of Fig. 3.4) that correlate the change of radius of the target (R) as a function of time (t) at four different inner concentrations and at a constant outer concentration of 1.0 M. We only measure the radii throughout the time the patterns are stable. The plots finish at the moment the patterns start breaking up (explained later in this chapter). It is significant from the

figure that the speeds of these waves are not constant. Moreover, the highest inner concentration engages the fastest pattern breakup, which can be reasoned to be an outcome of highest initial excitability causing the pattern to lose stability at an earlier stage. In addition, we also note that at this concentration we record relatively the highest velocity of wave propagation. The time power law equation of the form $R \sim t^\alpha$, fits perfectly the diffusion curves and their log-log plots are shown in Fig. 3.4. It is noticeable that the power α values, for all cases studied, are well above 0.5, which is the expected value in normal diffusive (Fickian) dynamics. The values of the power α increase ranging from 0.65 to 0.84, as the inner concentration increases from 0.20 M to 0.26 M. This confirms that Fickian diffusion is not governing these patterns and the more significant role is being played by the reaction kinetics in judging their dynamics. It is important to mention that at every experiment we choose, at random, up to 5 targets and perform the same previously mentioned curve fitting, only to obtain a similar reproduced value of the exponent α . We also execute analogous measurements on spirals and ripples with different initial outer and inner concentrations. The dynamics also confirm to be superdiffusive in all the measurements. Figure 3.5 shows the evolution of a target expressing superdiffusive dynamics.

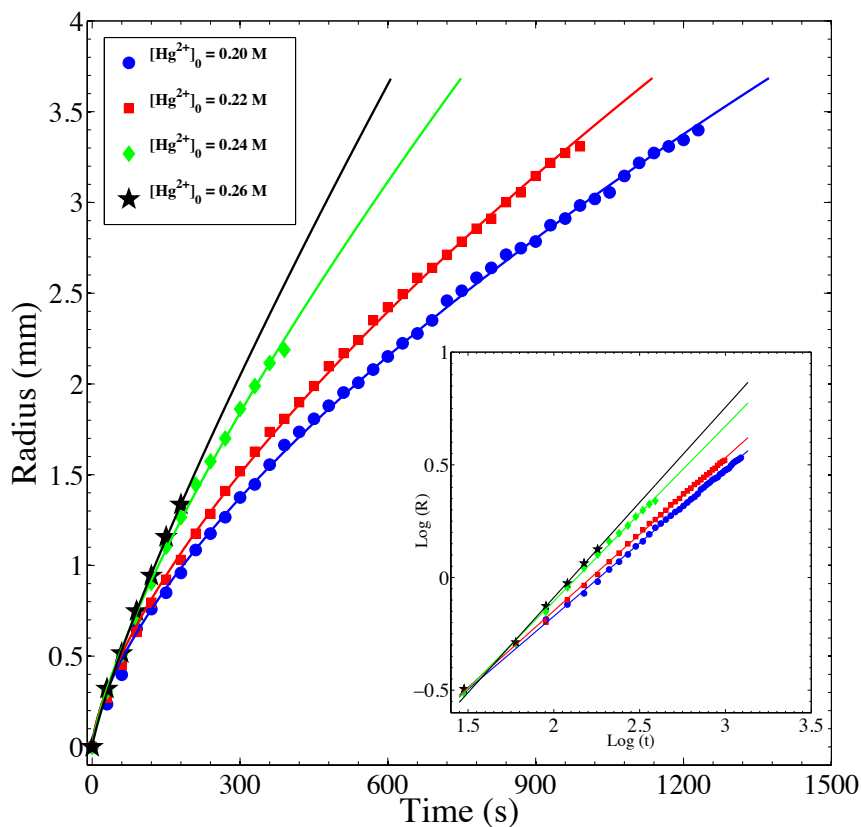


Fig. 3. 4 Radius (R) vs. time (t) plots of the spatio-temporal propagation of targets. Inset appears the $\text{Log}(R)$ vs. $\text{Log}(t)$ plot. Initial conditions: 1% agar gel, inner $[\text{Hg}^{2+}]_0 = 0.20 \text{ M}$, 0.22 M , 0.24 M , 0.26 M and constant outer $[\text{I}^-]_0 = 1.0 \text{ M}$. Plots are fitted to a power equation relating $R \sim t^\alpha$. Powers α (circle) = 0.65 ± 0.01 , α (square) = 0.67 ± 0.01 , α (diamond) = 0.76 ± 0.03 , α (star) = 0.84 ± 0.05 .

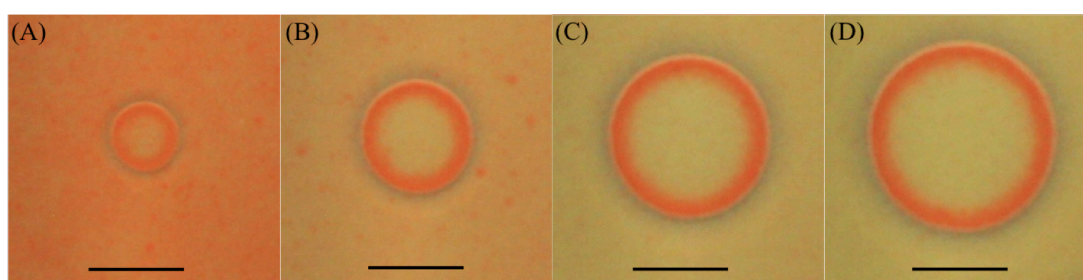


Fig. 3. 5 Top view snapshots displaying the spatio-temporal evolution of the target patterns forming in HgI_2 precipitate in gel medium. Initial conditions: 1% agar gel, inner $[\text{Hg}^{2+}]_0 = 0.22 \text{ M}$, outer $[\text{I}^-]_0 = 1.0 \text{ M}$. Time after initialization (A) 100 s; (B) 200 s; (C) 350 s (D) 450 s. The scale bar represents 0.5 cm. The width of the traveling red wave front is about twice that of the redissolution region ($\sim 0.7 \text{ mm}$).

Upon collision of two targets, no overlapping takes place yet they actually merge and form a larger yet distorted pattern. This is caused by the depletion of red- α - HgI_2 , comprising the chemical wave, from the section of collision, which transforms to an unperturbed quasi-steady β - HgI_2 . After prolonged evolution, no patterns survive, all are destined to lose their stability, leading to their breakup and followed by chemical turbulence.

To enrich the characterization of the targets, we also measure the width of the propagating wave. Throughout the whole propagation, it is found to be fairly constant. The width persists to be unchangeable with time, yet we confirm that a decrease in width occurs as a function of increasing $[\text{Hg}^{2+}]_0$. The values we measure range between 120–240 μm . This circumstance shares similarity with the BZ reaction in the experimental and theoretical work conducted by Bugrim *et al.*¹²⁶ and by Pagola and Vidal¹²⁷ where it is accomplished that the width of the targets remains constant during propagation.

c. Three-Dimensional Targets

We also study our targets under a high-resolution scanning electron microscope (MIRA3 LMU FE SEM) using an SE detector to determine its dimensional features. We prepare the sample for measurement, by first pouring the outer electrolyte to initiate the reaction and allow the precipitate to diffuse for less than a minute. Next we discard the outer, which causes the reaction to slowdown, since a small amount of iodide ions remains. By doing this, we allow the targets to nucleate and grow to the size appropriate for investigation. Afterwards, we place the Petri dishes in a freeze-drying

machine that reduces any moisture remaining and solidifies the gel thus quenching completely the propagation of the target.

After two hours, we end up with a frozen gel having an undamaged precipitate layer on top of it. This layer is easy to peel and cut to be placed on a SEM stub. Figure 3.6(A) shows an example of target pattern chosen for inspection and Fig. 3.6(C) represents the SEM image of the magnified area on the propagating wave of the target. From our analysis of many different samples, we measure and discover that the boundary (Fig. 3.6C(II)) of the circular target, that is the traveling chemical wave, is actually elevated as compared to the internal section (Fig. 3.6C(I)), which unveils that the self-organizing pattern has a remarkable three-dimensional wave. We also conclude that the outer section (Fig. 3.6C(III)) of the target is also at an elevated position from the inner section yet still lower than the chemical wave itself. The wave measures to be higher than the inner section by around 70 to 100 μm while the outer section is only around 20 to 40 μm lower than the wave.

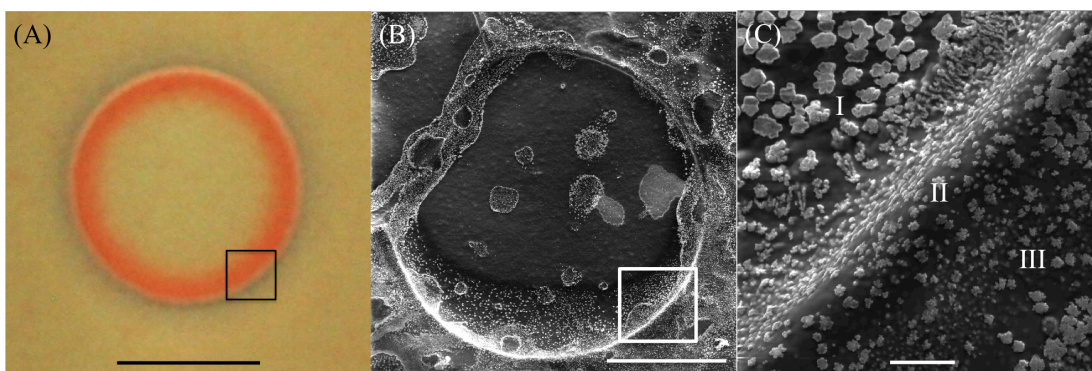


Fig. 3. 6 (A) A Target captured after 350 s of propagation, with $[\text{Hg}^{2+}]_0 = 0.22 \text{ M}$, $[\text{I}^-]_0 = 1.0 \text{ M}$. Scale bar represents 0.25 cm. The square on the image indicates the cropped area imaged in (C) using SEM. (B) SEM image of the target presented in (A). Scale bar represents 500 μm . (C) Zoomed in image on the chemical wave of the target. (I) The inner part of the target. (II) The wave front of the target. (III) The outer part of the target. Scale bar represents 20 μm .

d. Spirals and Ripples

Next, we shift our discussion to another rather interesting pattern that is abundant in our system, the rotating spiral wave. This pattern has achieved high interest owing to its universal characteristics: spiral waves are commonly witnessed in spontaneous oscillatory media as well^{128,129} and, from a topological point of view, they are equivalent¹³⁰ to dislocation type defects in striped patterns like convective rolls¹³¹. In this system, as presented in Figure 3.2(B), the spiral waves uniformly rotate around fixed centers having their tip pinned to the initial nucleation site. Their curvature stays persistent until the spiral encounters an instability and breaks up into a chaotic pattern⁴⁶. Fig. 3.7 displays the spatio-temporal evolution of rotating spirals appearing in our system.

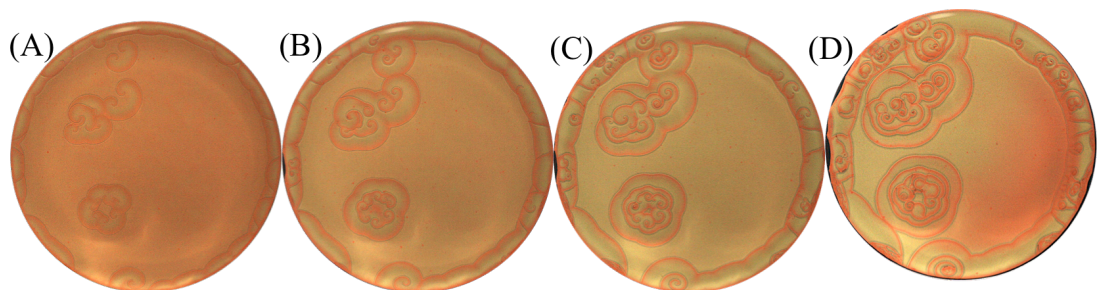


Fig. 3. 7 Top view snapshots, of the whole area of our Petri dishes (47 mm diameter), displaying the spatio-temporal evolution of the spiral patterns forming in HgI_2 precipitate in gel medium. Initial conditions: 1% agar gel, inner $[\text{Hg}^{2+}]_0 = 0.24 \text{ M}$, outer $[\text{I}^-]_0 = 5.0 \text{ M}$. Time after initialization (A) 340 s; (B) 460 s; (C) 550 s (D) 670 s.

Another type of pattern we encounter, presented in Fig. 3.2(C) is the ripple-like or cardioid structure. Dissimilar to the case of the targets, the nucleation site of the cardioid structures exhibits continuous stimulation, thus giving rise to a group of pulses

producing a wavetrain and appearing like a ripple pattern. We measure and calculate the characteristic separation and velocities of the consecutive waves and discover that they are unequal. The correlation between the characteristic wavelength and velocities of these wavetrains can be accounted for by the dispersion relation, therefore we predict that a slower propagation velocity brings upon a shorter wavelength⁴⁶.

We measure the wavelengths of spirals for the same pair of inner/outer concentrations and at different times of the reaction. The wavelengths average to be equal in all patterns studied. Figure 3.8 shows plots representing the variation of wavelengths as a function of the tested inner $[\text{Hg}^{2+}]_0$ range at a constant outer $[\text{I}^-]_0$. The wavelengths show an inverse dependence on the value of inner concentration. In all four plots we see a similar trend, in which from the highest to the lowest concentrations tested; the values of the wavelengths are doubled. On the contrary, the variation of the outer $[\text{I}^-]_0$, at constant inner $[\text{Hg}^{2+}]_0$, shows an opposite effect on the wavelengths, as can be seen in Fig. 3.9. The lowest $[\text{I}^-]_0$ has a wavelength measurement of about half that of the highest $[\text{I}^-]_0$. In the figures described, the values of wavelengths vary between 0.26 and 1.37 mm. Similar tests performed by Plesser *et al.*¹³² also conclude a decrease in spiral wavelengths as a function of increasing proton concentration in the measurements carried out on the BZ reaction patterns.

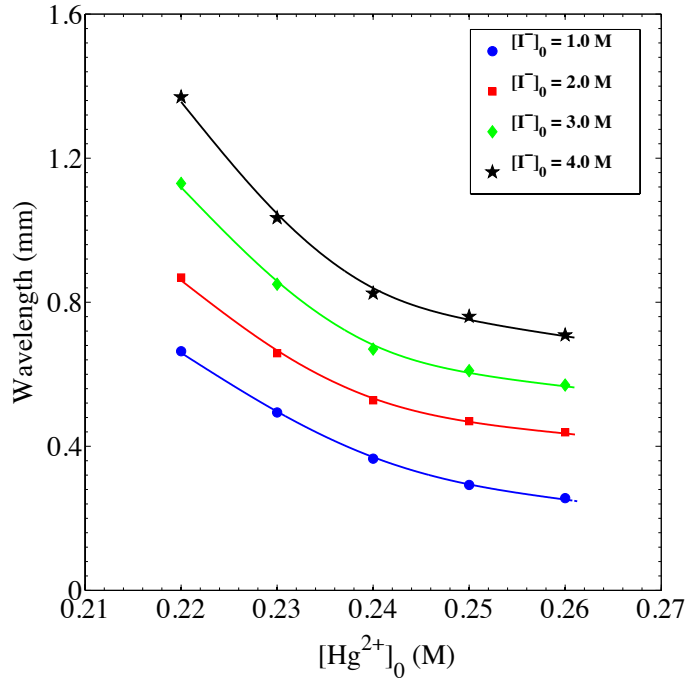


Fig. 3. 8 Plots of wavelength of spiral and ripple patterns versus inner $[\text{Hg}^{2+}]_0$. Initial conditions: 1% agar gel, inner $[\text{Hg}^{2+}]_0 = 0.22\text{--}0.26$ M, $[\text{I}^-]_0 = 1.0\text{--}4.0$ M.

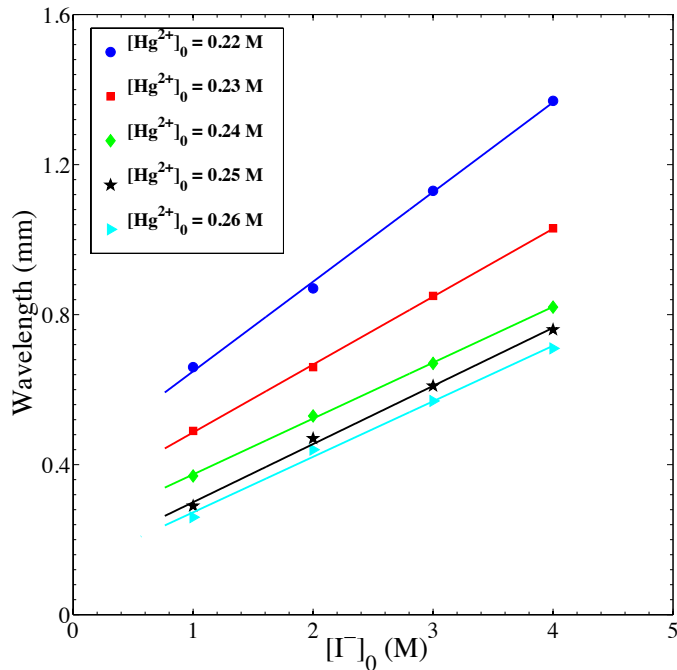


Fig. 3. 9 Plots of wavelength of spiral and ripple patterns versus outer $[\text{I}^-]_0$. Initial conditions: 1% agar gel, inner $[\text{Hg}^{2+}]_0 = 0.22\text{--}0.26$ M, $[\text{I}^-]_0 = 1.0\text{--}4.0$ M. Plots were fitted to a linear equation relating wavelength as a function of $[\text{I}^-]_0$. β (circle) = 0.24 ± 0.03 , β (square) = 0.18 ± 0.01 , β (diamond) = 0.15 ± 0.01 , β (star) = 0.16 ± 0.03 , β (triangle) = 0.15 ± 0.03 .

Figure 3.10 shows the displacement, with time, of three consecutive waves of a single ripple-like structure. The measurement of each wave starts at the moment the wave appears. From this figure, we deduce that the first wave leading the three travels at a relatively slower rate than the ones following it. As it appears on the plots, the velocities are relatively unequal, at a specified time interval (circled region on the plot) the velocity of the leading wave drops while the velocity of the second wave stays the same which allows it to gain up on it and gradually collide with it. Upon this front-to-back collision, the waves merge and form one large propagating front. The transition described between first and second wave, is clearly evident on the plot and is regularly expected to take place in ripples dynamics in this system. Such merging occurs when waves are separated by about 1 mm. A third wave also appears from the same nucleation site and follows the initial two waves. This wave is also expected to be faster than the wave directly in front of it, implying that it will also eventually collide with it. The part on the right in Fig 3.10 displays the spatio-temporal evolution of the ripple structure that is analyzed in the plots on the left and clarifies the described three waves and how they collide with each other leading to the breakup of the pattern. The plots in Fig. 3.10 also fit a time power law ($R \sim t^\alpha$), with power values all significantly above 0.5, clearly signifying superdiffusive dynamics. The first wave, appearing to be the slowest, has a power value of 0.62 followed by the second wave with power 0.84. This clarifies the reason leading the second wave to catch up with the first wave relatively fast. The third wave expressed a power value very close to 0.9, which could be evaluated to be traveling at a constant speed.

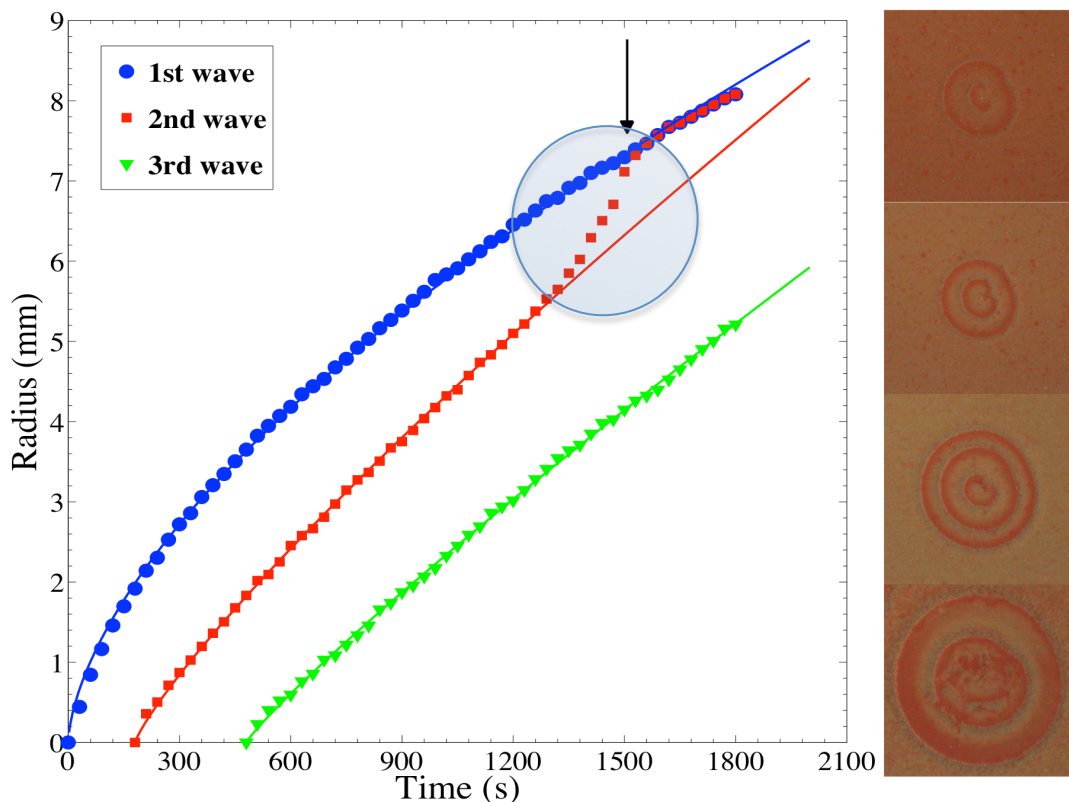


Fig. 3. 10 Plots of the radius traveled by the wavetrain of ripples, shown in the panels at the right-hand side of the graph, from nucleation site versus time. Represented are plots of three consecutive waves and their relative speeds. Initial conditions: 1% agar gel, inner $[\text{Hg}^{2+}]_0 = 0.23 \text{ M}$, $[\Gamma]_0 = 4.0 \text{ M}$. Plots were fitted to a power equation relating Radius $\sim (\text{Time})^\mu$. μ (circle) = 0.62 ± 0.01 , μ (square) = 0.84 ± 0.01 , μ (triangle) = 0.90 ± 0.01 . The arrow indicates the time at which the collision between wave 1 and 2 occurs. The circle indicates the transition dynamics when waves are about 1 mm close to each other.

e. Phase Wave

In our numerous experiments, we encountered a fourth very remarkable pattern that captured our attention. This pattern only survived for a short period of time of about 40–50 seconds. We named this pattern a “phase wave” owing to the way it evolves like a firing wave that invades the entire surface of the gel and comprises a mixture of the yellow and red polymorphs of HgI_2 . Figure 3.11 shows snapshots of the spatio-temporal evolution of a phase wave. The curious aspect about this pattern is that it does not arise

from any certain nucleation site, but it actually appears all over the area of the Petri dish forming a large spiral wave that eventually vanishes in the background. It has been reported that such phase waves have a crucial role in the creation of patterns in excitable media, but only when coupled with actual RD waves⁴⁰. Furthermore, we only observe this pattern instantly after initialization and it has the highest probability of occurrence specifically at outer iodide concentration of 1.0 M. There exist some rare occasions when this pattern appeared at an outer iodide concentration of 2.0 M, but is completely absent at concentrations of 3.0 M and above.

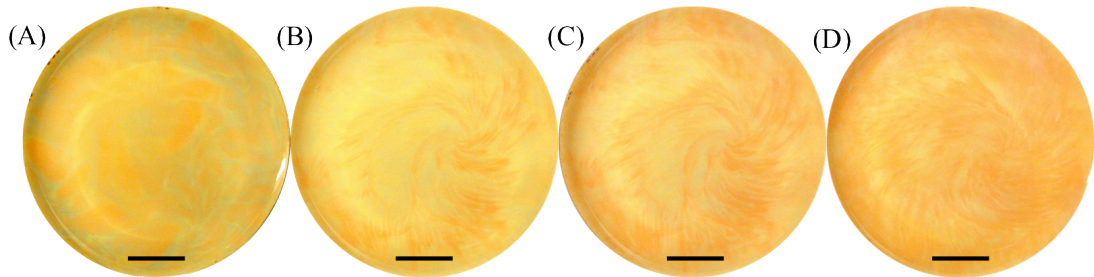


Fig. 3. 11 Evolution of the phase wave in HgI_2 with time (top view). Initial conditions: 1% agar gel, inner $[\text{Hg}^{2+}]_0 = 0.23 \text{ M}$, outer $[\text{I}^-]_0 = 1.0 \text{ M}$. (A) 5s (B) 15s (C) 25s (D) 35s, after initialization. The scale bar represents 1 cm.

f. Pattern Breakup

The transition from uniform patterns to spatio-temporal chaotic states has been encountered in many systems including RD processes¹³³⁻¹³⁶, fluid flows^{137,138}, cardiac tissue^{29,44}, and bacterial colonies¹³⁹. Specifically, a subject under extensive investigations is the spiral wave instability in a RD systems leading to shift to a state of defect-mediated turbulence^{140,141}. In this chapter, we also study the breakup dynamics the targets and spirals/ripples that are illustrated in Fig. 3.12. Even though the breakup

mechanisms appear to be different in the two cases, ultimately, in both, the entire system ends up in a state of defect-mediated turbulence.

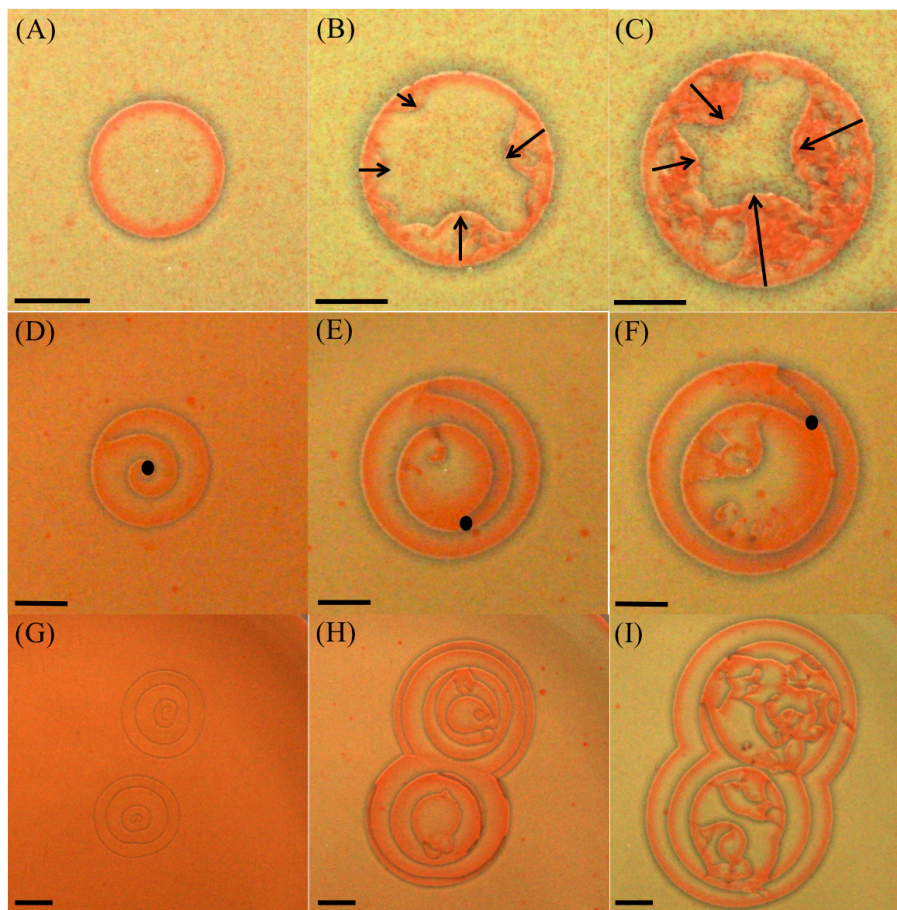


Fig. 3.12 Time evolution of the propagating wave patterns until their breakup. Initial conditions: 1% agar. Target breakup: $[\text{Hg}^{2+}]_0 = 0.26 \text{ M}$, $[\text{I}^-]_0 = 3.0 \text{ M}$; (A) 230 s (B) 395 s (C) 535 s; arrows indicate the direction of propagation of the defects. Spiral breakup: $[\text{Hg}^{2+}]_0 = 0.23 \text{ M}$, $[\text{I}^-]_0 = 4.0 \text{ M}$; (D) 180s (E) 345 s (F) 445 s; the black dots indicate the location of the tip of the spiral. Ripple breakup: $[\text{Hg}^{2+}]_0 = 0.24 \text{ M}$, $[\text{I}^-]_0 = 5.0 \text{ M}$; (G) 195 s (H) 425 s (I) 680 s. What is also interesting in this last series of snapshots is the merging of two ripples before destruction. Times reported represent the period after initialization. The scale bars represents 0.25 cm.

In Fig. 3.12 (A-C), we present the case of targets. Their breakup originates at the boundaries of the pattern, as defects at different locations distort the wave itself and form an irregular structure. These defects are special in the sense that they propagate inwards towards the nucleation center of the pattern, ending in a state of chemical

turbulence. The reason behind these defects is not entirely understood yet. However, bubbles that are still available in the gel and have not already nucleated a pattern or did not cause an adequate perturbation to nucleate a pattern, can sometimes behave as destabilizing factors. Furthermore, we confirm that at higher inner, $[\text{Hg}^{2+}]_0$ or outer, $[\Gamma]_0$ concentrations, the onset of the instability occurs earlier and the smaller the radius is before the target distorts.

Figure 3.12 (D-F) represents the case of spirals and Figure 3.12 (G-I) represents the case of ripples. Their breakup initiates at the core of the pattern and evolves outwards to form a number of new growths of smaller spirals leading to eventual chemical turbulence. The cause of the instability confronted by the spirals can be attributed to the Doppler effect similar to what is encountered in the BZ reaction¹³⁶. A Hopf bifurcation initiates this instability by operating on the spiral core, thus eventually resulting in significant meandering of the spiral tip towards its adjacent wave. As the tip meanders, it causes the whole pattern to breakup and produce additional perturbation sites, which in their turn increase the instability of the structure. Figure 3.12 (D-F) shows black dots that identify the position of the tip as it detaches and meanders from its initial pinning site (nucleation site). The aforementioned new perturbation sites also nucleate small spirals, which themselves meander causing an even more chaotic state. The new defects give rise to more defects, which in their turn add more to the pattern chaos producing a saturation of deformity and finally producing a state of chemical turbulence¹⁴². The increase in the control parameter $[\text{Hg}^{2+}]_0$, causes the acceleration in the transition to turbulence. As shown in Fig. 3.12 (D-I), the Doppler effect induces a continuous change in the local wavelength of the spiral or ripple, leading to the pattern breakup.

In our system, there also exists another way for the pattern to breakup and that is particular to spirals and ripples. As it is clear from their structures, they exhibit several propagating waves, developing from the same initial nucleation site. In ripples, as the first wave propagates temporally, its speed decreases thus allowing the second wave to catch up and collide with it (as previously explained). Upon this collision, a larger diffusing front is produced and in most of the cases the pattern loses its stability and breakups into a chaotic state.

It is important to note that the total number of waves fired, in the case of ripples, before breakup increases as a function of increasing initial concentration of the outer electrolyte $[I^-]_0$. Examples show in the case of $[I^-]_0$ more than or equal to 5.0 M, more than 5 waves can be fired by a single ripple, whereas in the case of $[I^-]_0$ less than or equal to 4.0 M, one can distinguish a maximum of 4 propagating waves for each ripple before breakup. The same breakup mechanism appears in spirals, in that the innermost turns become faster than the outer turn, therefore leading to their front-to-back collision and deformation of the structure. When obvious spatially altered waves emerge, the distance in space between consecutive waves varies. As the $[Hg^{2+}]_0$ increases, the amount of alterations increases thus leading to this kind of breakup¹⁴².

3. Relationship between chemical waves and cusped precipitation band

After investigating our system in both two- and three-dimensional setups, we design a new setup that can incorporate both dimensions at the same time. We construct a reactor made from plexi-glass having a rectangular prism structure. The dimensions of the prism are: 5 cm length \times 1 cm width \times 5 cm height. This prism is closed from all

sides except from one rectangular side through which we pour in the gel/inner (Hg^{2+}) mixture. The gel fills up two-thirds of the volume, thus leaving enough room for the outer (I^-) to be delivered at a later stage. This setup allows us to analyze what is happening from a top view on the surface of the gel, in terms of spirals and targets, and what is happening on the side view (under the spirals and targets), in terms of precipitation band and cusped wavefront. As always, we monitor all the experiments under our camera, which captures a snapshot every 5 seconds, thus producing an informative spatio-temporal evolution of the RD process. We place the camera in a way that forms an angle above the setup making it possible to capture both the surface and the side of the gel slab.

The early stages of the wavefront/pattern propagation show the clearest interpretation of what is happening on both the surface and the side of the gel. Figure 3.13 displays the evolution of two chemical waves on the surface and the cusp that is forming between them (all the forming cusps are a result of two chemical waves approaching each other). It is clear that from both sides of the appearing trapezoidal structure that the passive edges are extensions of the chemical wave, inserted inside the gel surface. As the two waves of the targets approach each other, we observe the two passive edges also approaching each other and the consequential decrease in length of the regressing edge of the wavefront. The formation of the pointy, triangular cusp does not indicate the collision of the two targets. The curved wavefront in the precipitation free region indicates that exact position of the chemical wave above it. Therefore, the moment when the two curved wavefronts in wedge-like, precipitate-free regions merge horizontally and become a straight propagating wavefront is the moment when the target waves collide. When this collision occurs, on the surface the red polymorph wave

is depleted and replaced by the quasi-steady yellow polymorph, which is also reflected in the stabilization of the wavefront in the precipitation band when it becomes linear.

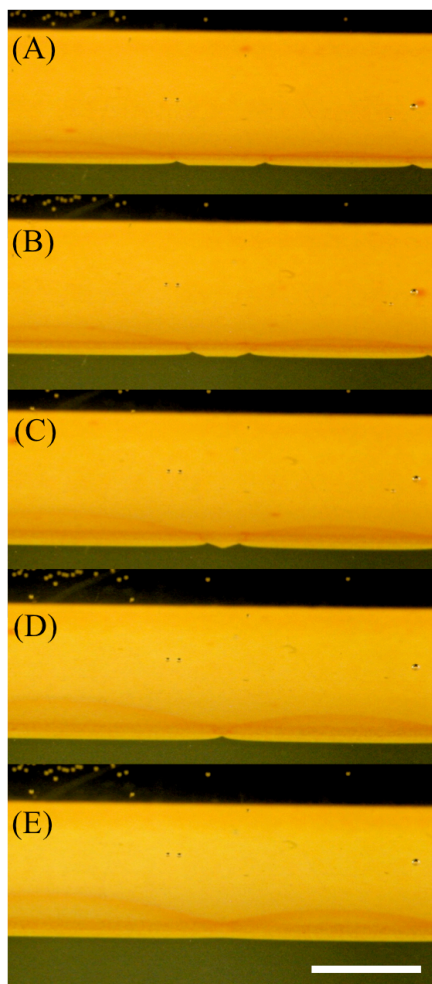


Fig. 3.13 Spatio-temporal evolution of the precipitation band in a rectangular gel slab, displaying both the features of the forming patterns on the surface and the cusps on the wavefront at the side-view of the gel. (A-B) Display the trapezoidal shape forming at the wavefront of the precipitation band with the passive edges protruding to form the chemical wave at the surface. (C) Formation of the triangular cusp. (D) Collision of the two chemical waves at the surface. (E) Annihilation of the both the chemical wave and cusp at the wavefront. Time after initialization: (A) 295 s, (B) 370 s, (C) 435 s, (D) 520 s, (E) 575 s. Initial conditions: 1% agar gel, inner $[\text{Hg}^{2+}]_0 = 0.21 \text{ M}$, $[\text{I}^-]_0 = 4.0 \text{ M}$. The scale bar represents 1.0 cm.

It is significant to notice that at the time the chemical waves, on the surface, lose stability and result in a chaotic state, several chemical waves collide with each other. From this we accordingly observe, on the side-view, a large amount of small cusp

pattern formations on the precipitation band that have very similar chaotic characteristics of what is happening on the surface.

Herein, we also inspect the impact of the initial reaction concentrations. As we have mentioned previously, the chemical wave patterns forming on the surface are constricted to nucleate in the so-called “excitable region” of inner mercuric concentration, which we find to exist between 0.16 and 0.26 M. The region appears to be in correlation with the aforementioned inflection region ($[\text{Hg}^{2+}]_0 = 0.16\text{--}0.19\text{ M}$) where the cusp formation on the precipitation band starts disappearing. Therefore, it is accurate to say that below 0.16 M inner mercuric concentration, no chemical waves or cusps in the precipitation band will appear.

CHAPTER IV

ALTERNATING METASTABLE/STABLE PATTERN OF THE CRYSTALLINE POLYMORPHS OUTSIDE THE OSTWALD RULE OF STAGES

The kinetic pathway leading to phase transformations during crystallization from amorphous phases and melts plays a crucial role in influencing the shapes and sizes of crystalline materials. Ultimately, this pathway expresses the final physical properties of the structures¹⁴³. In the remarkable work of Wilhelm Ostwald entitled “Studien ueber die Bildung und Umwandlung fester Koerper” (Studies of the formation and transformation of solid substances)¹⁰⁶, he writes a sentence that nowadays has shown great significance on research concerning transformations of crystalline states of different stabilities. The sentence reads: “When leaving a given state and in transforming to another state, the state which is sought out is not the thermodynamically stable one, but the state nearest in stability to the original state.” Today this statement is commonly recognized as the Ostwald’s Rule of Stages. To reformulate it in a simple manner, if a material is able to crystallize in several various forms, the initial structure it attains, by the means of, spontaneous crystallization, would have the least stability of all. This structure is consequently succeeded by structures of increasing stability until a final, most thermodynamically stable form is achieved. This brings forward the fact that there must exist intermediate metastable states appearing in the crystal growth process. Therefore, new perception about the kinetics of transformation during crystallization can be deduced from understanding the origin of these intermediate states. This as well

could be the primary crucial step towards controlling the overall crystallization behavior¹⁴⁴.

In this chapter, we present a system in which the precipitating mercuric iodide forms in a thin tube. The crystalline precipitate, as always, is produced in a gel media, which enforces steady growth of the crystals. This allows every stage of the HgI_2 polymorphic transformation to be thoroughly analyzed. A rather interesting phenomenon was discovered upon alteration of initial reaction concentrations. A region was found where the crystal growth progressed in an alternating method in which both the stable and metastable forms of HgI_2 coexisted.

A. Experimental Setup

In these experiments, the preparation of the gel mixture is exactly the same as previously explained, but the only difference is that the inner and outer electrolytes are swapped. After the completion of the gel/solution mixtures containing the inner electrolyte (I^-), we transfer them, by the means of a Pasteur pipette, to a thin tube of 6 mm diameter and about 20 cm length. We deliver around 2 mL of the solution, which fills up about two-thirds of the tube. We then cover the tubes with paraffin film and place them in the thermostatic chamber that maintains the temperature at 24.0 ± 0.2 °C. The gels are left for 2 hours for their gelation and aging processes to complete. After the mixtures have gelled, we transfer the outer electrolyte (Hg^{2+}) into the tube, also by the means of a Pasteur pipette, which initiates the reaction and produces a small circular precipitation layer that diffuses perpendicularly into the gel. The tubes are left for days for reaction and diffusion to proceed sufficiently. A snapshot of the tubes is taken every

24 hours to monitor the different stages of the diffusion accompanied by the polymorphic transformation.

B. Results and Discussion

At ambient conditions, it is very difficult to isolate the metastable orange and yellow polymorphs of HgI_2 , hence upon the slightest mechanical disturbance they readily transform into the thermodynamically stable red phase.

When the gel mixtures are ready, we initiate the reaction-diffusion process by simply delivering the outer electrolyte, Hg^{2+} , into the thin tubes. Directly at the moment the two initially separated electrolytes meet (gel interface), a ring of kinetically favored, unstable orange HgI_2 appears and starts diffusing down the tube forming a band of microscopically structured crystals. After a short period of time these crystals gradually transform to the metastable yellow (yellow^M) form. As the diffusion progresses, the major portion of the precipitation band is dominated by the yellow^M polymorph. Moreover, it exhibits a crystal structure that is more significant than the previously observed orange polymorph, in which it takes the form of fractals and threads with branching structures along their lengths. As the size of the precipitation band increases, a captivating polymorphic transformation occurs and converts the yellow^M polymorph into the final and thermodynamically favored form of HgI_2 , the red polymorph. The red crystals assume the structure of sharp needles and appear as if they are protruding out of the yellow fractals. The yellow^M crystals are always the main component of the leading front of the precipitation band. In the wake of this front, appears the polymorphic transformation, mostly happening at the center of the precipitation band where the

previously formed yellow^M crystals exist. The expected redissolution reaction, resulting from excess outer ions, also takes place in this setup, where the colorless K_2HgI_4 complex extends from the gel interface to the waveback of the precipitation band.

Typically in all our experiments the described sequence of diffusion and polymorphic transformation is what we regularly encounter. Yet while expanding our investigation to cover various alterations of initial concentrations (i.e. inner concentration, outer concentration and gel percentage), we discover a region that does not follow the typical evolution. The behavior of the precipitate formation and polymorphic transformation shows significant dependence on the inner electrolyte, $[I^-]_0$ concentration. To test this result, we prepare a range of different inner concentrations at constant outer concentration and constant gel percentage. We use outer, $[Hg^{2+}]_0 = 0.25$ M and inner, $[I^-]_0 = (0.005, 0.05, 0.10, 0.15)$ M in 1% agar gel. After reaction and diffusion proceed for a significant period of time (~ 1 week), we capture a snapshot of the tubes that we report in Fig. 4.1. Figure 4.1(A & B) represent the highest inner concentrations exhibiting the typical behavior of precipitation previously described. However, as we decrease the concentration (Fig. 4.1C) we realize that an alteration occurs in both the color and alignment of the precipitation band. In Fig. 4.1D, the behavior develops and actually becomes more noticeable in the tube containing the lowest concentration of the inner electrolyte. An interesting and abnormal coexistence of the metastable (yellow) polymorph and the stable (red) polymorph appears. The bands seem to arise from a mechanism very similar to what is previously perceived in the famous Liesegang bands^{2,145-149}. Nevertheless there happens to be a deviation in this type of banding, since the precipitate is continuous and no voids of none or minimal nucleation appear between precipitation rings. If it is to be compared with Liesegang

banding, we can assume that the red regions take the role of the nucleating bands and the yellow regions take the place of the voids. Furthermore, the tubes with high concentration gradients between the inner and outer electrolytes show the most significant redissolution reaction, occurring at the interface.

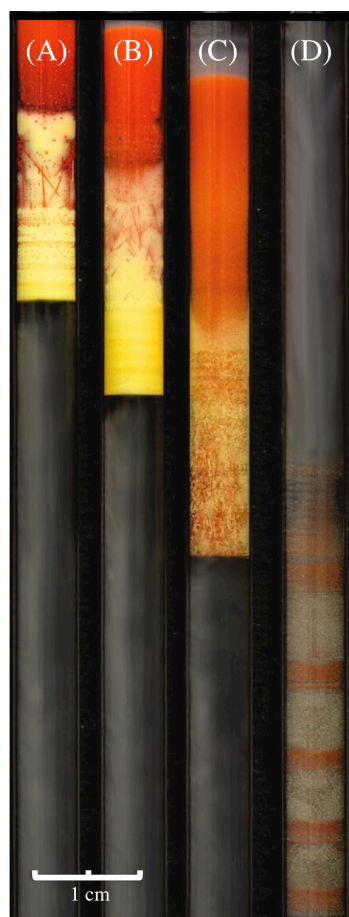


Fig. 4. 1 Snapshot of four tubes with different initial inner iodide concentrations expressing the features of the three concomitant HgI_2 polymorphs (orange-yellow-red). The tubes display the transition from the regular polymorphic transformation progression to the alternating regime. The black line at the edge of the tubes indicates the outer/inner electrolytes intersection (gel interface). Initial conditions: inner iodide concentration, $[\text{I}^-]_0 =$ (A) 0.15 M, (B) 0.10 M, (C) 0.05 M, (D) 0.005 M, all in 1% by volume agar gel; at constant outer mercuric concentration, $[\text{Hg}^{2+}]_0 = 0.25$ M. Scale bar represents 1.0 cm.

To particularly confirm this occurrence, we prepare a set of inner concentrations above and below this specific concentration (0.005 M) and we conclude that this behavior reproduces in the range between 0.003 and 0.006 M of inner $[\text{I}^-]_0$. We

reproduce the tube with the experimental parameters of: inner, $[I^-]_0 = 0.005$ M in 1% agar gel; outer $[Hg^{2+}]_0 = 0.25$ M many times and monitor its diffusion hourly. We then capture a snapshot every 24 hours to assemble a panel, reported in Fig. 4.2, representing the spatio-temporal progression of the precipitation band over a period of 9 days. From Fig. 4.2, we can clearly identify that at the early stages of the diffusion the major polymorph is the orange, which promptly transforms to the yellow^M polymorph. As the diffusion proceeds, the unexpected occurs, the metastable yellow polymorph does not actually transform to the stable red polymorph. From the thorough examination of numerous consecutive snapshots we capture of the evolution, we predict that each of the polymorphs appears separately. Initially the yellow grows for some time after which its production stops; next the red starts forming in the same manner. Ultimately through alternation of formation turns, the metastable/stable pattern is constructed. From Fig. 4.2, it is very evident that each produced band is perfectly stationary and does not diffuse through the length of the tube. At the late stages of the evolution, it is interesting to notice that the 'older' yellow^M bands that appear do not undergo the transformation to the stable red polymorph, yet actually dissolve upon the redissolution reaction taking place due to the excess outer ions. This aspect is clearly seen in the last 3 days in Fig. 4.2, because the formerly produced yellow parts have become nearly colorless and the remains in those regions are not entirely red. It is also worthy to state that the redissolution region increases proportionally as a function of time elapsed on the reaction.

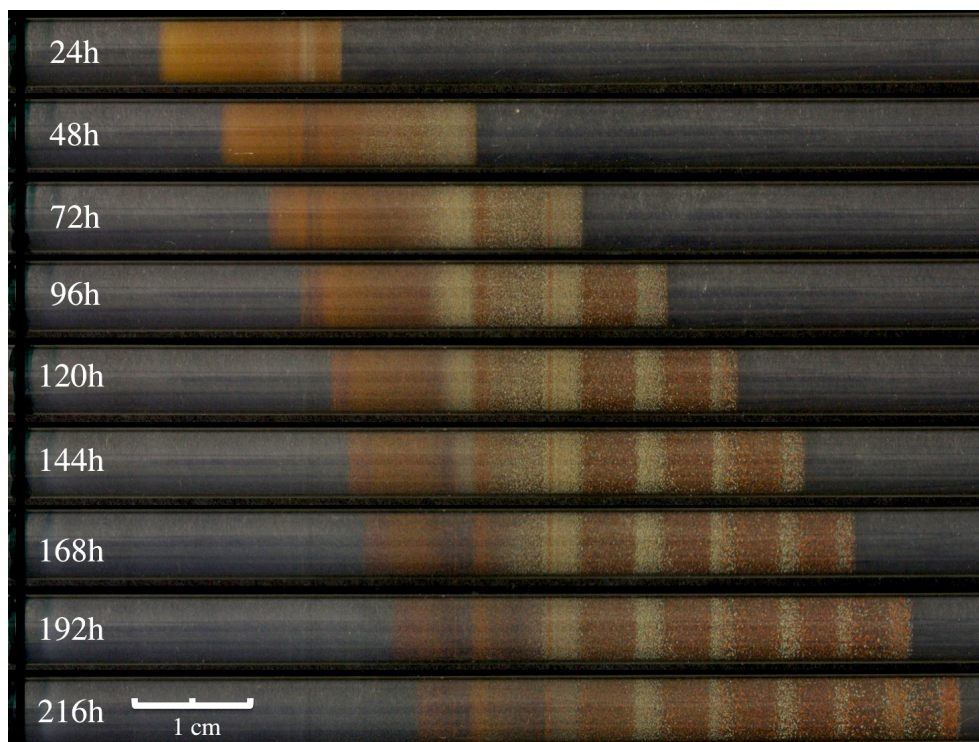


Fig. 4. 2 Panel of compiled snapshots of the daily evolution of the alternating yellow (metastable)/red (stable) pattern of the HgI_2 crystals. The black line at the edge of the tubes indicates the outer/inner electrolytes intersection (gel interface). Initial conditions: inner iodide concentration, $[\text{I}^-]_0 = 0.005 \text{ M}$ in 1% by volume agar gel; at constant outer mercuric concentration, $[\text{Hg}^{2+}]_0 = 0.25 \text{ M}$. Scale bar represents 1.0 cm.

In 1897, Ostwald implied, in his step rule of stages, that there exists metastable intermediate states, when he stated it is not necessary for system in an unstable state to transform directly into the most thermodynamically stable state¹⁰⁶. This rule unquestionably applies to many experimental processes, including our system and many other formerly reported systems similar to ours. Such cases have been encountered in the polymorphic transformation of nickel and cobalt hydroxide precipitates^{90,145,150,151}. Yet in the mercuric iodide system, the alternating pattern between the metastable and stable forms of the crystals is not ordinary. In this region of concentration ($[\text{I}^-]_0 = 0.003\text{--}0.006 \text{ M}$), the system adopts a behavior that favors oscillatory crystal formation after a transition happens in which the crystal transformation stops abiding by the

Ostwald rule of stages. This unusual behavior might be due to a physical instability caused by a bifurcation, where the interplay of reaction-diffusion with nucleation, growth and competitive particle sizes, all play a fundamental role.

CHAPTER V

CONCLUSION

A. Summary

In this work, we carry out reaction-diffusion experiments comprising the growth of crystalline mercuric iodide precipitate, in an agar gel media, from the coprecipitates mercuric chloride and potassium iodide. One solution is placed in the gel mixture and forms the inner electrolyte system and the second solution serves as the outer electrolyte. The mercuric iodide precipitate undergoes a spectacular polymorphic transformation between its three concomitant polymorphs. This transformation is also accompanied by the redissolution of the precipitate upon excess outer concentrations.

First, we study this system in a two dimensional setup, which produces a thin radially propagating precipitation band. Altering initial reaction conditions lead to the formation of cusp-like patterns of the precipitation front. The inner mercuric concentration in this case, imposed an effect on the structure of the band. At high concentrations the band formed irregular cusp patterns of the wavefront and waveback, yet at low concentrations the irregularity vanishes to expose a regular ring-like band. On the other hand, the outer iodide concentration played an important role in changing the dynamics of the reaction. As the concentration of the outer increased from 1.0 M to 6.0 M, the diffusivity of the propagating band changed from being superdiffusive (4.0 M and below) to being normally diffusive and abiding by the Fickian law (at around 5.0 M) then reaching a subdiffusive regime (at values above 5.0 M). The concentration of

the gel exhibited no influence on cusp pattern formation or on the anomalous diffusion of the precipitation band, but only altered the speed of propagation in which the higher percentages showed slower propagation. On the microscopic level, the situation was also complex. SEM images displayed the morphology of the crystal structures and sizes of both yellow^M and red polymorphs and revealed the existence of an Ostwald ripening mechanism accompanying the polymorphic transformation.

Second, we investigated the system in a three-dimensional setup, in which an interesting collection of self-organized patterns was observed in this heterogeneous system that consists of a reaction-diffusion process. The patterns that nucleated include: single-wave circular targets, spirals and ripples appearing like cardioid structures. They all undergo the HgI₂ polymorphic transformation and also experience instabilities that cause their breakup and lead to chemical turbulence. We present that the dynamics of the propagating waves are superdiffusive and this fact constitutes the first example of this kind in chemistry without external forcing. This finding will definitely open new realms of investigation aiming towards understanding this anomalous behavior and predicting theoretical modeling of the forming patterns.

Third, we analyze in a thin tube (one-dimensional setup) the mercuric iodide system precipitating and undergoing the polymorphic transformation of its three coexistent polymorphs: the orange (unstable), yellow (metastable) and red (stable). The usual progression of crystal conversion is established to initiate with the unstable orange polymorph and terminate with the most thermodynamically stable red polymorph via the metastable yellow polymorph (intermediate). This confirms that the kinetic pathway of crystalline form alteration abides by the Ostwald rule of stages. However, we discover a region of specific inner mercuric concentration at which a pattern of

alternating metastable and stable crystals unveils. In this region, the crystal growth mechanism undergoes an oscillatory behavior rather than the usual sequence of growth, which leads to the formation of a stationary pattern of yellow and red HgI_2 crystals. A model that incorporates reaction-diffusion, nucleation and growth to interpret the polymorphic alternation pattern, is under construction.

B. Future Work

A main concern in future endeavors is to propose a feasible mechanism that includes precipitation of the initial unstable HgI_2 precipitate. This first precipitate could be either the orange polymorph or at a different probability the yellow polymorph ($\beta\text{-HgI}_2$). Next, the mechanism must somehow explain the polymorphic transformation that readily converts the $\beta\text{-HgI}_2$ to $\alpha\text{-HgI}_2$, and also include the important redissolution reaction occurring as a result of excess outer concentration. In addition, a feedback intermediate reaction should be predicted that could aid explain the origin of creation of the patterns perceived in the HgI_2 precipitate. The propagation mechanism, generally, incorporates the coupling of transport with a positive feedback process, such as the coupling of autocatalytic chemical reaction with diffusion in the classic example of chemical waves⁴¹. A very important feature, yet complex parameter that should be explained in the model is the superdiffusive behavior of the chemical waves. This brings upon even further difficulty in achieving a complete mathematical model that can describe our system.

A second major interest is the aspect of being able to stabilize the nucleating patterns and reducing their breakup and thus decreasing the chaotic states of the system.

This is going to be investigated by applying external forcing onto the patterns. Such forcing would include: thermal, chemical, electrical, etc. alterations^{152,153} to reduce or suppress pattern instabilities and chemical turbulence¹⁵⁴.

REFERENCES

- (1) Grzybowski, B. *Chemistry in Motion: Reaction-diffusion Systems for Micro- and Nanotechnology*; Wiley Online Library: 2009.
- (2) Liesegang, R., Ueber Einige Eigenschaften Von Gallerten, *Naturwissenschaftliche Wochenschrift* **1896**, *10*, 353-362.
- (3) Zrinyi, M.; Galfi, L.; Smidroczi, E.; Racz, Z.; Horkay, F., Direct Observation of a Crossover from Heterogeneous Traveling Wave to Liesegang Pattern Formation, *Journal of Physical Chemistry* **1991**, *95*, 1618-1620.
- (4) Lagzi, I.; Ueyama, D., Pattern Transition between Periodic Liesegang Pattern and Crystal Growth Regime in Reaction–Diffusion Systems, *Chemical Physics Letters* **2009**, *468*, 188-192.
- (5) Leduc, S. *Théorie Physico-Chimique De La Vie Et Générations Spontanées*; A. Poinat, 1910; Vol. 1.
- (6) Murray, J. D. *Mathematical Biology*; New York: Springer, 2002; Vol. 2.
- (7) Newman, E. A.; Zahs, K. R., Calcium Waves in Retinal Glial Cells, *Science* **1997**, *275*, 844-847.
- (8) Ben-Jacob, E.; Schochet, O.; Tenenbaum, A.; Cohen, I.; Czirok, A.; Vicsek, T., Generic Modelling of Cooperative Growth Patterns in Bacterial Colonies, *Nature* **1994**, *368*, 46-49.
- (9) Jackson, J. A.; Mehl, J. P.; Neuendorf, K. K. E. *Glossary of Geology*; New York: Springer, 2005.
- (10) Meinhardt, H. *The Algorithmic Beauty of Sea Shells*; New York: Springer, 2009.
- (11) Turing, A. M., Chemical Basis of Morphogenesis, *Transactions of the Royal Society (London)* **1952**, *B237*, 37-72.
- (12) Zaikin, A.; Zhabotinsky, A., Concentration Wave Propagation in Two-Dimensional Liquid-Phase Self-Oscillating System, *Nature* **1970**, *225*, 535-537.
- (13) Castets, V.; Dulos, E.; Boissonade, J.; De Kepper, P., Experimental Evidence of a Sustained Standing Turing-Type Nonequilibrium Chemical Pattern, *Physical Review Letters* **1990**, *64*, 2953-2956.

- (14) Asakura, K.; Konishi, R.; Nakatani, T.; Nakano, T.; Kamata, M., Turing Pattern Formation by the Cima Reaction in a Chemical System Consisting of Quaternary Alkyl Ammonium Cationic Groups, *Journal of Physical Chemistry B* **2011**, *115*, 3959-3963.
- (15) Ball, P. *The Self-Made Tapestry: Pattern Formation in Nature*; Oxford Univ. Press, Oxford, 1999.
- (16) Bading, H., Nuclear Calcium Signalling in the Regulation of Brain Function, *Nature Reviews Neuroscience* **2013**, *14*, 593-608.
- (17) Dolmetsch, R. E.; Xu, K.; Lewis, R. S., Calcium Oscillations Increase the Efficiency and Specificity of Gene Expression, *Nature* **1998**, *392*, 933-936.
- (18) Straub, S. V.; Giovannucci, D. R.; Yule, D. I., Calcium Wave Propagation in Pancreatic Acinar Cells Functional Interaction of Inositol 1, 4, 5-Trisphosphate Receptors, Ryanodine Receptors, and Mitochondria, *The Journal of General Physiology* **2000**, *116*, 547-560.
- (19) Mair, T.; Warnke, C.; Tsuji, K.; Müller, S. C., Control of Glycolytic Oscillations by Temperature, *Biophysical Journal* **2005**, *88*, 639-646.
- (20) Dzeja, P. P.; Terzic, A., Phosphotransfer Reactions in the Regulation of ATP-Sensitive K⁺ Channels, *The FASEB journal* **1998**, *12*, 523-529.
- (21) Dzeja, P. P.; Terzic, A., Phosphotransfer Networks and Cellular Energetics, *Journal of Experimental Biology* **2003**, *206*, 2039-2047.
- (22) Hess, B., Periodic Patterns in Biology, *Naturwissenschaften* **2000**, *87*, 199-211.
- (23) Garfinkel, A.; Kim, Y.-H.; Voroshilovsky, O.; Qu, Z.; Kil, J. R.; Lee, M.-H.; Karagueuzian, H. S.; Weiss, J. N.; Chen, P.-S., Preventing Ventricular Fibrillation by Flattening Cardiac Restitution, *Proceedings of the National Academy of Sciences* **2000**, *97*, 6061-6066.
- (24) Weiss, J. N.; Garfinkel, A.; Karagueuzian, H. S.; Qu, Z.; Chen, P.-S., Chaos and the Transition to Ventricular Fibrillation a New Approach to Antiarrhythmic Drug Evaluation, *Circulation* **1999**, *99*, 2819-2826.
- (25) Newman, S. A.; Frisch, H. L., Dynamics of Skeletal Pattern Formation in Developing Chick Limb, *Science* **1979**, *205*, 662-668.
- (26) Camazine, S. *Self-Organization in Biological Systems*; Princeton University Press, 2003.
- (27) Nelkin, M.; Meneveau, C.; Sreenivasan, K. R.; Peng, C. K., Dynamics of Formation of Symmetrical Patterns by Chemotactic Bacteria, *Nature* **1995**, *376*, 49-53.

- (28) Kondo, S., The Reaction-Diffusion System: A Mechanism for Autonomous Pattern Formation in the Animal Skin, *Genes to Cells* **2002**, *7*, 535-541.
- (29) Gilmour, R. F., A Novel Approach to Identifying Antiarrhythmic Drug Targets, *Drug Discovery Today* **2003**, *8*, 162-167.
- (30) Göktepe, S.; Wong, J.; Kuhl, E., Atrial and Ventricular Fibrillation: Computational Simulation of Spiral Waves in Cardiac Tissue, *Archive of Applied Mechanics* **2010**, *80*, 569-580.
- (31) Allègre, C. J.; Provost, A.; Jaupart, C., Oscillatory Zoning: A Pathological Case of Crystal Growth, *Nature* **1981**, *294*, 223-228.
- (32) Haase, C. S.; Chadam, J.; Feinn, D.; Ortoleva, P., Oscillatory Zoning in Plagioclase Feldspar, *Science* **1980**, *209*, 272-274.
- (33) Reeder, R. J.; Fagioli, R. O.; Meyers, W. J., Oscillatory Zoning of Mn in Solution-Grown Calcite Crystals, *Earth-Science Reviews* **1990**, *29*, 39-46.
- (34) Heaney, P. J.; Davis, A. M., Observation and Origin of Self-Organized Textures in Agates, *Science* **1995**, *269*, 1562-1565.
- (35) Short, M. B.; Baygents, J. C.; Beck, J. W.; Stone, D. A.; Toomey III, R. S.; Goldstein, R. E., Stalactite Growth as a Free-Boundary Problem: A Geometric Law and Its Platonic Ideal, *Physical Review Letters* **2005**, *94*, 018501.
- (36) Chopard, B.; Herrmann, H. J.; Vicsek, T., Structure and Growth Mechanism of Mineral Dendrites, *Nature* **1991**, *353*, 409-412.
- (37) Grzybowski, B. A.; Bishop, K. J.; Campbell, C. J.; Fialkowski, M.; Smoukov, S. K., Micro- and Nanotechnology Via Reaction-Diffusion, *Soft Matter* **2005**, *1*, 114-128.
- (38) Kapral, R.; Showalter, K. *Chemical Waves and Patterns*; Kluwer Academic Pub, 1995.
- (39) Mikhailov, A. S.; Showalter, K., Control of Waves, Patterns and Turbulence in Chemical Systems, *Physics Reports* **2006**, *425*, 79-194.
- (40) Ross, J.; Muller, S. C.; Vidal, C., Chemical Waves, *Science* **1988**, *240*, 460-465.
- (41) Cross, M. C.; Hohenberg, P. C., Pattern Formation Outside of Equilibrium, *Reviews of Modern Physics* **1993**, *65*, 851-1112.
- (42) Panfilov, A.; Keldermann, R.; Nash, M., Drift and Breakup of Spiral Waves in Reaction-Diffusion-Mechanics Systems, *Proceedings of the National Academy of Sciences* **2007**, *104*, 7922-7926.

- (43) Loose, M.; Fischer-Friedrich, E.; Ries, J.; Kruse, K.; Schwille, P., Spatial Regulators for Bacterial Cell Division Self-Organize into Surface Waves in Vitro, *Science* **2008**, *320*, 789-792.
- (44) Weise, L. D.; Panfilov, A. V., New Mechanism of Spiral Wave Initiation in a Reaction-Diffusion-Mechanics System, *PloS one* **2011**, *6*, e27264.
- (45) Field, R. J.; Burger, M., Oscillations and Traveling Waves in Chemical Systems, New York: Wiley, 1985.
- (46) Meron, E., Pattern Formation in Excitable Media, *Physics Reports* **1992**, *218*, 1-66.
- (47) Luther, R., II. Sitzung Am Dienstag, Den 22. Mai, Vormittags 9 Uhr, Im Grossen Auditorium Des Chemischen Laboratoriums Der Technischen Hochschule. Räumliche Fortpflanzung Chemischer Reaktionen, *Zeitschrift für Elektrochemie Und Angewandte Physikalische Chemie* **1906**, *12*, 596-600.
- (48) Fisher, R. A., The Wave of Advance of Advantageous Genes, *Annals of Eugenics* **1937**, *7*, 355-369.
- (49) Kolmogorov, A.; Petrovsky, I.; Piskunov, N., Investigation of a Diffusion Equation Connected to the Growth of Materials, and Application to a Problem in Biology, *Bull. Univ. Moscow, Ser. Int. Sec. A* **1937**, 1-25.
- (50) Bray, W. C., A Periodic Chemical Reaction and Its Mechanism, *Journal of the American Chemical Society* **1921**, *43*, 1262.
- (51) Zhabotinsky, A. M., Periodic Liquid Phase Reactions, *Proceedings of the National Academy of Sciences USSR* **1964**, *157*, 392-395.
- (52) Zhabotinsky, A. M.; Zaikin, A. N., Autowave Processes in a Distributed Chemical System, *Journal of Theoretical Biology* **1973**, *40*, 45-61.
- (53) Winfree, A. T., Spiral Waves of Chemical Activity, *Science* **1972**, *175*, 634-636.
- (54) Winfree, A. T., Scroll-Shaped Waves of Chemical Activity in Three Dimensions, *Science* **1973**, *181*, 937-939.
- (55) Zhabotinsky, A. M.; Zaikin, A. N., Spatial Effects in a Self-Oscillating Chemical System, *Oscillatory Processes in Biological and Chemical Systems II*, Sel'Kov E. E. Ed., Science Publications, Puschino, **1971**.
- (56) Müller, S. C.; Plesser, T.; Hess, B., The Structure of the Core of the Spiral Wave in the Belousov-Zhabotinskii Reaction, *Science* **1985**, *230*, 661-663.

- (57) Müller, S. C.; Plesser, T.; Hess, B., Two-Dimensional Spectrophotometry and Pseudo-Color Representation of Chemical Reaction Patterns, *Naturwissenschaften* **1986**, *73*, 165-179.
- (58) Field, R. J.; Koros, E.; Noyes, R. M., Oscillations in Chemical Systems. II. Thorough Analysis of Temporal Oscillation in the Bromate-Cerium-Malonic Acid System, *Journal of the American Chemical Society* **1972**, *94*, 8649-8664.
- (59) Field, R. J.; Noyes, R. M. In *Faraday Symp. Chem. Soc.*; The Royal Society of Chemistry **1974**, *9*, 21-27.
- (60) Turanyi, T.; Gyorgyi, L.; Field, R. J., Analysis and Simplification of the GTF Model of the Belousov-Zhabotinskii Reaction, *Journal of Physical Chemistry* **1993**, *97*, 1931-1941.
- (61) Gray, P.; Scott, S. K. *Chemical Oscillations and Instabilities: Non-Linear Chemical Kinetics*; Clarendon Press. Oxford University Press, 1990.
- (62) Rotermund, H. H., Imaging of Dynamic Processes on Surfaces by Light, *Surface Science Reports* **1997**, *29*, 265-364.
- (63) Imbihl, R.; Ertl, G., Oscillatory Kinetics in Heterogeneous Catalysis, *Chemical Reviews* **1995**, *95*, 697-733.
- (64) Bär, M.; Zülicke, C.; Eiswirth, M.; Ertl, G., Theoretical Modeling of Spatiotemporal Self - Organization in a Surface Catalyzed Reaction Exhibiting Bistable Kinetics, *The Journal of Chemical Physics* **1992**, *96*, 8595-8604.
- (65) Nettesheim, S.; Von Oertzen, A.; Rotermund, H. H.; Ertl, G., Reaction Diffusion Patterns in the Catalytic Co Oxidation on Pt (110): Front Propagation and Spiral Waves, *The Journal of Chemical Physics* **1993**, *98*, 9977-9985.
- (66) Jakubith, S.; Rotermund, H.; Engel, W.; Von Oertzen, A.; Ertl, G., Spatiotemporal Concentration Patterns in a Surface Reaction: Propagating and Standing Waves, Rotating Spirals, and Turbulence, *Physical Review Letters* **1990**, *65*, 3013-3016.
- (67) Rotermund, H. H.; Engel, W.; Kordesch, M.; Ertl, G., Imaging of Spatio-Temporal Pattern Evolution During Carbon Monoxide Oxidation on Platinum, *Nature* **1990**, *343*, 355-357.
- (68) Ziff, R. M.; Gulari, E.; Barshad, Y., Kinetic Phase Transitions in an Irreversible Surface-Reaction Model, *Physical Review Letters* **1986**, *56*, 2553-2556.
- (69) Imbihl, R.; Cox, M. P.; Ertl, G.; Müller, H.; Brenig, W., Kinetic Oscillations in the Catalytic Co Oxidation on Pt (100): Theory, *The Journal of Chemical Physics* **1985**, *83*, 1578-1587.

- (70) Krischer, K.; Eiswirth, M.; Ertl, G., Oscillatory Co Oxidation on Pt (110): Modeling of Temporal Self - Organization, *The Journal of Chemical Physics* **1992**, *96*, 9161-9172.
- (71) Falcke, M.; Engel, H., Pattern Formation During the Co Oxidation on Pt (110) Surfaces under Global Coupling, *The Journal of Chemical Physics* **1994**, *101*, 6255-6263.
- (72) Bertram, M.; Beta, C.; Pollmann, M.; Mikhailov, A. S.; Rotermund, H. H.; Ertl, G., Pattern Formation on the Edge of Chaos: Experiments with Co Oxidation on a Pt (110) Surface under Global Delayed Feedback, *Physical Review E* **2003**, *67*, 036208.
- (73) Bär, M.; Eiswirth, M., Turbulence Due to Spiral Breakup in a Continuous Excitable Medium, *Physical Review E* **1993**, *48*, R1635.
- (74) Naota, T.; Koori, H., Molecules That Assemble by Sound: An Application to the Instant Gelation of Stable Organic Fluids, *Journal of the American Chemical Society* **2005**, *127*, 9324-9325.
- (75) Rahbani, J.; Behzad, A. R.; Khashab, N. M.; Al-Ghoul, M., Characterization of Internal Structure of Hydrated Agar and Gelatin Matrices by Cryo-Sem, *Electrophoresis* **2013**, *34*, 405-408.
- (76) Cudney, R.; Patel, S.; McPherson, A., Crystallization of Macromolecules in Silica Gels, *Acta Crystallographica Section D: Biological Crystallography* **1994**, *50*, 479-483.
- (77) Hensch, H. K. *Crystals in Gels and Liesegang Rings*; Cambridge University Press, 2005.
- (78) Hantz, P., Pattern Formation in the NaOH + CuCl₂ Reaction, *The Journal of Physical Chemistry B* **2000**, *104*, 4266-4272.
- (79) Hantz, P., Pattern formation in a new class of precipitation reactions, Doctorate of Sciences thesis (Physics), University of Geneva, 2006.
- (80) Volford, A.; Izsák, F.; Ripszám, M.; Lagzi, I., Pattern Formation and Self-Organization in a Simple Precipitation System, *Langmuir* **2007**, *23*, 961-964.
- (81) Murray, J. D. *Mathematical biology*; New York: Springer: 2002.
- (82) Tang, J.; Yi, M.; Chen, P.; Luo, J.; Ma, J.; Xia, H., The Influence of Diversity on Spiral Wave in the Cardiac Tissue, *EPL (Europhysics Letters)* **2012**, *97*, 28003.
- (83) Klages, R.; Radons, G.; Sokolov, I. M. *Anomalous Transport: Foundations and Applications*; Wiley, 2008.

- (84) Dubkov, A. A.; Spagnolo, B.; Uchaikin, V. V., Lévy Flight Superdiffusion: An Introduction, *International Journal of Bifurcation and Chaos* **2008**, *18*, 2649-2672.
- (85) von Kameke, A.; Huhn, F.; Fernández-García, G.; Muñuzuri, A.; Pérez-Muñuzuri, V., Propagation of a Chemical Wave Front in a Quasi-Two-Dimensional Superdiffusive Flow, *Physical Review E* **2010**, *81*, 066211.
- (86) Fernández-García, G.; Pérez-Muñuzuri, V., Superdiffusive Wave Front Propagation in a Chemical Active Flow, *The European Physical Journal Special Topics* **2008**, *165*, 169-174.
- (87) Han, S.; Hermans, T. M.; Fuller, P. E.; Wei, Y.; Grzybowski, B. A., Transport into Metal–Organic Frameworks from Solution Is Not Purely Diffusive, *Angewandte Chemie* **2012**, *124*, 2716-2720.
- (88) Vanag, V. K.; Epstein, I. R., Inwardly Rotating Spiral Waves in a Reaction-Diffusion System, *Science* **2001**, *294*, 835-837.
- (89) Wood, P. M.; Ross, J., A Quantitative Study of Chemical Waves in the Belousov–Zhabotinsky Reaction, *The Journal of Chemical Physics* **1985**, *82*, 1924-1936.
- (90) Al-Ghoul, M.; Ammar, M.; Al-Kaysi, R. O., Band Propagation, Scaling Laws and Phase Transition in a Precipitate System. I: Experimental Study, *Journal of Physical Chemistry A* **2012**, *116*, 4427-4437.
- (91) Boffetta, G.; De Lillo, F.; Musacchio, S., Anomalous Diffusion in Confined Turbulent Convection, *Physical Review E* **2012**, *85*, 066322.
- (92) Paoletti, M.; Nugent, C.; Solomon, T., Synchronization of Oscillating Reactions in an Extended Fluid System, *Physical Review Letters* **2006**, *96*, 124101.
- (93) Bouchaud, J.-P.; Georges, A., Anomalous Diffusion in Disordered Media: Statistical Mechanisms, Models and Physical Applications, *Physics Reports* **1990**, *195*, 127-293.
- (94) Noszticzius, Z.; Bodnar, Z.; Garamszegi, L.; Wittmann, M., Hydrodynamic Turbulence and Diffusion-Controlled Reactions: Simulation of the Effect of Stirring on the Oscillating Belousov-Zhabotinskii Reaction with the Radicalator Model, *Journal of Physical Chemistry* **1991**, *95*, 6575-6580.
- (95) Bube, R. H., Opto-Electronic Properties of Mercuric Iodide, *Physical Review* **1957**, *106*, 703.
- (96) Piechotka, M., Mercuric Iodide for Room Temperature Radiation Detectors. Synthesis, Purification, Crystal Growth and Defect Formation, *Materials Science and Engineering: R: Reports* **1997**, *18*, 1-98.

- (97) Hostettler, M.; Birkedal, H.; Schwarzenbach, D., Polymorphs and Structures of Mercuric Iodide, *CHIMIA International Journal for Chemistry* **2001**, *55*, 541-545.
- (98) Das, I.; Pushkarna, A.; Agrawal, N. R., Chemical Waves and Light-Induced Spatial Bifurcation in the Mercuric Chloride-Potassium Iodide System in Gel Media, *Journal of Physical Chemistry* **1989**, *93*, 7269-7275.
- (99) Das, I.; Pushkarna, A.; Bhattacharjee, A., New Results on Light-Induced Spatial Bifurcation and Electrical Field Effect on Chemical Waves in the Mercury (II) Chloride-Potassium Iodide System in Gel Media, *Journal of Physical Chemistry* **1990**, *94*, 8968-8973.
- (100) Das, I.; Pushkarna, A.; Bhattacharjee, A., Dynamic Instability and Light-Induced Spatial Bifurcation of Mercuric Iodide and External Electric Field Experiments in Two-Dimensional Gel Media, *Journal of Physical Chemistry* **1991**, *95*, 3866-3873.
- (101) Jeffrey, G. A.; Vlasse, M., Crystal Structures of the Red, Yellow, and Orange Forms of Mercuric Iodide, *Inorganic Chemistry* **1967**, *6*, 396-399.
- (102) Hostettler, M.; Birkedal, H.; Schwarzenbach, D., The Structure of Orange HgI₂. I. Polytypic Layer Structure, *Acta Crystallographica Section B: Structural Science* **2002**, *58*, 903-913.
- (103) Hostettler, M.; Schwarzenbach, D., The Structure of Orange HgI₂. II. Diamond-Type Structure and Twinning, *Acta Crystallographica Section B: Structural Science* **2002**, *58*, 914-920.
- (104) Hostettler, M.; Birkedal, H.; Schwarzenbach, D., The Yellow Polymorphs of Mercuric Iodide (HgI₂), *Helvetica Chimica Acta* **2003**, *86*, 1410-1422.
- (105) Hostettler, M.; Schwarzenbach, D., Phase Diagrams and Structures of HgX₂ (X= I, Br, Cl, F), *Comptes Rendus Chimie* **2005**, *8*, 147-156.
- (106) Ostwald, W., Studies on the Formation and Inversion of Solids. First Paper: Supersaturation and Supercooling, *Zeitschrift für Physikalische Chemie, Stoechiometrie und Verwandtschaftslehre* **1897**, *22*, 289.
- (107) Deutsch, A.; Dormann, S. *Cellular Automaton Modeling of Biological Pattern Formation: Characterization, Applications, and Analysis*; Springer, 2005.
- (108) Gálfi, L.; Rácz, Z., Properties of the Reaction Front in an A+ B→ C Type Reaction-Diffusion Process, *Physical Review A* **1988**, *38*, 3151.
- (109) Koza, Z.; Taitelbaum, H., Motion of the Reaction Front in the A+ B→ C Reaction-Diffusion System, *Physical Review E* **1996**, *54*, R1040.

- (110) Mansour, A. A.; Al Ghouli, M., Scaling and Crossover Dynamics in the Hyperbolic Reaction-Diffusion Equations of Initially Separated Components, *Physical Review E* **2011**, *84*, 026107.
- (111) van Baalen, G.; Schenkel, A.; Wittwer, P., Asymptotics of Solutions in $A + B \rightarrow C$ Reaction-Diffusion Systems, *Communications in Mathematical Physics* **2000**, *210*, 145-176.
- (112) Cornell, S.; Droz, M.; Chopard, B., Role of Fluctuations for Inhomogeneous Reaction-Diffusion Phenomena, *Physical Review A* **1991**, *44*, 4826.
- (113) Larralde, H.; Araujo, M.; Havlin, S.; Stanley, H. E., Reaction Front for $A + B \rightarrow C$ Diffusion-Reaction Systems with Initially Separated Reactants, *Physical Review A* **1992**, *46*, 855.
- (114) Taitelbaum, H.; Yen, A.; Kopelman, R.; Havlin, S.; Weiss, G. H., Effects of Bias on the Kinetics of $A + B \rightarrow C$ with Initially Separated Reactants, *Physical Review E* **1996**, *54*, 5942.
- (115) Horvát, S.; Hantz, P., Pattern Formation Induced by Ion-Selective Surfaces: Models and Simulations, *The Journal of Chemical Physics* **2005**, *123*, 034707.
- (116) Koo, Y. E.; Li, L.; Kopelman, R., Reaction Front Dynamics in Diffusion-Controlled Particle-Antiparticle Annihilation: Experiments and Simulations, *Molecular Crystals and Liquid Crystals* **1990**, *183*, 187-192.
- (117) Léger, C.; Argoul, F.; Bazant, M. Z., Front Dynamics During Diffusion-Limited Corrosion of Ramified Electrodeposits, *Journal of Physical Chemistry B* **1999**, *103*, 5841-5851.
- (118) Tinsley, M. R.; Collison, D.; Showalter, K., Propagating Precipitation Waves: Experiments and Modeling, *Journal of Physical Chemistry A* **2013**, *117*, 12719-12725.
- (119) Sultan, R.; Sadek, S., Patterning Trends and Chaotic Behavior in $\text{Co}^{2+}/\text{NH}_4\text{OH}$ Liesegang Systems, *Journal of Physical Chemistry* **1996**, *100*, 16912-16920.
- (120) Kleber, W.; Raidt, H.; Leupold, K. O., Ein Beitrag Zur Züchtung Von Quecksilber (II) - Jodid - Einkristallen, *Kristall und Technik* **1968**, *3*, 65-7
- (121) Greenwell, H. C.; Bindley, L. A.; Unwin, P. R.; Holliman, P. J.; Jones, W.; Coveney, P. V.; Barnes, S. L., In Situ Monitoring of Crystal Growth and Dissolution of Oriented Layered Double-Hydroxide Crystals Immobilized on Silicon, *Journal of Crystal Growth* **2006**, *294*, 53-59.
- (122) Pande, A.; Sinha, S.; Pandit, R., Spiral Turbulence: From the Oxidation of Co on Pt (110) to Ventricular Fibrillation, *arXiv preprint nlin/0001063* **2000**.

- (123) Field, R. J.; Noyes, R. M., Oscillations in Chemical Systems. V. Quantitative Explanation of Band Migration in the Belousov-Zhabotinskii Reaction, *Journal of the American Chemical Society* **1974**, *96*, 2001-2006.
- (124) Kuramoto, Y. *Chemical Oscillations, Waves, and Turbulence*; Courier Dover Publications, 2003.
- (125) Stich, M.; Mikhailov, A. S., Complex Pacemakers and Wave Sinks in Heterogeneous Oscillatory Chemical Systems, *Zeitschrift für Physikalische Chemie* **2002**, *216*, 521.
- (126) Bugrim, A. E.; Dolnik, M.; Zhabotinsky, A. M.; Epstein, I. R., Heterogeneous Sources of Target Patterns in Reaction-Diffusion Systems, *Journal of Physical Chemistry* **1996**, *100*, 19017-19022.
- (127) Pagola, A.; Vidal, C., Wave Profile and Speed near the Core of a Target Pattern in the Belousov-Zhabotinsky Reaction, *Journal of Physical Chemistry* **1987**, *91*, 501-503.
- (128) Hagan, P. S., Spiral Waves in Reaction-Diffusion Equations, *SIAM Journal on Applied Mathematics* **1982**, *42*, 762-786.
- (129) Ma, J.; Hu, B.; Wang, C.; Jin, W., Simulating the Formation of Spiral Wave in the Neuronal System, *Nonlinear Dynamics* **2013**, 1-11.
- (130) Bodenschatz, E.; Walter, T.; Pesch, W., Dislocation Dynamics in Rayleigh-Benard Convection, In *APS Meeting Abstracts* **2001**, *1*, 15008.
- (131) Siggia, E. D.; Zippelius, A., Dynamics of Defects in Rayleigh-Bénard Convection, *Physical Review A* **1981**, *24*, 1036.
- (132) Plessner, T.; Mueller, S. C.; Hess, B., Spiral Wave Dynamics as a Function of Proton Concentration in the Ferriin-Catalyzed Belousov-Zhabotinskii Reaction, *Journal of Physical Chemistry* **1990**, *94*, 7501-7507.
- (133) Belmonte, A.; Flesselles, J.-M.; Ouyang, Q., Spiral Instability to Line Sources in Forced Chemical Pattern Turbulence, *Europhysics Letters* **1996**, *35*, 665-670.
- (134) Ouyang, Q.; Flesselles, J.-M., Transition from Spirals to Defect Turbulence Driven by a Convective Instability, *Nature* **1996**, *379*, 143-146.
- (135) Ouyang, Q.; Swinney, H. L., Transition from a Uniform State to Hexagonal and Striped Turing Patterns, *Nature* **1991**, *352*, 610-612.
- (136) Ouyang, Q.; Swinney, H. L.; Li, G., Transition from Spirals to Defect-Mediated Turbulence Driven by a Doppler Instability, *Physical Review Letters* **2000**, *84*, 1047-1050.

- (137) Ecke, R. E.; Hu, Y.; Mainieri, R.; Ahlers, G., Excitation of Spirals and Chiral Symmetry Breaking in Rayleigh-Bénard Convection, *Science* **1995**, *269*, 1704-1707.
- (138) Mukolobwicz, N.; Chiffaudel, A.; Daviaud, F., Supercritical Eckhaus Instability for Surface-Tension-Driven Hydrothermal Waves, *Physical Review Letters* **1998**, *80*, 4661.
- (139) Lee, K. J.; Cox, E. C.; Goldstein, R. E., Competing Patterns of Signaling Activity in Dictyostelium Discoideum, *Physical Review Letters* **1996**, *76*, 1174.
- (140) Li, B.-W.; Deng, L.-Y.; Zhang, H., Chiral Symmetry Breaking in a Reaction-Diffusion System, *Physical Review E* **2013**, *87*, 042905.
- (141) Steinbock, O.; Engel, H., Wave Phenomena in Reaction-Diffusion Systems, *Engineering of Chemical Complexity* **2013**, *11*, 147.
- (142) Zhou, L. Q.; Ouyang, Q., Spiral Instabilities in a Reaction-Diffusion System, *Journal of Physical Chemistry A* **2001**, *105*, 112-118.
- (143) Burda, C.; Chen, X.; Narayanan, R.; El-Sayed, M. A., Chemistry and Properties of Nanocrystals of Different Shapes, *Chemical Reviews* **2005**, *105*, 1025-1102.
- (144) Chung, S.-Y.; Kim, Y.-M.; Kim, J.-G.; Kim, Y.-J., Multiphase Transformation and Ostwald's Rule of Stages During Crystallization of a Metal Phosphate, *Nature Physics* **2008**, *5*, 68-73.
- (145) Al-Ghoul, M.; Ammar, M., Polymorphic and Morphological Transformation During the Transition from a Propagating Band to Static Bands in the Nickel Hydroxide/Ammonia Liesegang System, *Defect and Diffusion Forum* **2011**, *312*, 800-805.
- (146) Al-Ghoul, M.; Sultan, R., Front Propagation in Patterned Precipitation. 1. Simulation of a Migrating Co(OH)₂ Liesegang Pattern, *Journal of Physical Chemistry A* **2001**, *105*, 8053-8058.
- (147) Antal, T.; Droz, M.; Magnin, J.; Rácz, Z.; Zrinyi, M., Derivation of the Matalon-Packter Law for Liesegang Patterns, *The Journal of Chemical Physics* **1998**, *109*, 9479-9486.
- (148) Karam, T.; El-Rassy, H.; Sultan, R., Mechanism of Revert Spacing in a PbCrO₄ Liesegang System, *Journal of Physical Chemistry A* **2011**, *115*, 2994-2998.
- (149) Lagzi, I., Simulation of Liesegang Patterns: Effect of Reversible Complex Formation of Precipitate, *Journal of Physical Chemistry B* **2003**, *107*, 13750-13753.

- (150) El-Batlouni, H.; El-Rassy, H.; Al-Ghoul, M., Cosynthesis, Coexistence, and Self-Organization of A-and B-Cobalt Hydroxide Based on Diffusion and Reaction in Organic Gels, *Journal of Physical Chemistry A* **2008**, *112*, 7755-7757.
- (151) Rahbani, J.; Khashab, N. M.; Patra, D.; Al-Ghoul, M., Kinetics and Mechanism of Ionic Intercalation/De-Intercalation During the Formation of A-Cobalt Hydroxide and Its Polymorphic Transition to B-Cobalt Hydroxide: Reaction–Diffusion Framework, *Journal of Materials Chemistry* **2012**, *22*, 16361-16369.
- (152) Lou, Q.; Chen, J.-X.; Zhao, Y.-H.; Shen, F.-R.; Fu, Y.; Wang, L.-L.; Liu, Y., Control of Turbulence in Heterogeneous Excitable Media, *Physical Review E* **2012**, *85*, 026213.
- (153) Kaštánek, P.; Kpsek, J.; Šnita, D.; Schreiber, I.; Marek, M., Reduction Waves in the Bz Reaction: Circles, Spirals and Effects of Electric Field, *Physica D: Nonlinear Phenomena* **1995**, *84*, 79-94.
- (154) Zhang, H.; Hu, B.; Hu, G., Suppression of Spiral Waves and Spatiotemporal Chaos by Generating Target Waves in Excitable Media, *Physical Review E* **2003**, *68*, 026134.